HIGH RESOLUTION SEISMIC IMAGING OF THE NEAR-SURFACE: COMPARISON OF ENERGY SOURCES

JIANGUANG XIANG

INFORMATION TO USERS

This manuscript has been reproduced from the microfilm master. UMI films the text directly from the original or copy submitted. Thus, some thesis and dissertation copies are in typewriter face, while others may be from any type of computer printer.

The quality of this reproduction is dependent upon the quality of the copy submitted. Broken or indistinct print, colored or poor quality illustrations and photographs, print bleedthrough, substandard margins, and improper alignment can adversely affect reproduction.

In the unlikely event that the author did not send UMI a complete manuscript and there are missing pages, these will be noted. Also, if unauthorized copyright material had to be removed, a note will indicate the deletion.

Oversize materials (e.g., maps, drawings, charts) are reproduced by sectioning the original, beginning at the upper left-hand corner and continuing from left to right in equal sections with small overlaps.

Photographs included in the original manuscript have been reproduced xerographically in this copy. Higher quality 6" x 9" black and white photographic prints are available for any photographs or illustrations appearing in this copy for an additional charge. Contact UMI directly to order.

Bell & Howell Information and Learning
300 North Zeeb Road, Ann Arbor, MI 48106-1346 USA
800-521-0600

High Resolution Seismic Imaging of the Near-Surface: Comparison of Energy Sources

By

©Jianguang Xiang

A thesis submitted to the

School of Graduate Studies

in partial fulfillment of the

requirements for the degree of

Master of Environmental Sciences

Environmental Science Program

Memorial University of Newfoundland

April, 2000

St. John's Newfoundland

Abstract

The shallow seismic reflection method plays an important role in helping to understand engineering, mining and environmental problems. For high resolution at shallow depth, choosing a seismic source to best meet the goals of the survey can be the most pivotal decision. This research is to study the characteristics of various portable and environmentally friendly seismic sources by comparing them to the source character of a shotgun source. The sources include two SIST (Swept Impact Seismic Technique) vibrators and a hammer. Data were collected in 1999 near St. John's, Newfoundland. They were compared with shotgun source in terms of radiated frequency spectrum and energy levels in an attempt to improve the resolving power.

Compared to the shotgun data, the SIST vibrators provide lower frequency range but higher frequency bandwidth. Their weaker energy limits the effective penetration depth for imaging to 150 m. However, the SIST vibrator yields a higher resolution in stacked section than the shotgun. Based on its overall performance, the SIST vibrator shows a great deal of potential to be a viable, environmentally friendly seismic source with high resolution capability. This is especially suitable for environmental surveys, in which depths are usually not more than 200 m.

Acknowledgement

I am most grateful to my supervisor, Dr. James Wright, for his kindly and effective guidance during the research and thesis writing and for his providing financial support to this research so that it could be finished smoothly.

This research was carried out through the Memorial University Seismic Imaging Consortium (MUSIC).

Many thanks are to Dr. Larry Lines, the other member of my supervisor committee, and Dr. Niall Gogan, the Chair of the Environmental Science Program. Dr. Lines provided financial aid in my first year study. Dr. Niall Gogan provided partial financial support. I also thank Memorial University of Newfoundland for the financial support of a Graduate Fellowship.

I want to thank Dr. Calin Cosma, Vibrometric OY, who assisted in the fieldwork and provided technical advice related to the mini-vibrator source.

I also highly appreciate the help from other members of seismic group. Discussions with Kebabonye Laletsang enlightened me on both research and processing skills. Mr. Paul Barnes and Ms. Christina Demerling assisted very much in data acquisition. Mr. Tony Kocurko managed the computers to ensure that the software worked well.

Contents

List of Figures

List of Tables

Chapter 1. Introduction

1.1. Statement of Objective

Over the last two decades, the application of seismic reflection methods to engineering, groundwater, mining, and environmental problems has become more and more popular (Steer et al., 1996; Steeples and Miller, 1990; Jongerious and Helbig, 1988; Pullan and MacAulay, 1987). To obtain high seismic resolution with these applications, numerous investigators have developed and applied a wide variety of shallow reflection seismic sources, of which most could be classified as impulsive or vibratory sources.

Seismic methods have been applied to many types of engineering problems, such as foundation testing, water table location, detection of abandoned mine shafts, and detection of metallic objects. Foundation testing includes determination of the depth to bedrock, and the properties of rock encountered in construction projects, such as power plants, dams, highways, subways and so on. The location of water is important for municipal engineering relating to water supply, sewage disposal, irrigation, and drainage problems.

Over past 50 years, seismic exploration has been applied widely in environmental problems, especially in the search for groundwater resources. In addition, by mapping geological structure, seismic exploration has been used for other environmental issues, such as the location of buried hazardous waste materials, landfills, safe sites for nuclear waste disposal, dams and reservoirs, tunnels and road foundations.

Groundwater is an important part of the Earth's environment, and many environmental problems are related to the location of groundwater and its protection from contamination sources. In favorable noise conditions, reflection seismic profiling can yield specific geological and hydrological information about possible aquifers. The presence or absence of fluid in pores and fissures affects density and seismic velocity manifest through the strength of reflections. Also, the degree of alteration varying with the nature and content of contaminant present significantly changes the acoustic properties of many rocks. This factor makes it possible for seismic methods to locate water-bearing structures, to map regions where the interstitial fluid is liquid and to distinguish them from ones where the pore fluid is gaseous.

The seismic reflection method is also used for coal exploration, in which the goal is to locate the coal zones and determine their extent. Previous work (Greenhalgh and Emerson, 1986, Spencer et al., 1993) indicates that coal generally has markedly low velocity and density compared with the surrounding rocks. Thus the interface between coal and adjacent rocks makes an excellent reflector but can cause multiple and transmission problems. On the other hand, the surrounding rocks with uniformly high velocities can produce reflections of only low amplitude. Usually, coal seams may be less than 2m thick and frequently contain steep dips and lateral heterogeneity. Due to these properties of coal, high-resolution seismic reflection is necessary to resolve the thin coal seams at several hundred-meter depths. Also, in conjunction with borehole data, high-resolution seismic reflection can furnish continuous profiles and show whether the coal seam is flat laying or dipping. Explosives have been the most common source for mineral

exploration. However, since explosives always generate significant ground roll that reduces the resolution and have severe environmental impact, non-explosive sources such as hammer and vibroseis are increasingly employed. Besides reducing environmental impact, the repeatable characteristics of these sources can allow source stacking to suppress ground roll and therefore lead to improvements in signal-to-noise ratio.

1.2. Previous Work

There are many factors that affect the seismic energy source selection, including cost, repeatability, spectral characteristics, convenience and efficiency, amount of energy and safety. To assist in the selection of a shallow seismic source best meeting the goals within the constraints of specific projects, the Engineering and Groundwater Committee of Society of Exploration Geophysicists (SEG) conducted a field comparison of shallow seismic sources in New Jersey (Miller et al., 1986) and near Chino, California (Miller et al., 1992). The experiments involved 26 different sources or variation of sources for testing. These can be classified as sledgehammer, explosives, weight drop, projectile impacts, and various guns.

Two tests indicated the similarities in wave presence, recording energy, and spectral characteristics. Besides reflection and refraction, the recorded signal also includes surface wave (ground roll and air blast), instrument noise, cultural noise, air coupled, and random source echoes. Surface waves can be clearly identified on the near offset traces by their high amplitude and long wavelength. The most noteworthy characteristic of the air blast is its very high frequency wavelet. Instrument noise affects all traces equally while cultural noise is generally observable on only a few traces near the noise source. The air coupled, random source echoes appear as high-frequency chatter trailing the air blast on near offset traces.

In the published tests, the recorded energy varies by more than an order of magnitude, both trace-to-trace and source-to-source. Among them, elastic wave generators (EWG)

produce the largest amplitude while a rifle shot at surface in a dry hole generates the smallest. Figure 1 illustrates the comparison of relative total amplitude recorded from various sources. The elastic wave generator requires continuous use of 4-cycle gasoline engine to power its hydraulic lift mechanism; thus, its frequency spectrum contains high-frequency engine noise. For the downhole shotgun, black powder loads generate almost triple the total recordable amplitude of a lead slug. Lowering the muzzle of the rifle below the ground surface not only increases the total seismic energy, but also decreases the amount of the air-coupled wave. For downhole sources (i.e., explosives, shotguns, and rifles), water-stemming can reduce the air-coupled wave by as much as one third and increase the seismic energy by almost double. For the certain applications, the downhole black powder capsule has become a popular alternative to high explosives, which yield more than twice the recordable energy of black powder capsule but produce a higher percentage of air-coupled waves to high frequency seismic energy.

Spectral characteristics in terms of amplitude versus frequency are also compared. For most records in the test, ground roll and seismic reflections are not the only arrivals on the seismic traces. The spectrum from the Fourier transform contains not only ground roll and reflection frequency, but also air blast frequency. On the amplitude versus frequency plots, the dominant frequency bands of both the ground roll and the reflection wave are

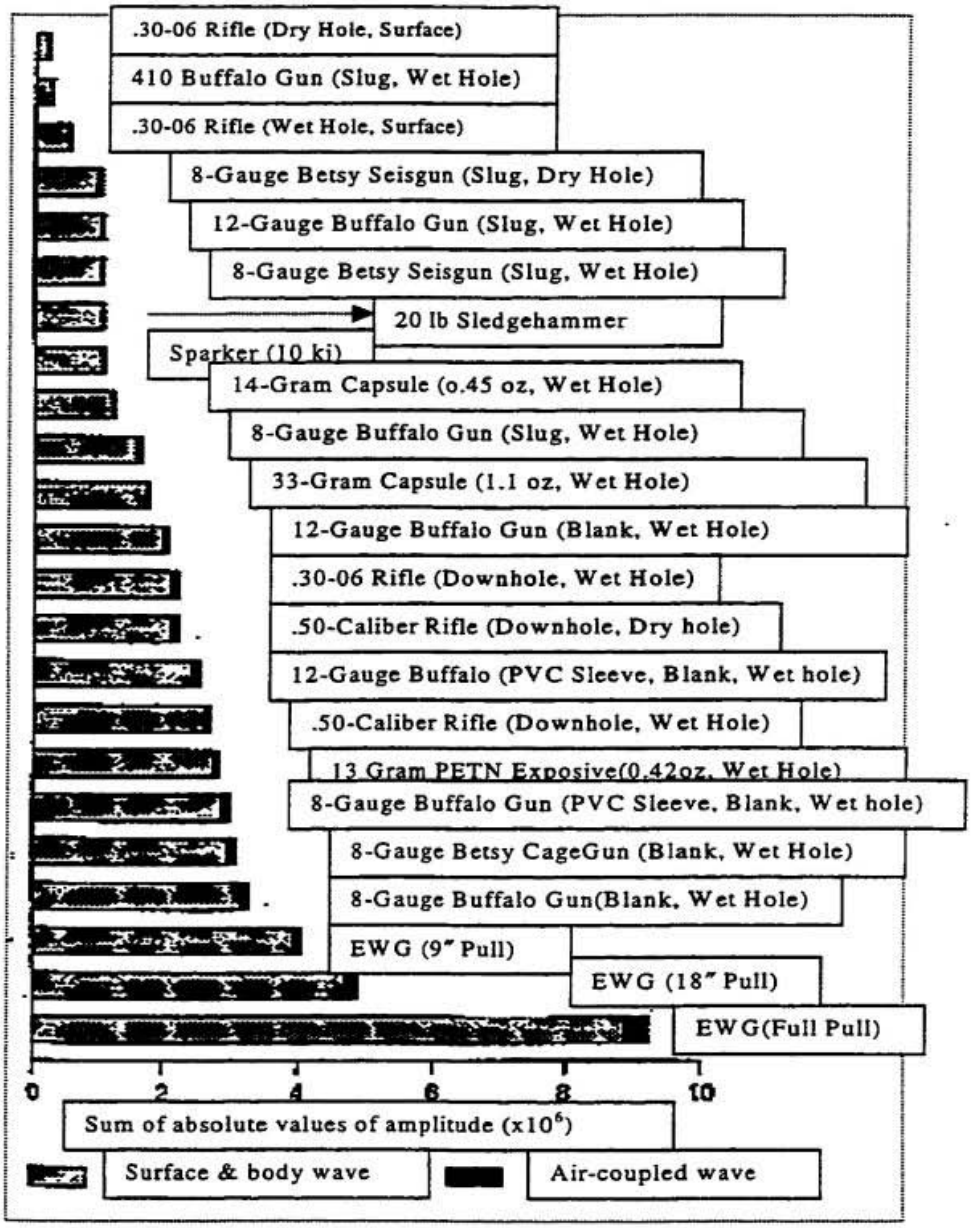

Figure 1 Amplitude comparison from 23 sources and configuration of sources recorded with analog low-cut filters out (open). (after Miller et al., 1992)

within the high amplitude maxima centered below about 400Hz and are easily compared. The air blast's dominant frequencies are contained within the peaks at about 600Hz. Beyond 600Hz, the majority of energy is either instrument noise or high frequency chatter from air-coupled or randomly arriving echoes source.

The results of two comparison tests reveal the basic nature of various seismic sources. The comparison indicates that the choice of a seismic source should be an important factor for successful seismic surveys designed to obtain a better understanding of the geological structure and the fluid content of the near surface of the Earth. However, all the data were obtained at particular sites, thus different results may be expected under different site conditions. With the extremely site-dependant nature of near surface reflections, some specific seismic sources in a specific geological setting are expected to generate more useful and higher quality seismic energy than others.

In a land survey, explosives and weight-drops are the most used impulsive seismic sources. The use of the weight-drop is now very limited, but explosives are still used often (Baeten and Ziolkowski, 1990). The explosive source, depending on its size as well as the burn time, can generate relatively high frequency output. However, explosives also have some disadvantages. First, they are destructive, and they are prohibited in a densely populated environment. Secondly, they may produce chemical residues that are harmful to the environment, especially if they enter the groundwater. Thirdly, drilling a hole for each shotpoint is costly. Finally, the frequency content of the radiated wave depends heavily on the charge size. Although the burn time of the dynamite is very brief compared with any time duration in seismic exploration, the high energy density of the

explosion produces a nonlinear zone around the explosion, and the size of this zone determines the frequency content of the radiated waves. The bandlimited signal radiated from the nonlinear zone cannot be measured directly because of its unknown shape.

As a non-explosive seismic source, Vibroseis® (Vibroseismic Prospecting), which was developed by Continental Oil Company in 1960's, has become very widespread in land surveying. In the Vibroseis method, the input wave generated by the vibroseis source persists for many seconds, and its frequency changes over the duration of the signal. By a special choice of input signal frequencies, a "sweep" signal with varied frequency, and a special data processing operation, Vibroseis can achieve good seismic character.

Vibroseis has distinct advantages over dynamite. First, because of the use of a long sweep, the energy density of the Vibroseis pulse is much less than that of dynamite. Therefore, destructive effects are much less severe. Secondly, drilling shot holes is no longer needed, so that the cost and environmental damage is greatly reduced. Thirdly, Vibroseis provides a direct means to measure and control the radiated signal. After data processing, Vibroseis data looks like impulsive seismic data but without the unwanted nonlinear and destructive effects. Therefore Vibroseis may have a higher signal/noise ratio than that for explosive sources.

The Swept Impact Seismic Technique (SIST) has been developed for high resolution seismic applications in recent years (Cosma et al., 1998). SIST combines both the Vibroseis swept-frequency and the Mini-Sosie multi-impact ideas (Black, 1996). With SIST, a low power impact source generates a series of seismic pulses, hence it relates to

Mini-Sosie. On the other hand, a varying swept impact rate is used so that SIST is similar to Vibroseis. Compared to Vibroseis, a firm coupling to the rock or ground is not as critical with SIST (Cosma et al., 1998). This is a clear advantage. In addition, the SIST apparatus is simpler and more portable than Vibroseis.

The optimum seismic source selection leads to the generation of higher resolution seismic imaging by considering a particular purpose, geological setting, and site and environmental logistics.

1.3. Resolution Considerations

Seismic resolution defines the amount of detail in the acoustic property variations both in vertical and horizontal directions that can be derived from seismic data. Vertical resolution measures the ability to distinguish two horizontal interfaces as separate reflectors, whereas horizontal resolution measures the ability to distinguish features at the same depth but separated horizontally (Figure 2).

The resolution in the vertical direction is involved with the "resolvable (separable) limit". Rayleigh (Jenkins and White, 1957) defined the resolvable limit as a quarter wavelength ($\lambda/4$). When the two reflectors are separated by $\lambda/4$, the interference effects are minimized. Widess (1973) provided a slightly less stringent criterion, in which the value for resolvable limit is one eighth of the dominant wavelength ($\lambda/8$). There are still other definitions, but all of them generally fall within this range.

The importance of the resolvable limit in stratigraphic interpretation becomes evident for calculating the thickness that corresponds to a quarter wavelength. When a wavelet with dominant frequency f travels to a reflector with velocity v, its wavelength λ is simply v/f, so the minimum resolving limit ($\lambda/4$) should be v/(4f). Generally, the velocity in shallow layers is almost constant and cannot be controlled. Thus, increasing frequency is the only means to sharpen the wavelet and increase the resolution.

The horizontal resolution on unmigrated seismic data is usually described in terms of the Fresnel zone, although some other factors such as signal/noise ratio, spatial sampling and three-dimensional effects also contribute. The first Fresnel zone is the area on a reflecting

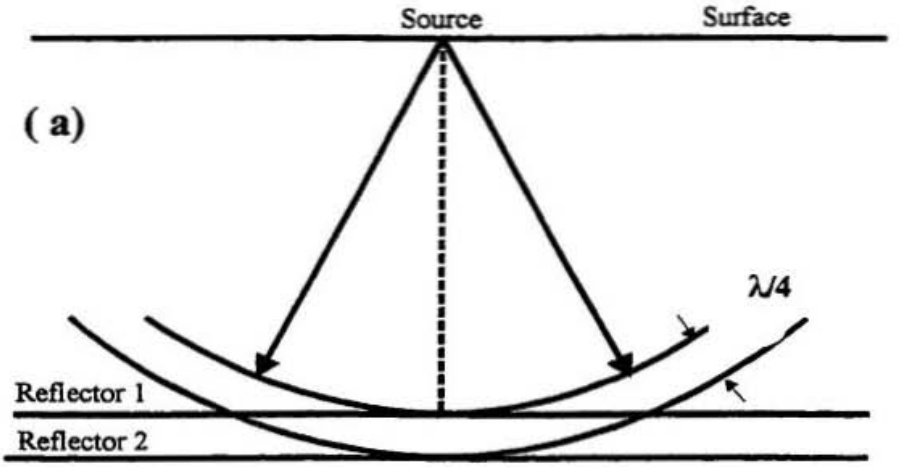

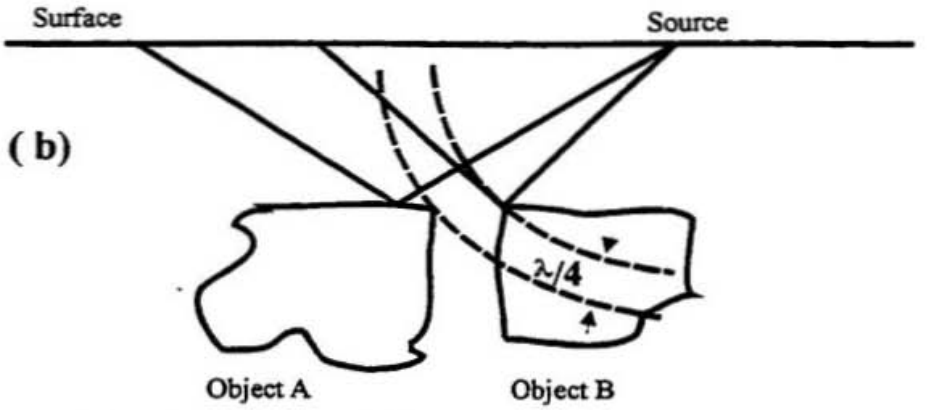

Figure 2 Seismic resolution. (a) Vertical and (b) Horizontal

surface from which reflected energy arriving at a detector has a phase difference of no more than 180°. This energy interference is more or less constructive; hence, the Fresnel zone is often taken as limiting horizontal resolution on unmigrated seismic data. However, in a migrated section, the Fresnel zone dimensions effectively shrink so that the Fresnel zone size is no longer used as a criterion for horizontal resolution, because migration is believed to collapse the Fresnel zone. After migration and deconvolution, the resolution is determined by the temporal bandwidth, the sub-surface velocity, and the dip distribution.

Extremely sharp input wavelets will generate high seismic resolution. However, actual seismic wavelets always involve a limited range of frequencies and hence have appreciable temporal breadth. Therefore, the most practical method to increase seismic resolution is to increase the dominant frequency of the source. On the other hand, a key point that needs to be considered for seismic source selection is the tradeoff between the maximum resolution and depth of penetration. A high frequency input wave may generate high resolution, however, when it travels in the earth, its energy attenuates quickly and the attenuation limits the penetration. Contrarily, a larger power source has more energy and better penetration, but the energy is concentrated in lower frequencies, therefore the resolution is decreased.

1.4. Outline of the Research

This research will compare impulsive and vibratory sources that are portable and applicable for near surface high-resolution seismic studies. Particular emphasis will be on comparing the radiated frequency spectrum and energy levels for the source in an attempt to improve the resolving power.

Chapter 2. Theory and Techniques for High Resolution Seismology

2.1. Fundamentals of Shallow Seismic Reflection

Among geophysical methods, seismic reflection is the most sensitive to mechanical properties of earth materials. The method has been used increasingly since the 1980's in application to the shallow subsurface. Because all the engineering and environmental tasks described in Chapter 1 exist in the near-surface, the seismic reflection method is an excellent choice to achieve high resolution in this domain.

Modern work using shallow seismic reflections by Schepers (1975) resulted in excellent data, but did little to encourage widespread use of the method (Sheriff and Geldart, 1995). The work of Hunter and Pullan (Hunter et al., 1984; Pullan and Hunter, 1985, 1990) and Helbig et al. (1985) was instrumental in establishing the shallow seismic reflection procedure. In particular, the optimum window-common offset technique (Hunter et al., 1984) has been widely used, in which the nearest geophone is located beyond the zone of ground roll so that the reflector is observed with minimum interference.

2.1.1. The Seismic Wave Equation and Propagation

External force causes elastic solids to undergo two types of deformation: compression and shear. According to the theory of the elasticity and the basic principles of dynamics,

these deformations give rise to two independent wave propagation mechanisms: compressional waves (P-waves) and shear waves (S-waves). The wave equation can be derived from Newton's second law of motion, that an unbalanced force on a mass produces acceleration. The wave equation can be expressed in vector as well as the more conventional scalar notation.

$$\nabla^2 \Delta = \frac{1}{Vp^2} \frac{\partial^2 \Delta}{\partial t^2}$$

$$\nabla^2 \bar{\Theta} = \frac{1}{V_s^2} \frac{\partial^2 \bar{\Theta}}{\partial t^2} \qquad \text{.....(2.1)}$$

here Δ is dilatational potential ($\varepsilon_{xx}+\varepsilon_{yy}+\varepsilon_{zz}$) and Θ (Θ_x, Θ_y, Θ_z) is rotational vector potential.

The first equation corresponds to the propagation of a compressional wave at velocity

$$V_p = \sqrt{\frac{\lambda + 2\mu}{\rho}}$$

and the second one corresponds to the propagation of a shear wave at velocity

$$V_s = \sqrt{\frac{\mu}{\rho}}$$

V_p and V_s above indicate that the shear wave velocity is always less than the compressional velocity, and shear waves do not propagate in a liquid medium with the zero rigidity modulus.

The passage of the seismic wave sets the subsurface particles in motion. The surface on which the particle movements are in phase is called the wavefront. In isotropic homogeneous media, the wavefronts propagate along rays perpendicular to the wavefront. While wavefronts have physical significance, they have no real existence. Raypaths are introduced for convenience and it is better to argue in terms of wavefronts in simple cases.

Huygen's Principle, which is useful in drawing successive positions of wavefronts, states that every point on a wavefront can be regarded as a new point source of waves, and the subsequent wavefronts are the envelopes of all the secondary wavefronts. Specifically, given the location of a wavefront at a certain time, the future positions of the wavefronts can be predicted by considering each point on the first wavefront as a new wave source.

When the wavefronts reach the subsurface interfaces, the energy is partly reflected and partly transmitted in accordance with the boundary conditions of elastic media. In homogeneous formations, where the seismic velocities are constant, the seismic raypaths are straight lines. When seismic rays pass from one homogeneous formation to another one, the raypaths are bent according to Snell's Law (Equation 2.2 & Figure 3): the reflected angle θ_1 is the same as incident angle θ_0 and transmitted angle θ_2 is larger or smaller than incident one depending on whether the velocity in second media is larger or smaller than that in the first.

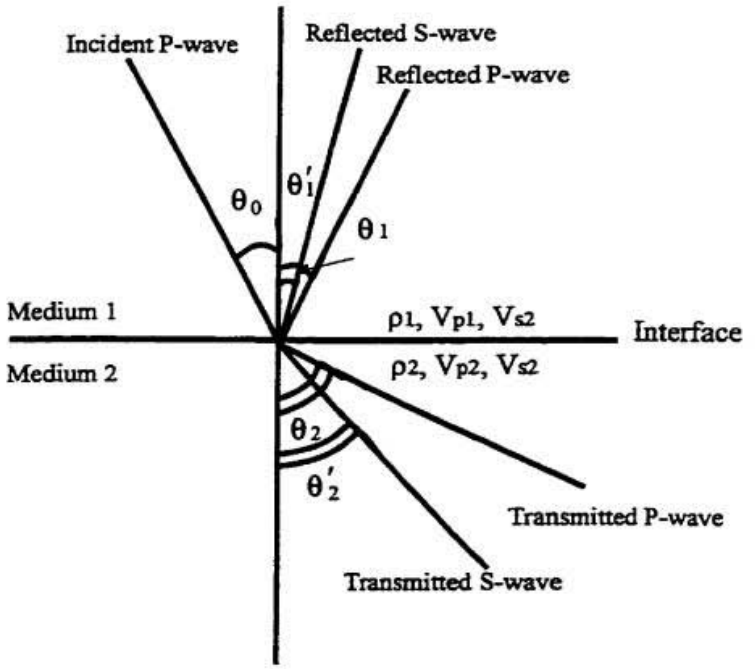

Figure 3 Angular relationships between incident, reflected and transmitted rays for different wave types.

$$\frac{\sin\theta_0}{V_{p1}} = \frac{\sin\theta_1}{V_{p1}} = \frac{\sin\theta_1'}{V_{s1}} = \frac{\sin\theta_2}{V_{p2}} = \frac{\sin\theta_2'}{V_{s2}} = p \quad \text{..... (2.2)}$$

In the case of normal incidence (θ_0=0), the reflection amplitude coefficient R, the ratio of reflected relative amplitudes to the incident waves, can be expressed in the form:

$$R = \frac{Z_2 - Z_1}{Z_2 + Z_1} \qquad \text{where } Z_i = \rho_i \cdot V_i \quad \text{.....(2.3-1)}$$

Similarly, the transmission amplitude coefficient T can be expressed as:

$$T = \frac{2Z_1}{Z_2 + Z_1} \quad \text{..... (2.3-2)}$$

The fractions of energy reflected and transmitted are given as E_R and E_T, which are also called reflection and transmission energy coefficients respectively.

$$E_R = \left(\frac{Z_2 - Z_1}{Z_2 + Z_1}\right)^2 = R^2 \qquad E_T = \left(\frac{2Z_1}{Z_2 + Z_1}\right)^2 = \frac{Z_2}{Z_1}T^2 \quad \text{.....(2.4)}$$

The equation (2.3) and (2.4) indicate that the reflection and transmission coefficients (both amplitude and energy) depend on the presence of acoustic contrasts in the subsurface. These acoustic contrasts, governed by acoustic impedance Z, occur at boundaries between geological layers, as well as at man-made boundaries such as tunnels and mines. An acoustic impedance ρV_p exists for compressional waves, and ρV_s for shear waves. Thus, the acoustic impedance occurs as a variation either in density or seismic velocity or both.

The simplest case of seismic reflection is a single layer over an infinitely thick half-space (Figure 4a). Energy is radiated spherically away from the source of seismic waves. One particular raypath originating at the source will convey energy to the subsurface layer, and then return an echo to the surface where a geophone will detect it.

It is more common that several layers exist beneath the Earth's surface (Figure 4b). According to Snell's law, the ray paths are not straight lines when they across boundaries; instead, the velocity and density discontinuities between layers bend the rays.

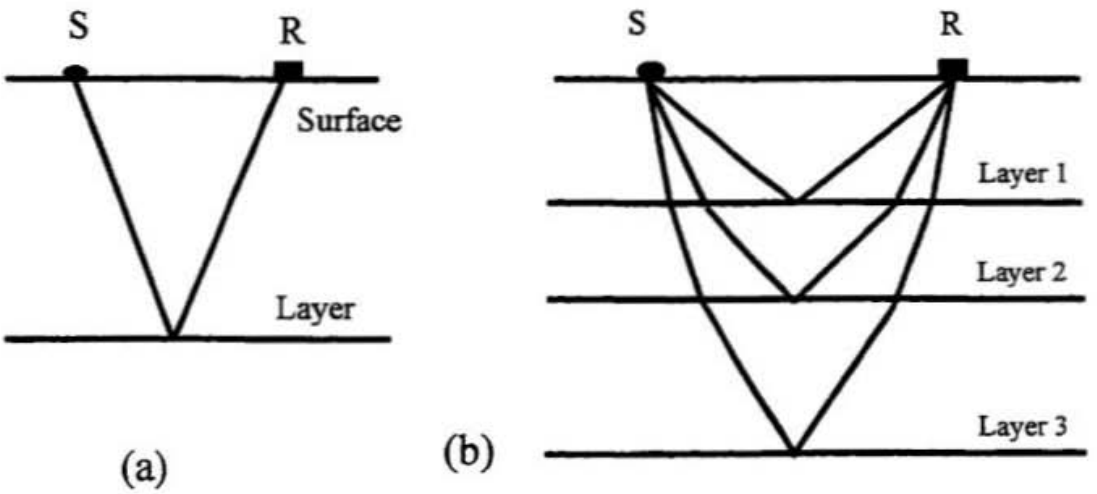

Figure 4 Shallow seismic reflection_ a) single layer case; b) multi-layer case

2.1.2. Data Acquisition and Instruments

Acquisition systems essentially comprise a geophone spread, a source pattern, and digital recording instruments.

2.1.2.1 Geophone Spread

The spread indicates the relative locations of the sources and the geophones or the centers of the geophone groups that are used to record the reflected energy. The geophone locations are usually laid out in a straight line in 2-D survey, and the spread types depend on the locations of source. In a split spread, the source is at the center of a line of regularly spaced geophones. A common asymmetrical spread is end-on, in which the source is at one end of regularly spaced geophones. The end-on arrangement also often involves in-line offset of source (Figure 5).

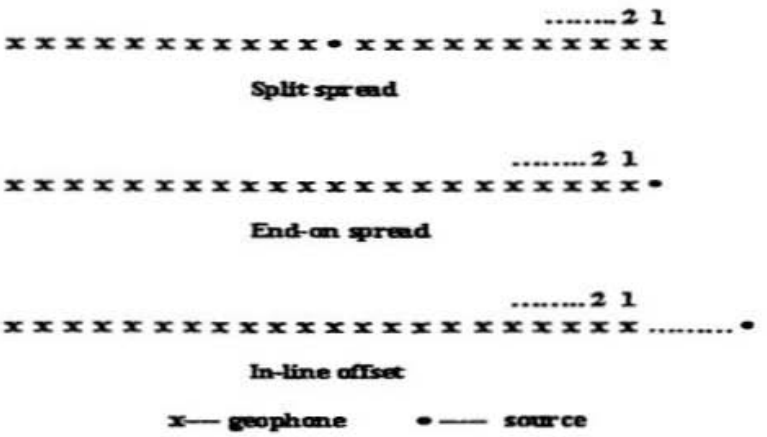

Figure 5 Types of reflection spreads

When a seismic source is discharged at a given shot point, the reflected waves are detected at geophones arrayed in a line each side of the shot (Figure 6). There are several points in the subsurface (equal to the number of geophones) that reflect seismic energy to the geophones. In the simple case of a straight line spread (2-D), the point of reflection is half-way between the source and the detecting geophone. The spacing between reflection points on the interface is always half that of geophone spacing. Consequently, the total sub-surface coverage of an interface, the length across all reflecting points, is exactly half the total geophone spread length.

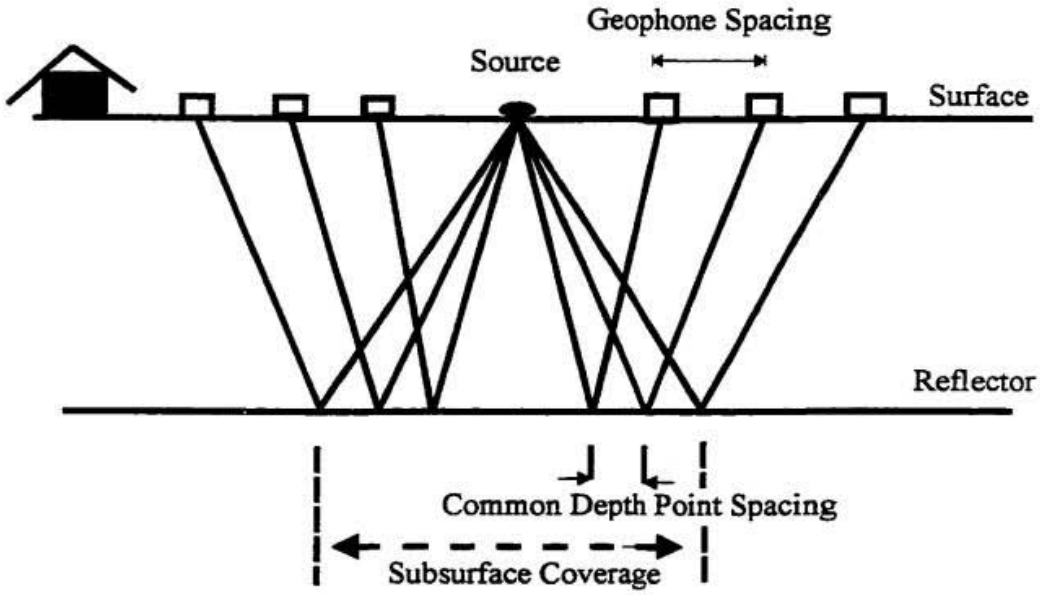

Figure 6 Schematic view of seismic raypaths for multi-channel acquisition

For shallow low velocity layers, there is much noise in the reflection data. Usually, more than one shot is used. Thus reflections arising from the same point on the interface will be detected at different geophones (Figure 7). This common point of reflection is known as the common midpoint (CMP) or common-depth point (CDP). A CMP gather is a grouping of all traces with the same midpoint location, while a CDP gather is a grouping of all those with same reflection point. CMP and CDP gather is a useful technique for combining traces to increase the signal/noise ratio.

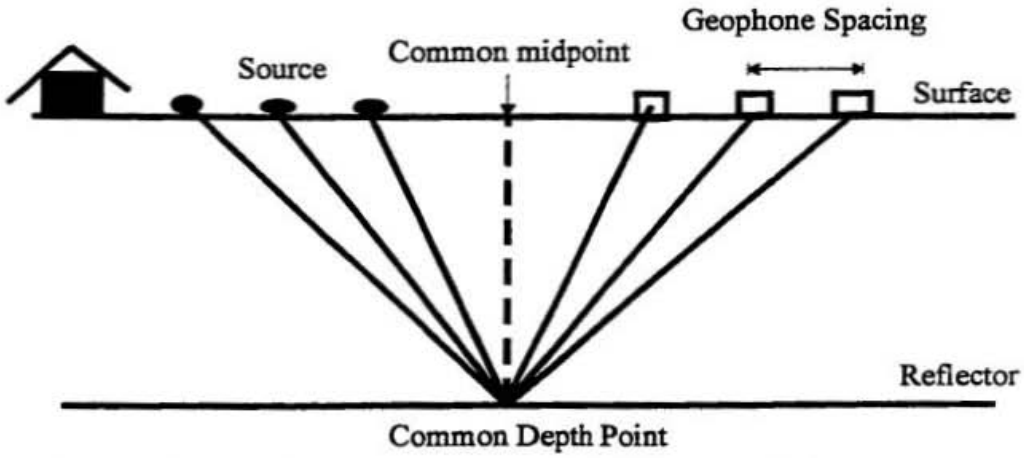

Figure 7 Common-depth-point (CDP) and the common midpoint (CMP) concept

A CDP gather is equivalent to a CMP gather only when the reflectors are horizontal and velocity does not vary horizontally. If the reflector in the subsurface dips, these two gathers are no longer equivalent and only the term CMP gather is used. The power of the CMP process is in the multiplicity of data that come from a particular subsurface location. Since the noise is generally random in nature, making a CMP gather and adding the traces can reduce noise and enhance the reflection signal. The degree of multiplicity of data from a particular location is known as "CMP fold". Theoretically, the signal-to-noise (S/N) ratio of reflections is improved proportionally to the square root of the CMP fold.

2.1.2.2. Source

Selection of the most appropriate seismic source type for a particular survey is very important. An ideal seismic source must produce a large enough signal into the ground to ensure sufficient depth penetration and a high enough resolution to image the subsurface.

There is a great number of different sources that can be used depending on the type of target. All sources are generally classified as three types: 1) impact, which includes hammer, drop weight and accelerated weight; 2) impulsive, which includes dynamite, airgun and shotgun; and 3) vibrator, includes vibroseis and vibrator plate (Reynolds, 1997).

As seismic waves propagate, part of their energy is converted into heat and energy is lost. This reduction in the elastic energy of the wave is termed absorption. The energy attenuation due to the absorption varies exponentially with the distance from the source. In a solid medium, the absorption is directly proportional to frequency (Al-Sadi, 1980). Thus, the energy losses with distance are much greater at higher frequencies than at lower frequencies. However, in a shallow reflection survey, higher frequency contents are required to achieve high resolution. The goal of source selecting is finding better ways to increase higher frequency components when generating energy and to be sensitive to detecting those higher frequencies rather than the lower ones.

From a practical standpoint, there are some differences between the sources for shallow seismic reflection and those for standard reflection surveying, say in the petroleum industry. Firstly, the amount of source energy required is often much less for shallow reflection. Secondly, low cost is preferred since the number of shotpoints per kilometer is often an order of magnitude greater for a shallow high resolution application. Thirdly, portability and efficiency are required to achieve the large amount of field work with ease. Fourthly, repeatability is required to ensure that stacking records from multiple input from the same energy source at the same shotpoint will enhance the reflection

signal. Finally, safety is an important factor to be considered to minimize any danger to the environment and any local community.

2.1.2.3. Detector

Seismic energy arriving at the surface of the ground is detected by geophones, which convert ground motion to an electrical signal whose amplitude is proportional to the amount of ground displacement. Performance characteristics of a geophone include its natural frequency, sensitivity, coil resistance, damping and harmonic distortion.

One of the most important aspects of a geophone is its natural frequency. This is the frequency for which the output of geophone has the greatest value. For high resolution shallow surveys, the geophone is needed to detect high frequency with minimum distortion in the output signal. The first rule of thumb is to choose a receiver with a natural frequency that is at least 10 percent of the highest frequency likely to be recorded (Sharma, 1997); i.e., if the likely highest frequency is 500 Hz, then a 50 Hz geophone is sufficient. Geophones with natural frequencies of 50 to 100 Hz are recommended for shallow reflection work (Burger, 1992).

Geophones have a response peak at their natural frequency, which can cause ringing in the data and an artificial peak in the spectrum of the recorded data. To counter this, damping resistors are used to flatten this peak relative to the other response frequencies. Usually, the damping resistors are installed at the factory, which makes it possible to change the damping coefficient easily to meet different needs. Present generation digital

acquisition systems have higher sample rates and larger data storage to record high frequency signal successfully.

Also, geophone-ground coupling affects a geophone response at high frequencies. If this coupling is not good enough, the motion of the geophone case does not faithfully follow ground motion at high frequencies. To improve the geophone-ground coupling, a large area of contacting with ground, by increasing the size of the spike or base plate of geophone, is desired.

For large scale survey, more than one geophone may be connected together to form a "group" of geophones, the output of which is summed and recorded in one channel. The geophone group is designed to enhance the near-vertical upward-travelling reflected waves and minimize any horizontal coherent noise (Reynolds, 1997). If the individual geophones in a group have a spacing equivalent to a half wavelength of coherent noise, for example, the Rayleigh wave, the signals at alternate geophones will be out of phase and will be cancelled by the summation of the outputs from the geophone group. A geophone group can also help to filter out some random noise and has a overall effect of increasing both signal strength and signal/noise ratio (Reynolds, 1997). Because of the small spacing between the geophones in the group, the entire group is approximately equivalent to a single geophone located at the center of the group.

2.1.2.4. Seismograph

The seismograph records the geophone output digitally by analog-to-digital converters. In playback, through filtering, time shifting, compositing, and other operations, the data are

put into the desired form for processing and presentation after digital-to-analog conversion. By using computer technology, the seismograph has a significant recording speed and storage capacity for handling multichannel seismic signal in real time. There are numerous different recording system settings. In a high resolution shallow seismic survey, a high frequency is needed to achieve high resolution. High frequency has a small wavelength that requires the recording system to sample at a high rate to avoid high frequency component losses. In some cases, like vibroseis, long records (more than 10 seconds) are employed to enhance signal. Thus the ability to record long records is important.

2.1.3. Data Processing

Data processing is applied to the seismic data to enhance the signal/noise ratio, highlight the geological features, and finally enable the geophysicist to interpret. Figure 8 illustrates a conventional data processing flowchart (after Yilmaz, 1987).

The multiplicity of seismic data gives rise to a variety of schemes to process the data and provide an image of the sub-surface. Generally, data processing for shallow seismic reflection data is similar to that for conventional seismic reflection data.

However, shallow layers generally have low velocity that varies abruptly with horizontal location. In addition, the reflections are often subtle and noisy. Thus, in contrast to conventional processing, more attention must be paid to some pitfalls of shallow reflection data processing. The primary pitfalls are spatial aliasing, removing of air-blast noise, and refraction muting.

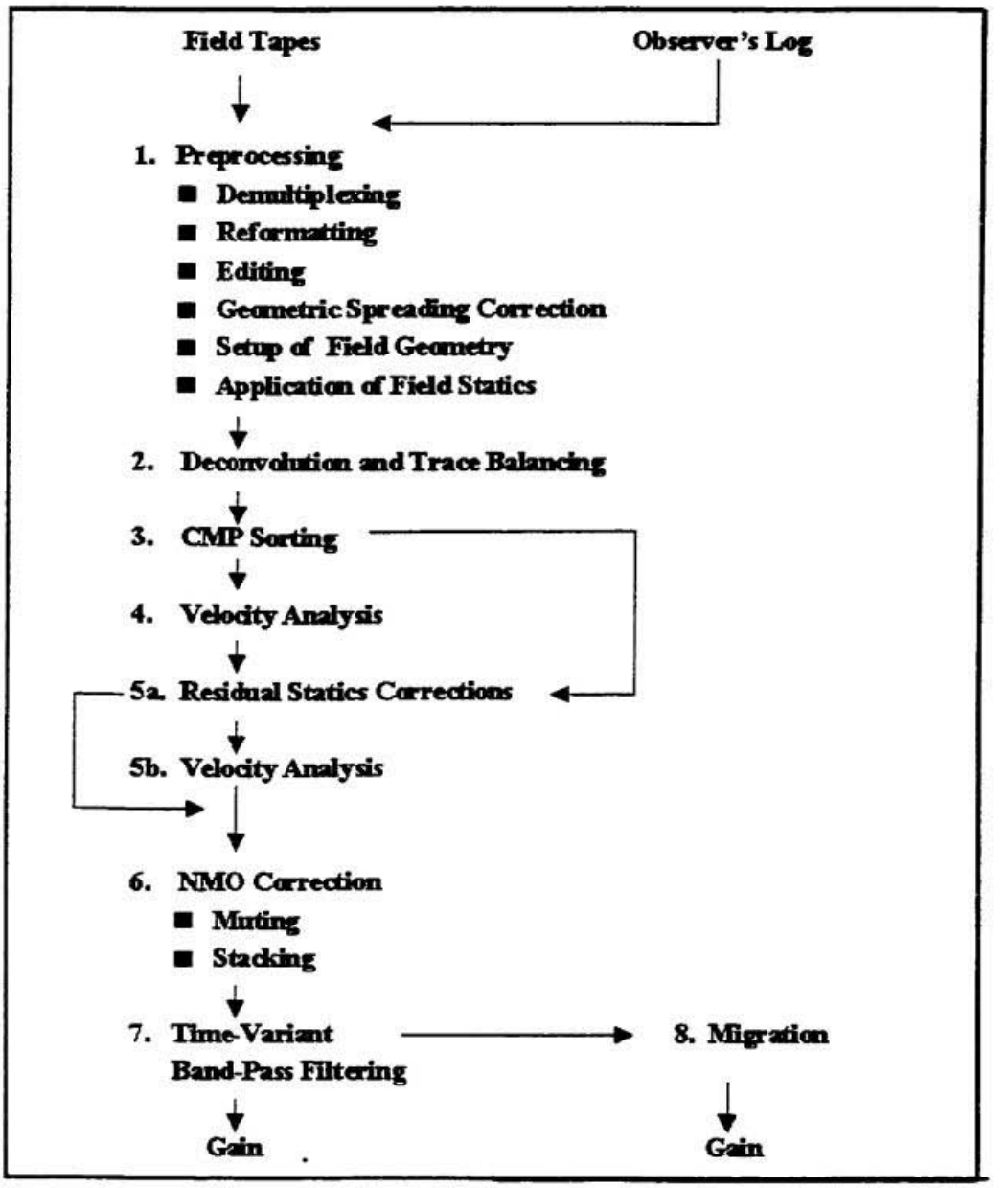

Figure 8 A typical data processing flowchart (After Yilmaz, 1987)

2.1.3.1. Preprocessing

Field data are recorded in a multiplexed mode using a certain type of format. Demultiplexing consists of separating the individual seismic channels, reassembling the series of samples corresponding to each geophone sequentially. Finally, the profile number, shot number and receiver number etc. are written into data as "headers".

A gain recovery function is applied to correct for the amplitude effects of wavefront divergence. Automatic Gain Control (AGC) can adjust the signal amplitude to an identical average value. An exponential gain function may be used to compensate for attenuation losses.

The most important step is field geometry setting, which, based on surveying information, stores coordinates of shot and receiver locations for all traces on trace headers. Many types of processing problems may arise from incorrectly setting up the field geometry. Elevation statics are also applied in this stage to correct travel times to a common datum level.

2.1.3.2. Deconvolution

Deconvolution is defined as a process convolving with an inverse filter. By compressing the effective source wavelet contained in the seismic trace to a spike, deconvolution extracts the reflectivity function from the seismic trace and thus improves the vertical resolution (Sheriff and Geldart, 1995). Because both high frequency noise and signal are boosted, the data often need filtering with a wide band-pass filter after deconvolution.

2.1.3.3. Remove Air-blast Noise and Ground Roll

Most seismic sources emit air-blast noise. Echoes from trees or other objects near the source generate air-blast and air-coupled waves, which are easily recorded. Air-coupled waves can cause enormous problems on shallow reflection data, particularly in the first 30ms of the record. Usually, the ground-coupled air wave arrives first, then the direct wave (Steeples and Miller, 1990).

Airwaves practically show a dominant frequency near that of the lower band edge of the low-cut filter (Steeples and Miller, 1998). Simple frequency filtering does little to attenuate the airwaves within the frequency range of reflection energy. Thus, trace muting, removal of part of traces, is preferred to remove airwaves. The air blast usually contains some frequency components between 200 to 500 Hz, so that spatial aliasing frequently occurs. Frequency-wave number filtering (f-k filtering) can be used to reduce air blast, but caution is necessary to avoid enhancing air-coupled waves and degrading reflection signals.

Ground roll, the surface wave, contributes lower frequency and high amplitude to contaminate reflections. It also needs to be removed to recover the reflection data.

2.1.3.4. CMP Sorting

CMP sorting is transforming all data from shot-receiver to midpoint-offset coordinates and grouping those traces with the same midpoint location together (Figure 7). The CMP technique uses redundant recording to improve the S/N ratio.

Given the total number of elements in the recording system N:

$$N = n_s \cdot n_g \cdot n_f \quad \text{..... (2.5)}$$

Where n_s is the sources per trace;

n_g is the receivers per traces;

n_f is the offset coverage of the same subsurface point.

The signal amplitude-to-rms noise ratio theoretically is improved by a factor of $N^{1/2}$. This improvement factor is based on the assumptions that the reflection signal on traces of a CMP gather is identical and the random noise is mutually uncorrelated from trace to trace (Yilmaz, 1987).

2.1.3.5. Velocity Analysis

In addition to improving the S/N ratio, multifold coverage with nonzero-offset recording yields velocity information about the subsurface. Velocity analysis is performed on selected CMP gathers, and the result is a table of numbers as a function of velocity versus two-way zero-offset travel time. These numbers represent some measure of signal coherency along the hyperbolic trajectories, governed by velocity, offset and travel time.

These velocity functions are spatially interpolated between the analysis points across the entire profile, so that each CMP gather is supplied a velocity function. In areas with complex structure, the velocity spectrum often fails to provide accurate velocity picking. Under this circumstance, the data are stacked with a range of constant velocities.

2.1.3.6. Normal Moveout (NMO) and Stacking

NMO-correction is applied to the data in order to yield zero-offset recordings. NMO correction depends only on time, offset and RMS (Root Mean Square) velocity. The arrival time of a seismic reflection event as a function of offset can be approximated by a

hyperbola. Figure 9 shows a hyperbolic curve obtained for each reflector. Curve t(x)is the time/distance curve, and the time variation with respect to its ordinate at the origin is the normal moveout (NMO).

$$\Delta t = t - t_n \cong \frac{x^2}{\bar{v}_n^{\,2}} \frac{1}{t + t_n} \qquad \text{.....(2.6)}$$

Δt is the NMO correction, which is applied to t makes the time/distance curve horizontal (Figure 9b). After NMO correction, the offset effect has been removed from traveltimes; however, NMO correction stretches the traces in a time-varying manner, and shifts their frequency content toward the low end of the spectrum. Also, frequency distortion increases at shallow times and large offset. To prevent the degradation, the stretch zone should be deleted (muted) before stack.

Finally, a CMP stack is obtained by summing those traces over offset. The stacked traces can now be presented in their correct position, each at the position of their common reflection point to create a seismic section.

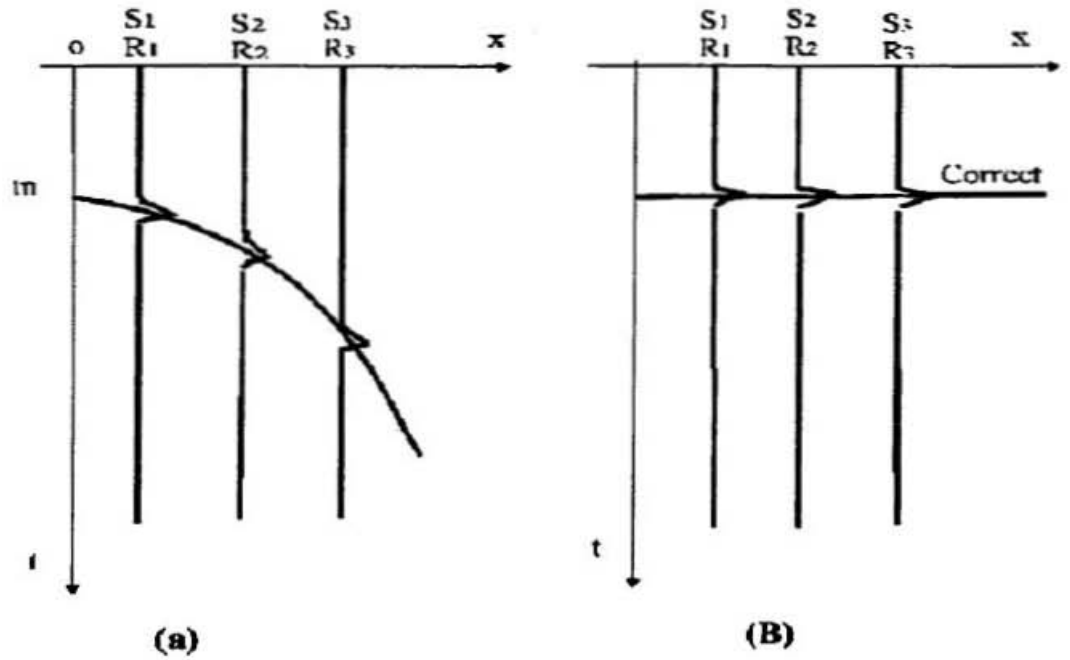

Figure 9 CMP display (a) before and (b) after NMO correction

2.1.3.7. Mute Refraction Arrival

Refracted arrivals should be muted from the data section during the early stage of processing; however, separating shallow reflection from shallow refraction is a potential pitfall. Because reflected energy near the surface tends to contain frequency components close to that of the early refracted arrivals on field files, it is difficult to separate them by means of frequency filtering. Furthermore, because of their similar phase velocities, wide-angle shallow reflection and shallow refraction may interfere with each other over a large offset range. Consequently, f-k filtering is ineffective to separate the shallow reflections from shallow refractions.

Even so, two indicators (Steeples and Miller, 1990) are useful for distinguishing them. One is frequency inversion with depth. Under normal geological conditions, the frequency of the reflections will decrease with depth because of attenuation with increasing travelpath length. If the apparent frequency of the coherent events changes from low at short reflection times to high at longer times, it may be a sign of a shallow refraction event. The other distinguishing feature is NMO correction. A reflection-time display will be transformed from a hyperbola to a straight line during NMO, and typically 20-30% of the high frequencies will be lost by NMO stretch (Miller, 1992). Refractions are also stretched by a similar amount, but their linear arrivals at near offset do not respond in-phase to hyperbolic time-distance moveout. Thus, in CMP stacking, refractions don't stack as coherently as reflections, and the misalignment of individual wavelets present may decrease their dominance in a stacked section.

2.2. Factors Controlling Seismic Resolution

The resolution of seismic data is the ability to tell that more than one feature is contributing to an observed effect (Sheriff, 1985), which is defined by the smallest features that can be observed in both the vertical and horizontal directions. Vertical resolution concerns the ability to distinguish that more than one reflecting interface is contributing to an observed reflection, while the horizontal resolution concerns the ability to distinguish features that are displaced horizontally with respect to each other.

Seismic resolution is controlled by many related factors, including frequency bandwidth and velocities of seismic wave, the size of Fresnel zone, the spatial sampling and survey depth. Each of these will be discussed below.

2.2.1. Waveshape and Frequency

For vertical resolution, the "resolvable limit" is defined to quantify whether two reflectors are resolvable or not. The most common definitions of resolvable limit are from Rayleigh (Jenkins and White, 1957) and Widess (1973). Rayleigh's definition is a quarter of the dominant wavelength $\lambda/4$ and Widess' is $\lambda/8$. Other definitions generally fall within this range. Thus, the wavelength, thereby the wavelet shape, affects the resolvable limit greatly.

According to Fourier synthesis, a seismic wavelet can be thought of as resulting from the superposition of many harmonic waves of different frequencies and amplitudes. Cosine waves with zero phase shift will have maximum constructive interference at t=0, thus,

producing the maximum possible amplitude there. At other certain time, the wave will add up to give smaller peak amplitudes. However, the broader the band of frequencies included, the farther one has to go from t=0 for these to achieve appreciable constructive interference. Higher frequency components in the bandwidth are necessary to produce a sharp peak. Therefore, the desired waveshape is best achieved with a sharp and narrow zero-phase wavelet with minimal sidelobes to interfere with other events.

Figure 10 is an example to illustrate the effect of a wedge (Sheriff and Geldart, 1995). Figure 10b shows a reflection from single interface (upper reflection) and the wedge which velocity is intermediate between that above and below it ($V_3>V_2>V_1$ or $V_3<V_2<V_1$). The waveshape clearly indicates more than one reflector when the wedge thickness exceeds $\lambda/4$ (12ms). Figure 10c shows the wedge with a velocity different from that of the surrounding material ($V_1=V_3\neq V_2$), The waveshape is nearly constant below a thickness of $\lambda/4$, where the amplitude is at the maximum because of constructive in interference. For wedge thickness less than $\lambda/4$, the waveshape is the derivative of that for a single interface.

Berkhout (1984) introduced the length L_t of the wavelet as a measure for its resolving power. To achieve this, the relative second-order moment of the time wavelet w(t) is used.

$$L_t^2 = \frac{\int (t-t_0)^2 w^2(t)\,dt}{\int w^2(t)\,dt} \qquad \text{.....(2.7)}$$

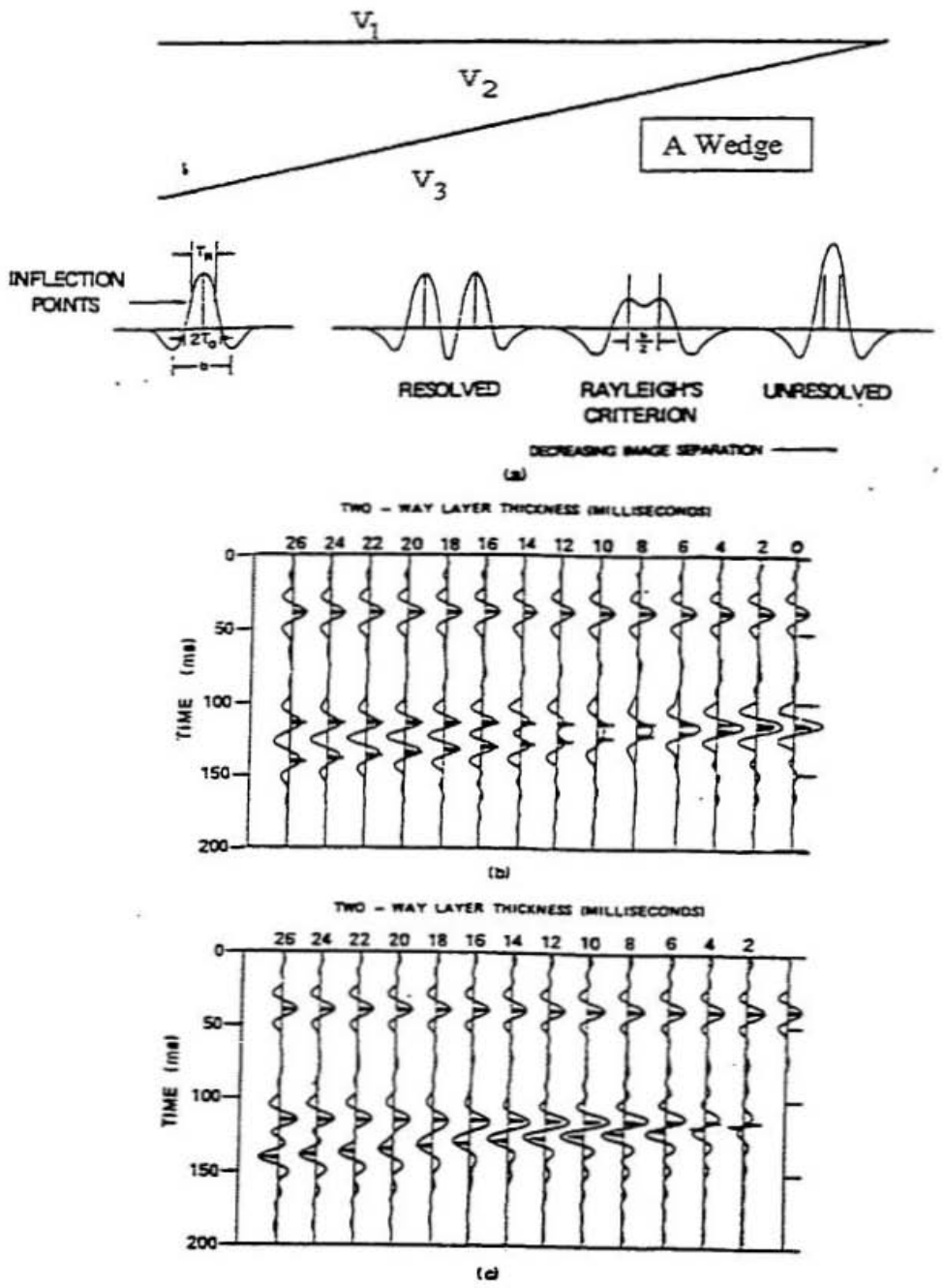

Figure 10 Reflections illustrating vertical resolution. (after Sheriff and Geldart, 1995)

Where t_0 is the center of the wavelet:

$$t_0 = \frac{\int t \; w^2(t)\, dt}{\int w^2(t)\, dt} \quad \text{..... (2.8)}$$

Evaluation of L_t in the frequency domain results in:

$$L_t^2 = \frac{1}{4\pi^2} \frac{\int |W(f)|^2 \left[\left(\frac{d \ln |W(f)|}{df} \right)^2 + \frac{d(\phi(f) + 2\pi f t_0)}{df} \right] df}{\int |W(f)|^2 df} \quad \text{... (2.9)}$$

Where W(f) and ϕ(f) are the amplitude and phase spectrum of the wavelet w(t).

From equation (2.9), it is clear that a band limited wavelet W(f) requires smoothing at the lower and upper frequency limits. Without smoothing the steep amplitude changes in the frequency domain result in an inferior wavelet. Berkout (1984) also defined a window function as

$$W(f) = \left(\cos \left(\pi \frac{f - f_c}{2\Delta f} \right) \right)^{\gamma} \quad \text{..... (2.10)}$$

$$f_c = \frac{f_{max} + f_{min}}{2} \qquad \Delta f = \frac{f_{max} - f_{min}}{2}$$

The exponent γ (≥ 0) is a smoothing parameter that controls the trade-off width of the main lobe and the side-lobe attenuation. Large γ results in a low side-lobe level and a small γ results in a small width of the main lobe. From the above equation, a high frequency can sharpen and narrow the waveshape thereby achieving higher resolution.

2.2.2. Fresnel Zone

The horizontal resolution is often quantified by the size of the first Fresnel zone. According to Huygens' principle, all points on a wave front are sources of secondary wave fronts; the reflection energy observed at a geophone position does not come from a single reflection point but a fairly large zone that contains all reflection points. This zone is termed the Fresnel zone (Figure 11), from which the two-way path length from source to receiver is at most $\lambda/4$ longer than the "nominal path length". The intensity scattered from points in the first Fresnel zone arrives less than half quarter period after the "nominal" arrival, and thus the energy interferes more or less constructively. In Figure 11(b), S is a source and a coincident detector. SP_0 is perpendicular to a reflecting plane, and R_1, R_2 are such that the distance SP_0, SP_1 and SP_2 differ by $\lambda/4$. Generally, $h_n >> R_n >> \lambda$.

The shape and size of the Fresnel zone depends on the position of source and receiver, the velocity contribution, wave length, and depth, dip, and curvature of the reflector. The magnitude of the Fresnel zone can be as indicated in Figure 11a. In the Fresnel zone, the area effectively contributing to a reflection is fairly large. The outer parts do not contribute as much as the inner parts. Sometimes an "effective" Fresnel zone is used,

which is half the radius of the Fresnel zone defined above. Figure 11c shows how high frequency decreases the size of Fresnel zone.

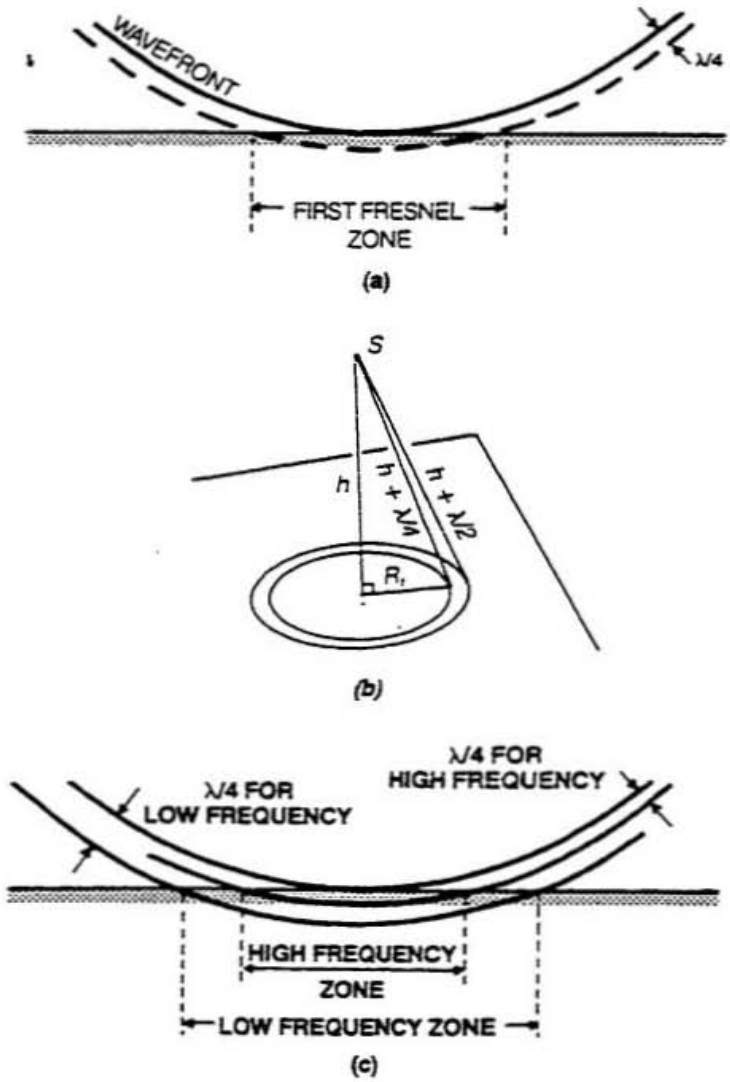

Figure 11 The Fresnel zone. (a) Determining the diameter of the first Fresnel zone for coincident source and detector. (b) Showing the second Fresnel zone. (c) Fresnel zone size depends on frequency or wavelength. (after Sheriff, 1985)

For the simplest case with source and receiver coincident (zero offset), homogeneous medium, and a plane horizontal reflector at depth z, the Fresnel zone is a circular disc with the radius r_F, as indicated in Figure 12,

$$z^2 + r_F^2 = \left(z + \frac{\lambda}{8}\right)^2 \Leftrightarrow r_F^2 = \frac{z\lambda}{4} + \frac{\lambda^2}{64}$$

$$r_F = \frac{1}{2}\sqrt{z\lambda} \qquad \text{..... (2.11)}$$

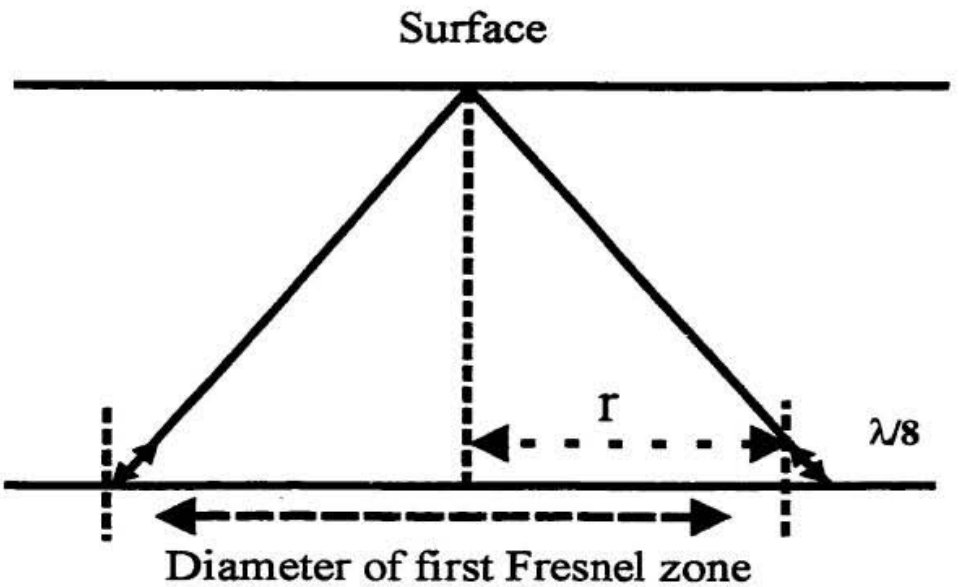

Figure 12 Fresnel zone for zero-offset acquisition geometry

2.2.3. Spatial Aliasing

Spatial aliasing occurs when data are not sampled frequently enough in space. Similar to the Nyquist frequency in time sampling, the Nyquist wave number, $k_N/2\pi$, is used in spatial sampling (Sheriff and Geldart, 1995).

$$k_N/2\pi = 1/\lambda_N = 1/2\Delta x \quad \text{..... (2.12)}$$

Δx is the geophone spacing and λ_N is the minimum wavelength detected without spatial aliasing.

Equation (2.12) indicates that signals should be sampled at least twice per wavelength to avoid spatial aliasing, or, in other words, aliasing occurs when the wavelength λ of energy is smaller than λ_N. For a survey with geophone spacing of 3 m, for example, the minimum wavelength λ_N is 6m. If λ is smaller than 6 m, then aliasing will occur.

Equation (2.12) also indicates the aliasing is mainly controlled by offset, geophone spacing and spatial sampling. The offset of the closest receiver determines the first common depth point position in the subsurface, so a different offset design could affect which point in the subsurface is being imaged. Because the smaller common depth point spacing can separate two closer features and hence guarantee high horizontal resolution, common depth point spacing, the distance between two nearest reflection points, is an important factor to distinguish two features displaced horizontally. The common depth point spacing is exactly half of the geophone spacing. Therefore, decreasing the

geophone spacing can shorten the common depth point spacing thereby increasing the horizontal resolution.

Among the three factors, spatial sampling is the most important for controlling the seismic resolution. A seismic signal is a continuous time function. In digital recording, the continuous seismic signal is sampled at a fixed rate in time (sampling rate or sampling interval). In order to reconstruct the seismic signal more exactly, a smaller sampling interval is required. If the sampling interval is not small enough, some details corresponding to the high frequency component will lost. Generally, the highest frequency that can be restored is $1/(2\Delta t)$, the Nyquist frequency.

If the signal is digitized at a coarser sampling rate, the amplitude spectrum would change, and those frequencies above Nyquist are folded back into the amplitude spectrum of the digital version of the signal. The discrete time series derived from undersampling of a continuous signal actually contains the contribution from high frequency components, but it appears as lower frequencies. This phenomenon is aliasing. The aliased frequency f_a can be calculated by means of $f_a=|2mf_n-f_s|$, where f_n is the folding frequency, f_s is the signal frequency, and m is an integer such that $f_a>f_n$.

Undersampling has two effects: (1) bandlimiting the spectrum of the continuous signal, with the maximum frequency being the Nyquist, and (2) contamination of the digital signal spectrum by high frequencies beyond the Nyquist, which may have been present in the continuous signal. Nothing can be done about the first problem. To keep the recoverable frequency band from zero to the Nyquist frequency free from aliased

frequencies, a high-cut anti-aliasing filter is needed in the field before analog-to-digital conversion. This filter can eliminate those frequency components that would be aliased during sampling. Typically, the high-cut anti-aliasing filter has a cutoff frequency that is either ¾ or ½ of the Nyquist frequency. This filter rolls off steeply so that the frequencies above Nyquist are highly attenuated.

To help to avoid spatial aliasing, Steeples and Miller (1998) put forward a few strategies:

(1) Moving the shotpoint one-half geophone interval closer or further away from the geophone spread will have essentially no effect on the appearance of the reflector, but will usually have a substantial effect on spatial aliasing of ground roll.

(2) Reducing the geophone interval by a factor of two or three will improve the coherency of a true reflector, and destroy the coherency of spatial aliased ground roll.

(3) Geologic or geophysical information from a site, if available, can help determine when the reflector is on the record and what its normal moveout should be.

(4) Energy reflected from shallow layers tends to have a frequency content close to that of the direct wave and the early refracted arrivals. When the observed reflected frequencies are considerably lower than those of the first arrivals, the recorded events are likely to be caused by ground roll rather than by reflectors.

2.2.4. Time-to-Depth Conversion

In data processing, after NMO correction and stacking, the final seismic section is presented as a time section. A time section may suffice to provide a general view of

subsurface structure, and it may not be warranted to develop a depth section. However, in the shallow subsurface, the velocities often vary with depth and may vary laterally, hence, the time section is not enough to deduce the correct nature of reflectors and may even result in an incorrect interpretation. In this situation, depth sections are always necessary for interpretation. To achieve this time-to-depth conversion, detailed knowledge of velocity values is required both vertically and along the seismic line.

As an example, Figure 13 illustrates the value of depth sections compared to time sections. Figure 13(a) is a schematic of several traces with well-defined reflection arrivals. It appears that the upper unit thickens to the right because the first reflection arrives progressively later from left to right. In the same manner, the second unit appears to thin to the right and third one appears significantly deeper to the right. In fact, unit boundaries are horizontal and unit thicknesses are constant across the entire section (Figure 13(b)). The reason for the displacement of the reflections in time from left to right on the time section is a variation in the velocities of the upper two units. Thus, a depth section is important in shallow reflections for high quality interpretation.

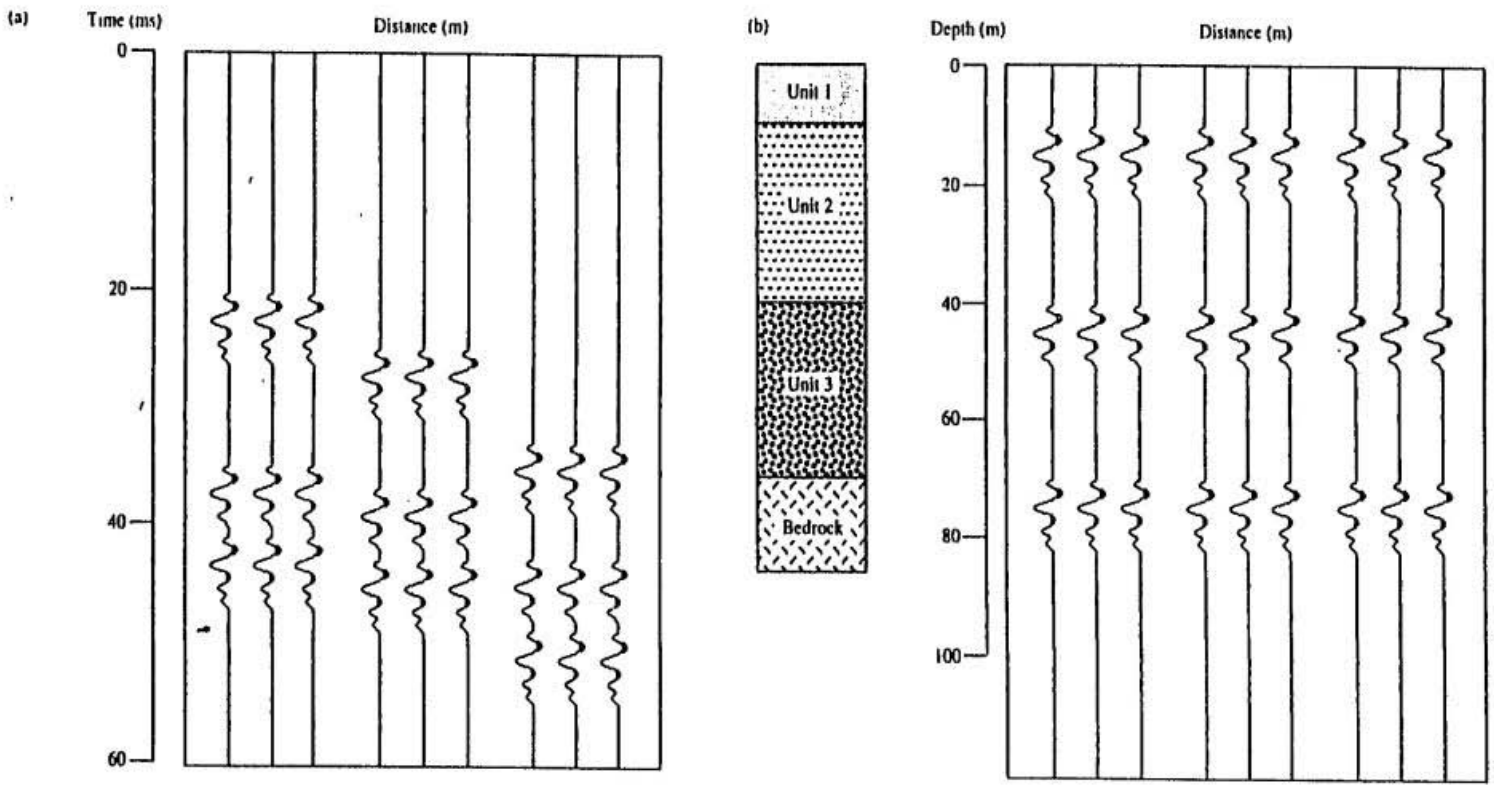

Figure 13 Time versus depth sections. (a) time section and (b) depth section (after Burger, 1992)

2.3. The Approaches to High Resolution

This research will investigate means to achieve high seismic resolution by the following approaches:

(1) Selecting a proper seismic energy source. Because little can be done about the velocity, the effort will focus on increasing seismic wave frequency so as to increase seismic resolution;

(2) In data acquisition, proper offset and geophone spacing will be considered carefully to avoid spatial aliasing; and

(3) By careful data processing, this research will finally develop stacked sections to preserve reflection information for high quality interpretation.

Chapter 3. Data Acquisition and Processing Techniques

The acquisition of seismic data always follows the same sequence: generation of a seismic signal by a source, propagation of signal through the subsurface, and conversion of the ground motion into an electric voltage by receivers. The prerequisite to all seismic surveying is the careful selection of acquisition parameters. The acquisition settings can affect the data quality greatly. In a high-resolution survey, it is essential to preserve high frequencies to image shallow reflections. The frequency content is controlled by the design parameters of the source and the receivers, as well as how they are deployed in the field (Brouwer and Helbig, 1998). The first part of this chapter will discuss in detail the acquisition parameters for this research.

Once high quality data have been collected, it is essential to process the data so that the high resolution character is maintained. For Vibroseis data, the processing is somewhat different from conventional processing. The processing of conventional impulse source data assumes the source is an approximation to a unit impulse. Vibroseis data must be transformed through processing from its inherent swept frequency form to that for an impulse function. The second part of this chapter deals with the special problems of transforming the high resolution data collected for this research

3.1. Data Acquisition

To compare the relative resolving power of different sources, three field tests were carried out in 1999 near St. John's, Newfoundland.

3.1.1. Location and Line Geometry

A preliminary field test (test 1) was held in September 1999 at an open site on the campus of Memorial University of Newfoundland. This test collected the data from a hammer source and was primarily used to check the instruments. The spread contains 25 single geophones at an interval 5m.

In October, the other two different tests were carried out at a site approximately 70 km north of St. John's. These two tests were mainly for collecting data from SIST vibrator sources and, for the sake of comparison, from an explosive source (shotgun). The spread was set along a straight section of a seldom-used road (Figure 14). The first test spread (test 2), consisting of 170 stations, was laid out on the shoulder of the road. Each successive eight stations were connected to a RAM II Module and then by digital telemetry to the ARAM 24 recorder. The second test (test 3) used the first 120 stations of test 2 except the geophones were moved perpendicular to the line into a ditch alongside the shoulder of the road. It was hoped that better coupling would occur away from the gravel of the shoulder.

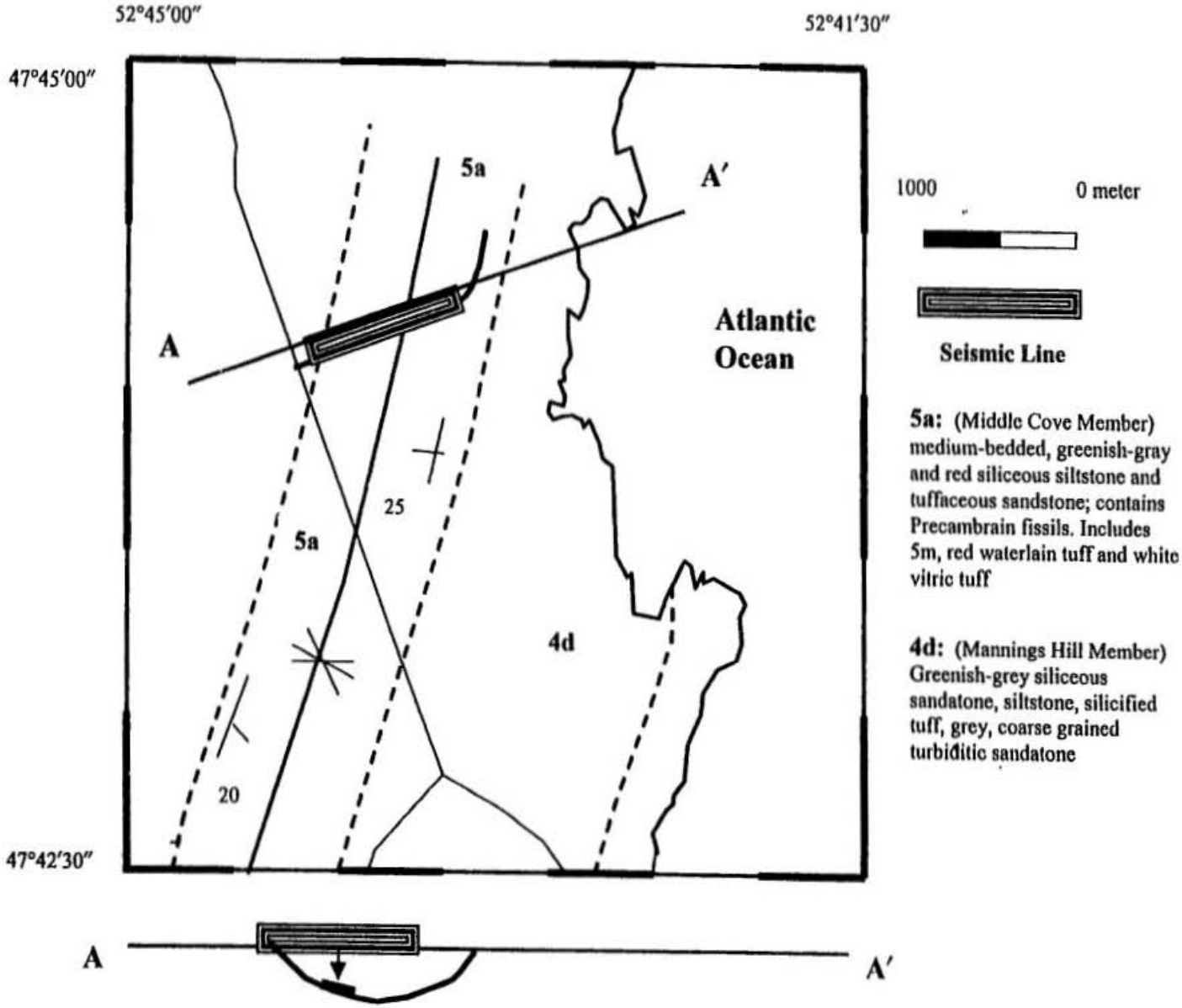

Figure 14 The location of test 2 and test 3

To try to avoid spatial aliasing, the geophone spacing for both test 2 and test 3 was cut to 3 m. In order to reduce the random noise, data were acquired for at least two sweeps at the same shotpoint.

The campus site (test 1) and the shoulder of the road (test 2) both have surface gravel, while in the ditch, the geophones were planted in fairly soft soil, which may result in a lower frequency spectral content. There are no documented previous surveys at either site; thus geological information is limited to regional geological mapping (see chapter 5).

3.1.2. Seismic Sources

The source selection is of critical importance in a high resolution seismic survey. The characteristic of an ideal energy source is that, first and foremost, it must impart sufficient energy to provide reflections and refractions. The amplitudes must be sufficient to be detected and displayed reasonably well for interpretative purposes. Thus, not only the total amount of energy imparted but also the shape of waveform and its spectral content affect the seismic resolution.

The emphasis of this research is on near-surface seismic studies, and the particular focus is on comparing impulsive and vibratory sources. Two SIST vibrators and a hammer source are used in this research. All of them are portable, repeatable, and capable of achieving high frequencies. For comparative purposes, a shotgun was also employed for data acquisition.

3.1.2.1. Hammer Blow

A hammer blow can be regarded as an accelerated weight drop, in which the operator provides the acceleration. Due to the limit of energy imparted, a hammer source is usually used for very shallow investigations. Under good conditions, a hammer source can detect an interface at a depth of 50 m (Burger, 1992).

A 4-kg hammer was used in this research. In order to effectively transfer the energy to the ground, the hammer was repeatedly struck against a base plate on the ground. The recording time was as long as 21 seconds, during which about 10 hammer blows were recorded. The long time recording enhanced the waveforms by allowing summing for a number of hammer impacts. Figure 15(a) illustrates 15s raw data.

3.1.2.2. Mini Vibrator

Two hand-held electric demolition hammers (large and small vibrators), (VIBROMETRIC, OY), were used as the main vibrator sources in this research. The small one was used for part of the shots in test 2, while the large one was used for the rest of the shots in test 2 and throughout test 3.

The large vibrator is a BOSCH Model GS9. It has a nominal power of 1800W and an energy of 50J/impact at 30 impacts/second. In this research, the impact rate is from 10 to 25 impacts per second. The energy per impact at lower impact rates is about 2/3 of the nominal value.

The small vibrator is a 1.5KW hammer that delivers 20 J per impact, at a mean impact rate of 25/second. The signal frequency extends well beyond 1 KHz.

With the SIST vibrator source, the amplitude of the pulse does not depend on the input voltage and the impact frequency varies linearly with the voltage. By adjusting the voltage as a function of time, these characteristics make the electromechanical source computer-controllable, so that various impact frequency codes can be generated.

The specific technique used in this research is the Swept Impact Seismic Technique (SIST). SIST combines the Vibroseis swept-frequency and the mini-Sosie multi-impact concepts. With SIST, a low power impact source generates a series of seismic impulses, which is similar in concept to Mini-Sosie (Barbier, 1982). Figure 15b illustrates some of the raw data from SIST. However, rather than a pseudo random coding of the impact rate, a deterministic, monotonously varying rate (i.e. a swept impact rate) is used. In this sense, SIST is similar to Vibroseis. Compared to Vibroseis, a compliant coupling to the rock or ground is not as critical in SIST. Considering the fact that a compliant contact over a wide band is difficult to achieve in all conditions because of the diversity of the experimental conditions encountered in a small-scale survey, SIST has a clear advantage (Cosma et al., 1998).

Cosma has applied SIST in many areas and his research indicates that SIST could be a viable solution for high-resolution, shallow seismic surveying both methodologically and logistically (Cosma et al., 1998, Cosma & Enescu, 1999). SIST is portable, easy to operate, and does not have any adverse environmental impact.

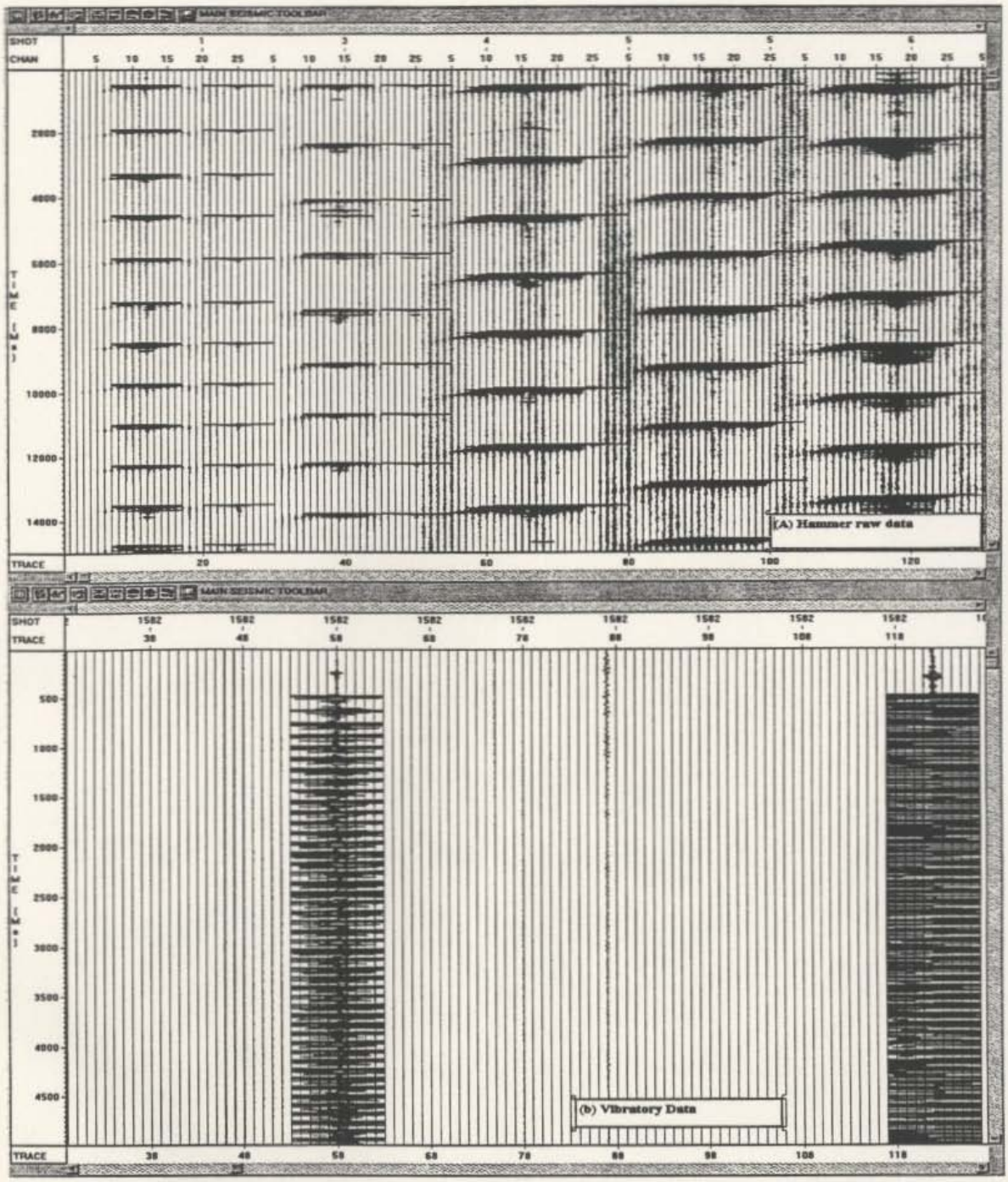

Figure 15 Raw data from (a) a hammer and (b) a vibrator source

3.1.2.3. Shotgun

Explosives were the sole energy sources used in seismic exploration until the weight drop was introduced in the 1950's (Sheriff and Geldart, 1995). Explosives can produce both high energy and high frequency in a burst because the high energy results from the high speed of the detonation, rather than from the slow movement of a large mass. However, explosives are not environmentally friendly and easy to use. Furthermore, due to their destructive nature, they can introduce unpredictable nonlinear effects in the vicinity of the source that tend to degrade the frequency spectrum. Explosives are not the emphasis of this research. However, for comparison with the hammer and the vibrator sources, a 12-gauge shotgun, one kind of explosive source, was applied in test 2 and test 3. Figure 16 shows some raw data from the shotgun source.

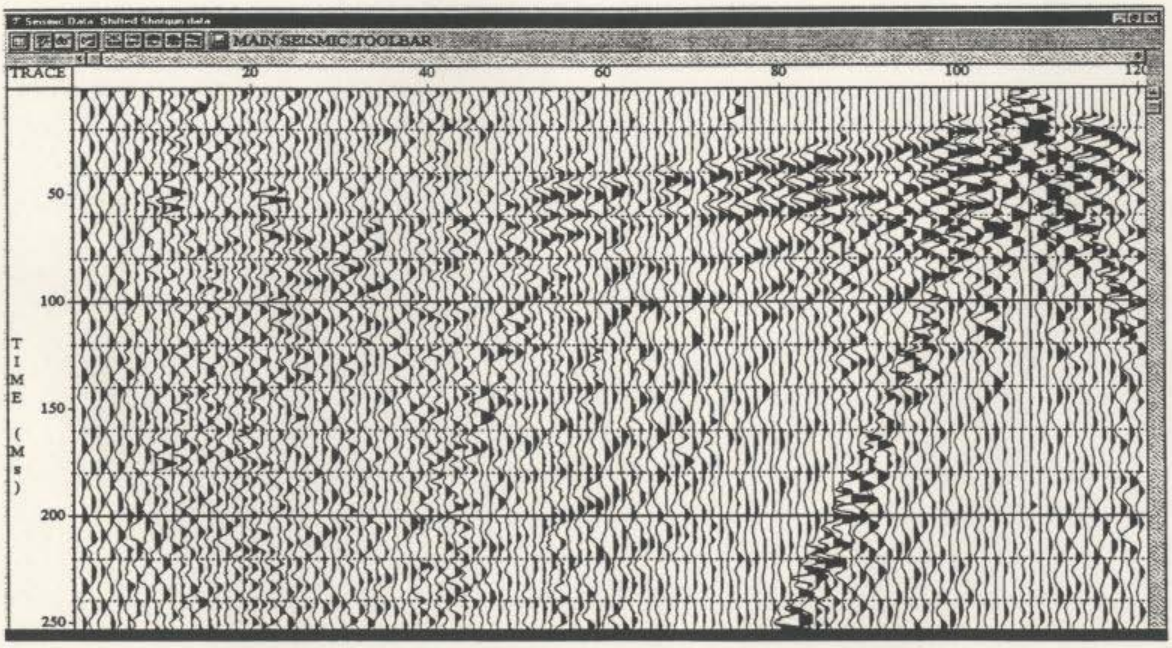

Figure 16 Raw data from 12-gauge shotgun energy source

3.1.3. Recording System

Mark Products L-40 high resolution geophones are employed. The geophone's natural frequency range is 30-40 Hz. As the natural frequency is at least 10 percent of the highest frequency likely to be recorded, the L-40 can record seismic energy with frequencies up to 400 Hz. The open circuit damping is 22.2/f, which decreases ringing in the data and flattens the resonance peak in the spectrum.

The recording system is a Geo-X Systems Ltd. ARAM24 seismic acquisition system, which is used for both the single shot energy source (dynamite and hammer) and the multishot and vibrator energy source. Figure 17 shows schematically the complete acquisition system.

A personal computer (PC) generates the pilot signal, which is then amplified by a power amplifier and fed to the vibrator. One geophone is set near the vibrator plate to record the pilot trace, which is used for cross-correlation of the raw geophone traces. The recording times are 21 s, 29 s and 15 s respectively for the three tests, with the sample rate set at 0.5 ms. The Low-cut filter setting is 3 Hz while the high-cut is 656 Hz. The receiver offsets ranged from 1.5 m for the nearest geophone to 500 m for the longest.

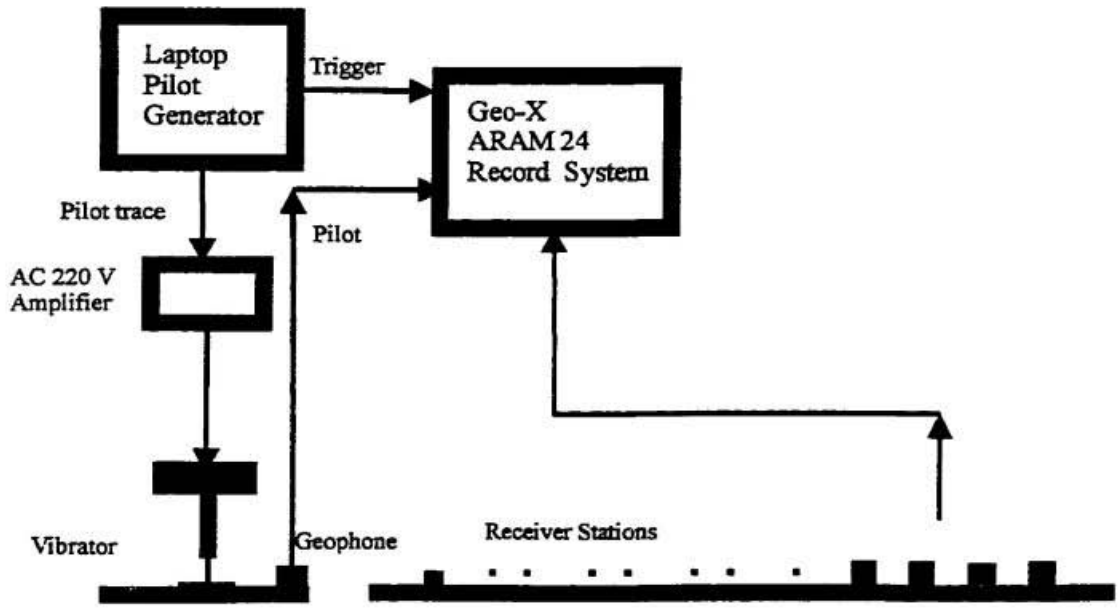

Figure 17 Portable vibrator recording system

3.2. Specific Processing Techniques

The purpose of data processing is to improve the reflection signal/noise ratio and geometrically arrange the seismic reflection information, in such a way that geological information can be easily extracted. Data processing is another important factor affecting seismic resolution in a shallow survey; poor processing can degrade resolution. The processing of shallow high resolution data can best be described in relation to standard seismic processing with some specific considerations.

For the data from the shotgun energy source, the processing procedure discussed in section 2.1.3 is applied. For the data from hammer and vibrator sources, the same seismic processing is still an appropriate approach after crosscorrelating the data. However, some pitfalls and differences must be considered cautiously, which are highlighted below.

In order to compare data from all the tests, it is important to use the same procedures and processing parameters on all data.

3.2.1. Processing Software

The VISTA for Windows™ 2D/3D seismic data processing software was employed throughout this research.

3.2.2. Basic Principles of the Vibroseis Method

Because SIST is a combination of Vibroseis swept-frequency and Mini-Sosie multi-impact ideas, the processing procedure for Vibroseis is applicable.

The Earth response h(t) is theoretically an impulse response to primary reflectors only. When a pilot signal s(t) is transmitted into the earth, it is convolved with the earth response to form the geophone input. Neglecting the geophone response itself this can be thought of as the geophone output, y(t).

$$y(t) = h(t)*s(t) \quad \text{.....(3.1)}$$

For a discrete series, convolution is defined as:

$$x(t) * y(t) = \sum_k x(k)y(t-k) = \sum_k x(t-k)y(k) \quad \text{..... (3.2)}$$

Equation (3.2) indicates that the convolution is commutative, therefore

$$x(t)*y(t) = y(t)*x(t)$$

and $[x(t)*y(t)]*z(t) = x(t)*[y(t)*z(t)]$

However, in our case, the pilot signal s(t) lasts much longer than the time interval between reflectors. Thus, individual reflectors cannot be distinguished in the output. In order to "compress" the signal into a relatively narrow wavelet or pulse to distinguish reflectors clearly, the cross-correlation procedure needs to be applied.

$$r(t) = s(t) \oplus y(t) \quad \text{.....(3.3)}$$

The cross-correlation function is a measure of the similarity between two data sets and is expressed as

$$\Phi_{xy}(\tau) = \Sigma\, x_k y_{k+\tau} = \Sigma\, y_k x_{-(\tau-k)}$$

so $\Phi_{xy}(\tau) = \Phi_{yx}(-\tau)$

$$= y_\tau * x_{-\tau} = x_{-\tau} * y_\tau \quad \text{.....(3.4)}$$

Hence, the cross-correlation can be performed by reversing the first data set and convolving.

Now, by replacing y(t) in (3.3) by (3.1) and employing equation (3.4), the equation (3.3) can be rewritten as

$$r(t) = y(t)*s(-t) = [h(t)*s(t)]*s(-t) = h(t)*[s(t)*s(-t)]$$

$$= h(t)*a(t) \quad \text{.....(3.5)}$$

Where a(t) is the autocorrelation of the pilot signal s(t).

According to equation (3.5), the "normal" seismic record can be obtained by cross-correlating the pilot trace with the geophone output.

A key assumption is that the autocorrelation a(t) is a reasonable representation of a delta function, which equals to zero everywhere except at zero-lag. In practice, the degree of compliance with this condition will provide a means of evaluating the data quality.

Figure 18 shows a practical example of data from the SIST method. Figure 18(a) is the recorded data (geophone output). For a clearer view, only 6000 ms out of 29000 ms are displayed. No processing has been done on the data so that just the zero-offset trace and pilot trace (trace 122) have significant amplitude. A "Normal" seismic record (Figure 18(b)) is obtained by correlating the pilot trace with all the other traces. The

autocorrelation of the pilot trace (Figure 18(c)) shows that more than 90 percent of the energy is concentrated at zero-lag.

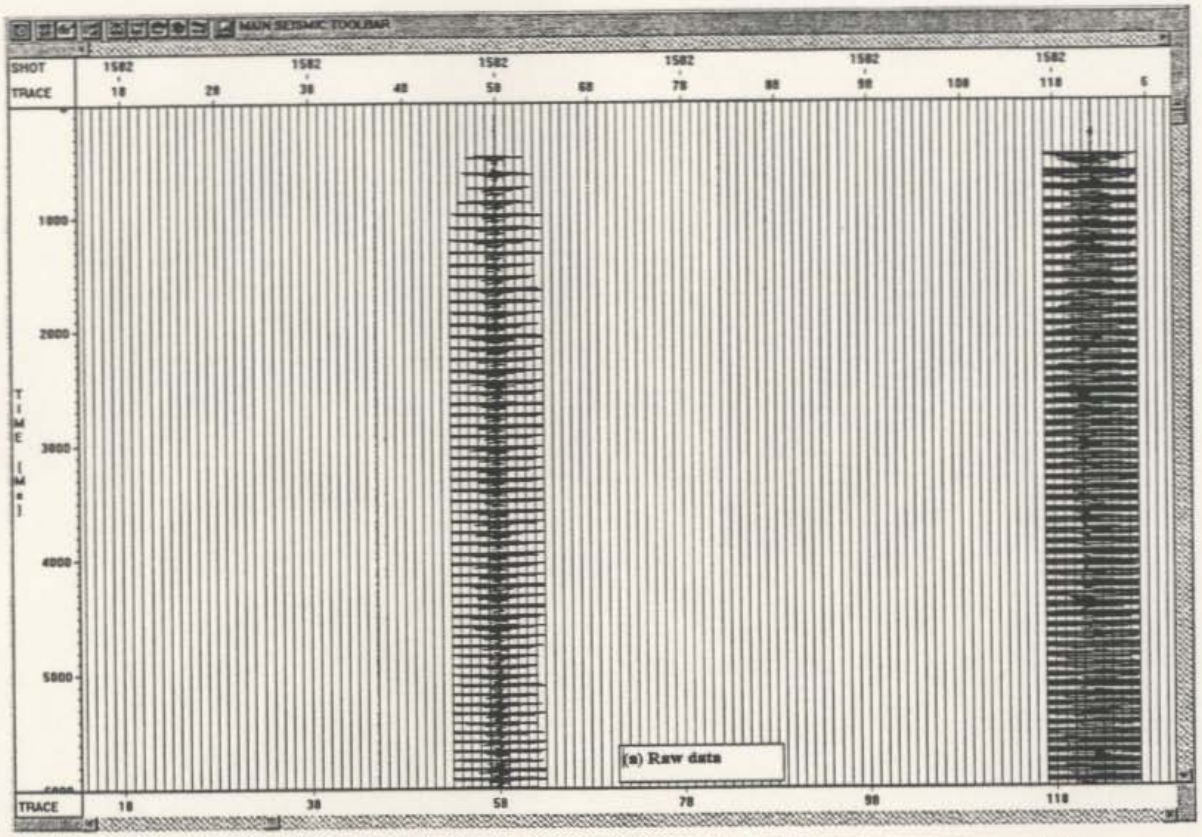

Figure 18 Practical vibrator data, (a)SIST recorded data, (b) correlated data, and (c) autocorrelation of pilot trace

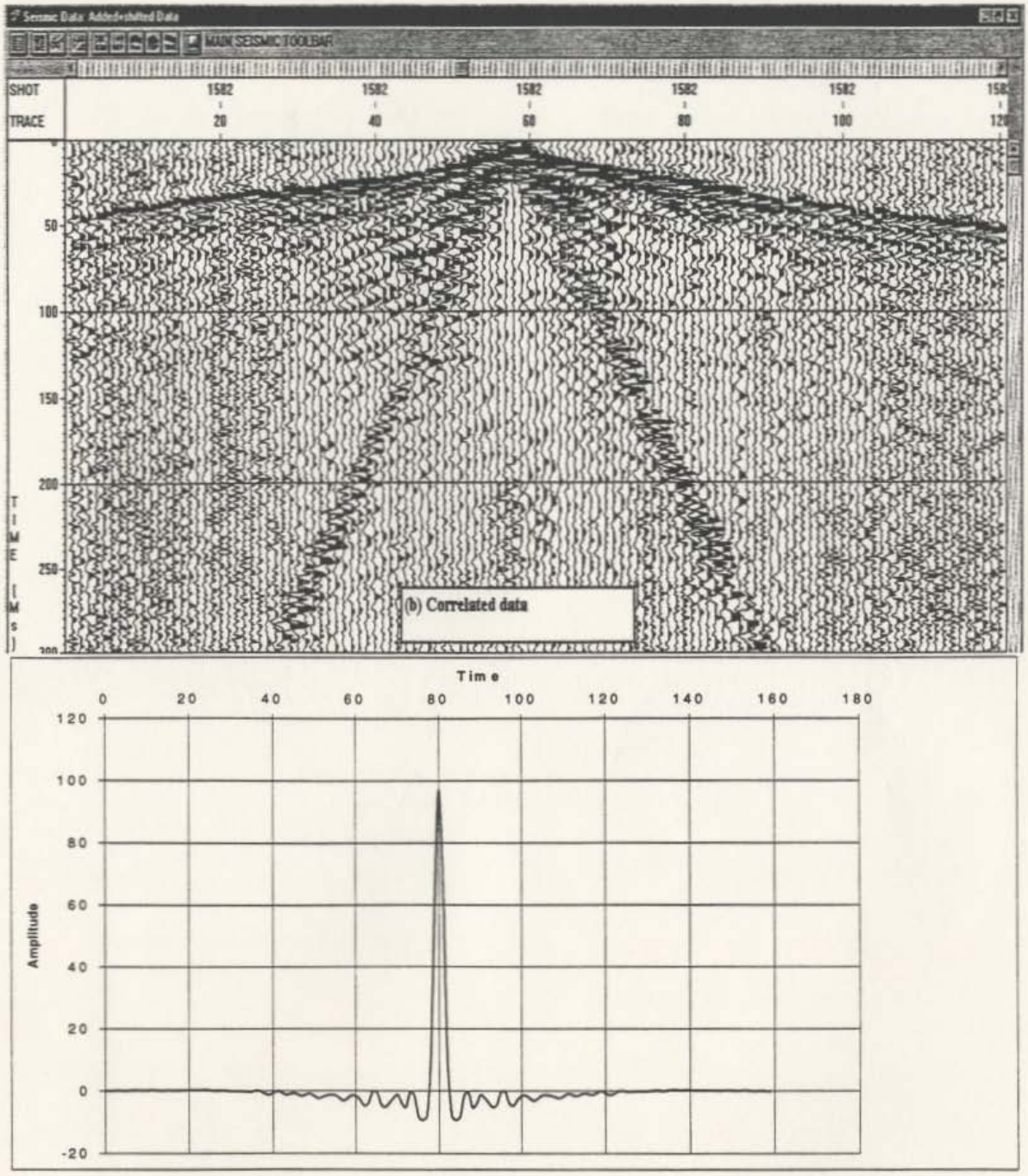

Figure 18 (continued) Practical vibrator data, (a)SIST recorded data, (b) correlated data, and (c) autocorrelation of pilot trace

3.2.3. The "Best" Pilot Trace

The pilot trace is used to correlate the geophone output data to obtain the "normal" seismogram; thus, the selection of the pilot trace greatly affects the quality of the correlated data. As illustrated in Figure 17, a series of impulse signals generated by the computer controller cause the vibrator to strike the base plate, thereby creating a base plate signal that is transmitted to the earth.

Sallas (1984) has presented a detailed discussion of the construction of the ground force signal, involving both the vibrator and the base plate (Figure 19). The equation governing the motion of the base plate is

$$-F_g = m_b \ddot{x}_b + m_r \ddot{x}_r \quad \cdots\cdots (3.6)$$

where m_b is the mass of the base plate

x_b is the base plate acceleration

m_r is the mass of the reaction mass

x_r is the reaction mass acceleration

Because it is closer to the actual signal propagating from the base plate into the earth, this ground force signal has been suggested many times as a preferred correlation signal (Baeten and Ziolkowaki 1990).

In the field work, one geophone was set near the vibrator to record the ground force signal (Figure 20). However, in test 3, the pilot trace from this geophone was clipped

making the correlation result of poor quality. Under this circumstance, as a replacement, the trace from the nearest offset receiver station (approximately 1 m away) was used for correlation. This trace is very similar to the base plate pilot trace and is an acceptable proxy. The quality of correlated data is satisfactory by correlating the near trace with the rest of the traces.

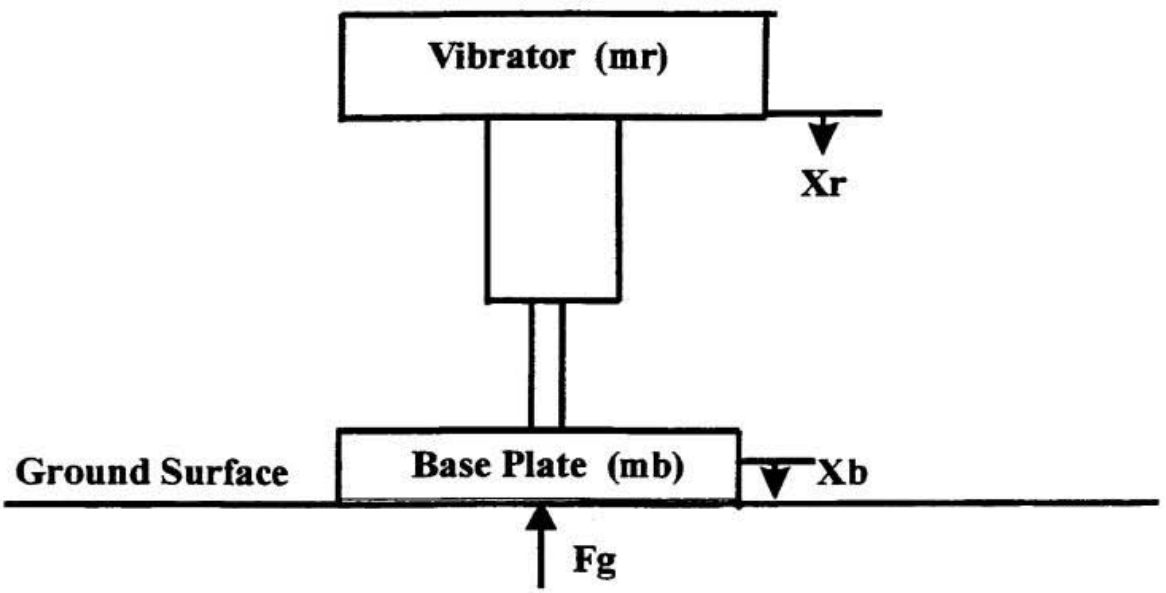

Figure 19 Mechanical model of the vibrator actuator

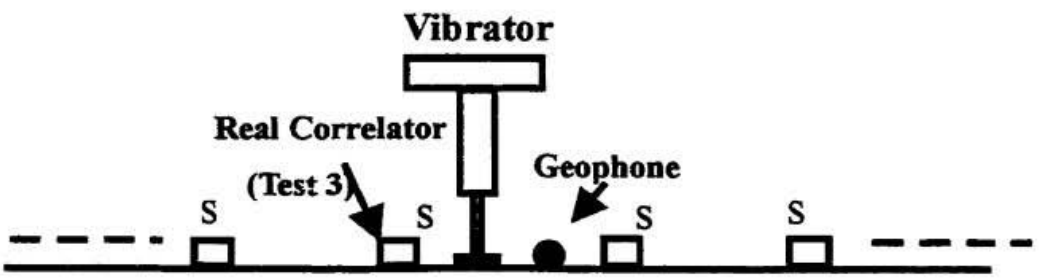

Figure 20 Pilot trace selection

3.2.4. Elimination of Ghost Noise

Generally, non-linear effects cause the actual base-plate signal that differs from the signal of the pilot signal. This difference results in harmonic distortion in most vibrator operations on land (Li, 1997). When the recorded ground force signal correlates the geophone output data, the correlogram resembles a shot seismogram, as well as containing the correlation ghost noise produced by severe harmonic distortions in the ground force signal both at negative and positive correlation times.

In order to eliminate the harmonic distortion and thereby eliminate ghost noise, numerous methods have been developed during the last thirty years. However, all existing methods used to reduce harmonic distortion have been with limited success, largely because they are difficult to implement and control (Martin and Bacon, 1993). Recently, Li et al. (1995) provided a new method known as the pure phase shift filter (PPSF), which can easily be implemented. Li (1997) put forward a deconvolution approach that uses deconvolution to process uncorrelated data to reduce the harmonic distortion.

In this research, the correlated data from the above methods still contain much ghost noise. To seek better results, Cosma (1999) suggested using deconvolution processing on the pilot trace before correlation. This procedure shortens and de-scrambles the transients. According to the Vibroseis theory, the Klauder wavelet with a narrow wave shape and a wide bandwidth ensures better-correlated data. Figure 21(a) shows the autocorrelation of a pilot trace, which is obviously not an ideal Klauder wavelet. The data correlated with the pilot trace presents poor quality with much noise (Figure 21(c)).

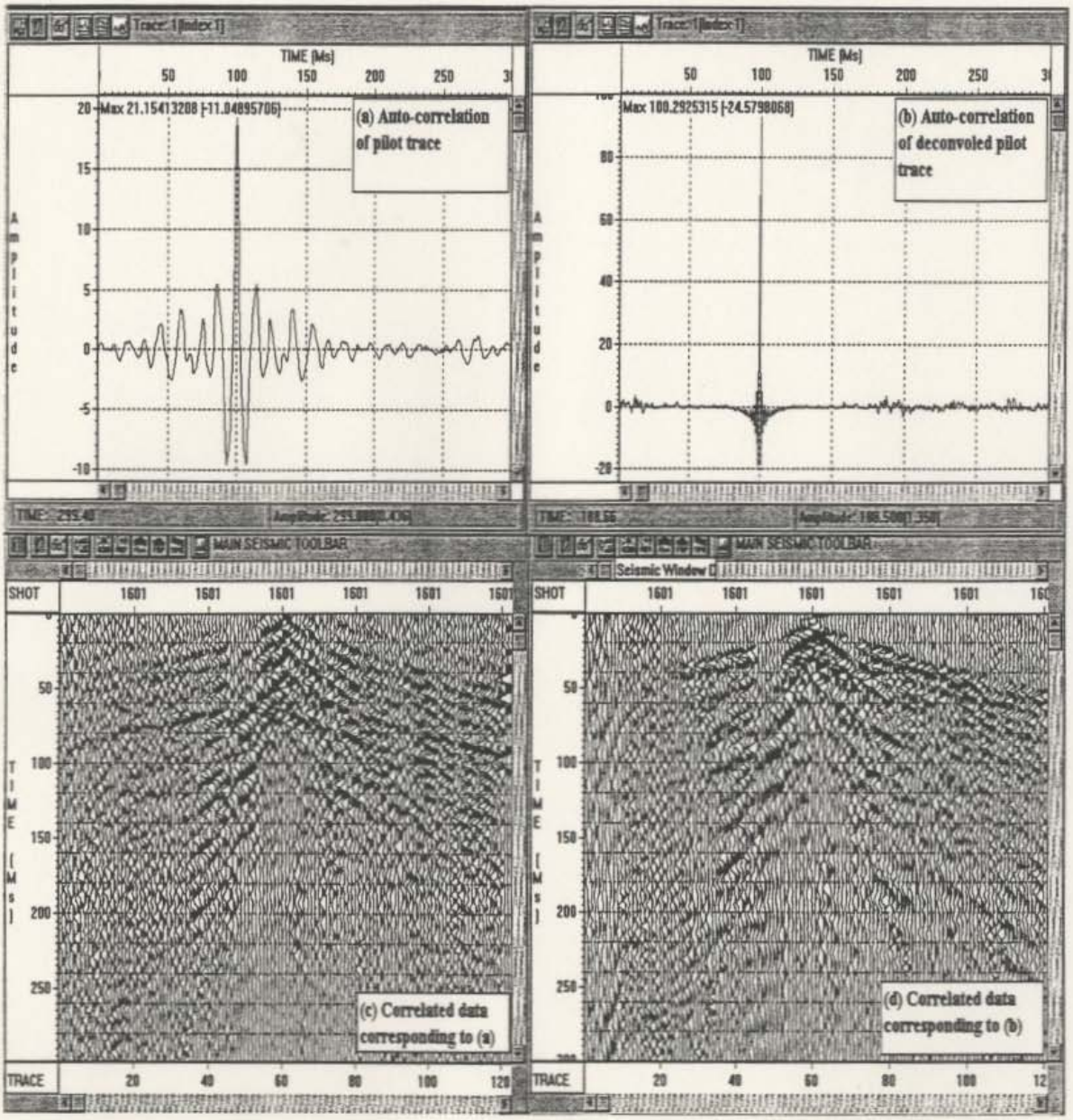

Figure 21 Autocorrelation of (a) pilot trace and (b) Deconvolution of pilot trace. (c) Correlated data for (a), (d) Correlated data for (b)

Applying deconvolution on the pilot trace before correlation sharpens the wavelet and broadens the frequency bandwidth. Figure 21(b) illustrates that more than 90% of the energy is concentrated at zero lag of the autocorrelation. This procedure improves the correlated data quality greatly in Figure 21(d).

3.2.5. Deconvolution of Correlated Data

After cross-correlation, the seismogram contains lower frequency content and much noise, which obscures the reflections. In order to recover the earth's reflectivity in the seismic trace, deconvolution is desired.

Deconvolution is a process that improves the temporal resolution of seismic data by compressing the basic seismic wavelet (Yilmaz, 1987). The wavelet is the response of seismic system to an impulse, which is theoretically the signal from a single perfect reflector. The earth's impulse response is that recorded if the wavelet is a simple spike. However, the wavelet practically combines the effects of the source signature, surface reflections, the recording filter, and the geophone response. Thus, the impulse response comprises primary reflections and all possible multiples and noise. Ideally, the deconvolution will shorten the wavelet, flatten and broaden the spectrum to standardize the wavelet from trace to trace. This will eliminate the multiples and noise and leave only the earth's reflectivity in the seismic trace.

Spiking deconvolution is employed in this research in order to achieve a zero-lag spike. In the application, several parameters are specified.

Operator length. Usually, the longer the deconvolution operator, the more perfectly the deconvolution filter approximates the true inverse of the wavelet. Nevertheless, very long operators may introduce artifacts. To choose the best operator, the autocorrelation of the seismic trace is referenced. For the data here, the wavelet autocorrelation should extend to a lag of about 50ms. Following Yilmaz (1987), several different operator lengths around 50 ms were tested and then 80 ms was selected as it yielded the best appearance in the seismic record.

Pre-Whitening. There is always noise in the seismogram that is additive in both the time and the frequency domain. Moreover, numerical noise is generated during the processing. Pre-whitening is a process to add a small constant value to the wavelet spectrum at all frequencies (white noise). This stabilizes the amplitude spectrum of the inverse wavelet so it does not grow without bound at high and low frequencies. The values for pre-whitening usually range from .01 to 1 percent (Yilmaz, 1987), and the typical value 1 percent is applied here.

Design Window. The seismic wavelet is not really constant in shape throughout the trace. It actually loses high frequencies due to absorption and geometrical spreading. Thus, the autocorrelation function should be calculated over a portion of rather than the whole trace. In practice, high resolution data requires the window to begin after the refracted first break and last 200 to 500 ms (Nickerson, 1993). Because the first break arrives at different times on different shot records, it is difficult to design the "gate" accurately. Yilmaz's (1987) recommended that the design window must be at least eight

times of operator length. This research tested several design windows with around eight times of the operator length (80ms) and chose 500 ms that yielded the best result.

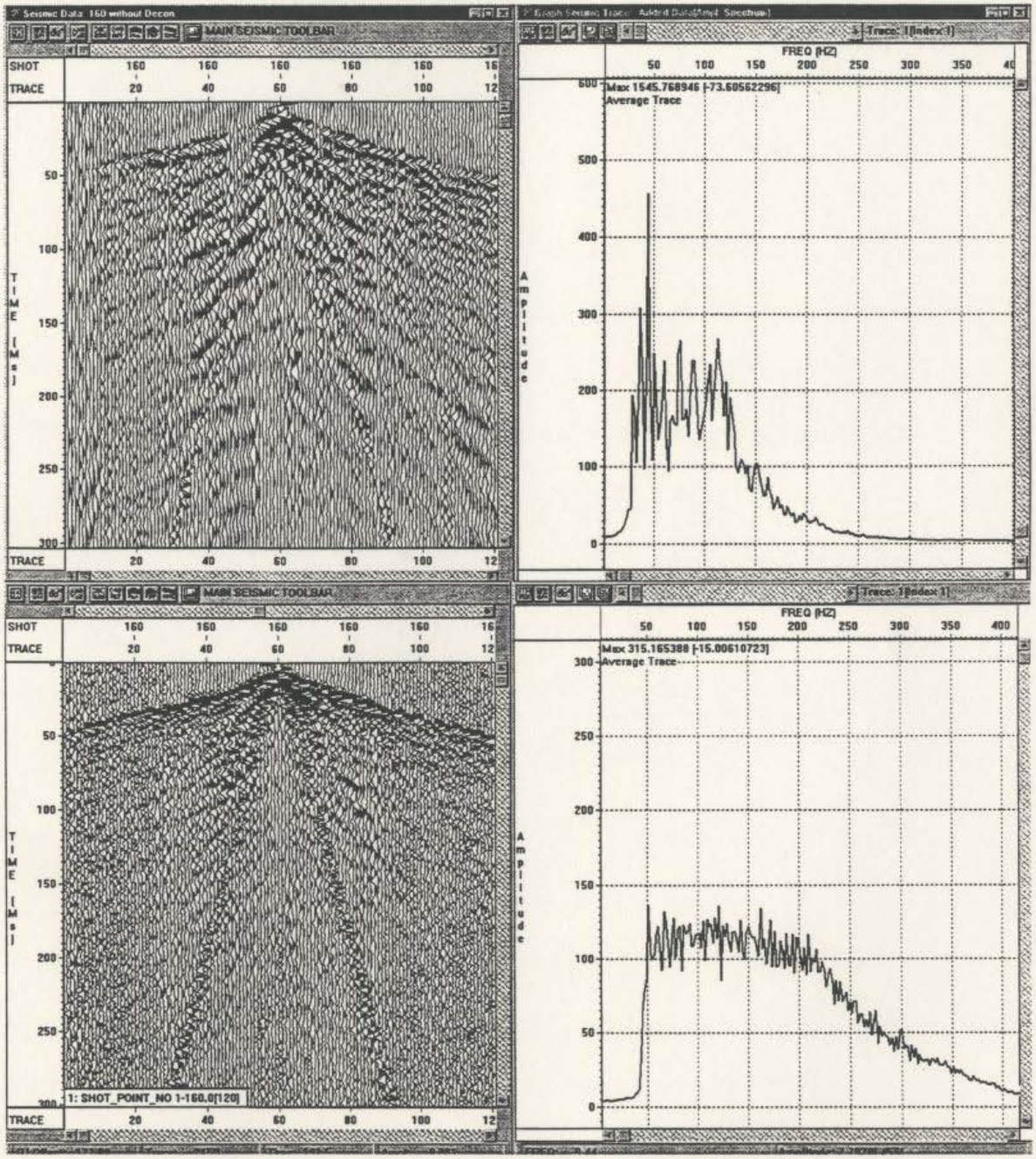

Figure 22 Shot gather and its spectrum (a) before and (b) after spiking deconvolution

After deconvolution, the seismic wavelet has been shortened and some noise and multiples have been removed (Figure 22). Also, the spectrum has been flattened and broadened greatly. However, this processing has also generated some high frequency noise, therefore bandpass filtering is required after deconvolution

3.2.6. Filtering

Besides the noise from the recording system, there still are other noises (i.e. wind, traffic) that mostly fall into a lower frequency range. In order to remove these and to enhance the reflection signal, an Ormsby bandpass filter is applied to all traces. Because the main concern of this research is on higher frequencies, the frequency parameters are set as

Low Truncation Freq:	40 Hz
Low Cut Freq:	60 Hz
High Cut Freq:	300 Hz
High Truncation Freq:	500 Hz

This setting not only removes the walk-away noise, but also removes the 60 Hz contamination generated by the generator in the field test.

Air blast and ground roll are the main factors that obscure the genuine reflections. Both of them are coherent linear noises with low frequency. The velocity of the air blast is around 340 m/s and that of the ground roll is about 1500 m/s. F-k filtering (wave number filter) is a useful way to separate these noises from reflection energy then remove them without hurting the reflections. Since the trace spacing on CMP gathers may be more than twice of that on shot gathers, f-k filter on CMP gather may result in aliasing. Therefore, this research applied an f-k filter on the shot gathers rather than CMP gathers.

In the f-k filter process, all the signal with velocities lower than 1700 m/s was rejected. After f-k filtering, the ground roll was removed successfully, but the aliased air blast was not (Figure 23). Fortunately, the depth of interest is just a few hundred meters; thus, except for the traces near the source, the air blast has no effect and can be ignored.

3.2.7. Shot Stacking

Four sets of data were collected at each shotpoint in test 2 and two sets in test 3. By adding all the shots at the same shotpoint together, the random noise is reduced while the coherent reflections are enhanced.

Theoretically, all shots at the same shotpoint should be identical. However, in practice, there are differences in the time domain because the receivers are difficult to trigger accurately at the same time. Thus, shifting all shots identically in the time domain is necessary before shot stacking. In order to determine the precise time to be shifted, the cross-correlation between each two shots was calculated. Cross-correlation represents the coherence of the two shots and the position of the maximum peak in time axis determines the optimum shift for stacking. Figure 24 illustrates that the signals are enhanced after shot stacking, especially on the far offset.

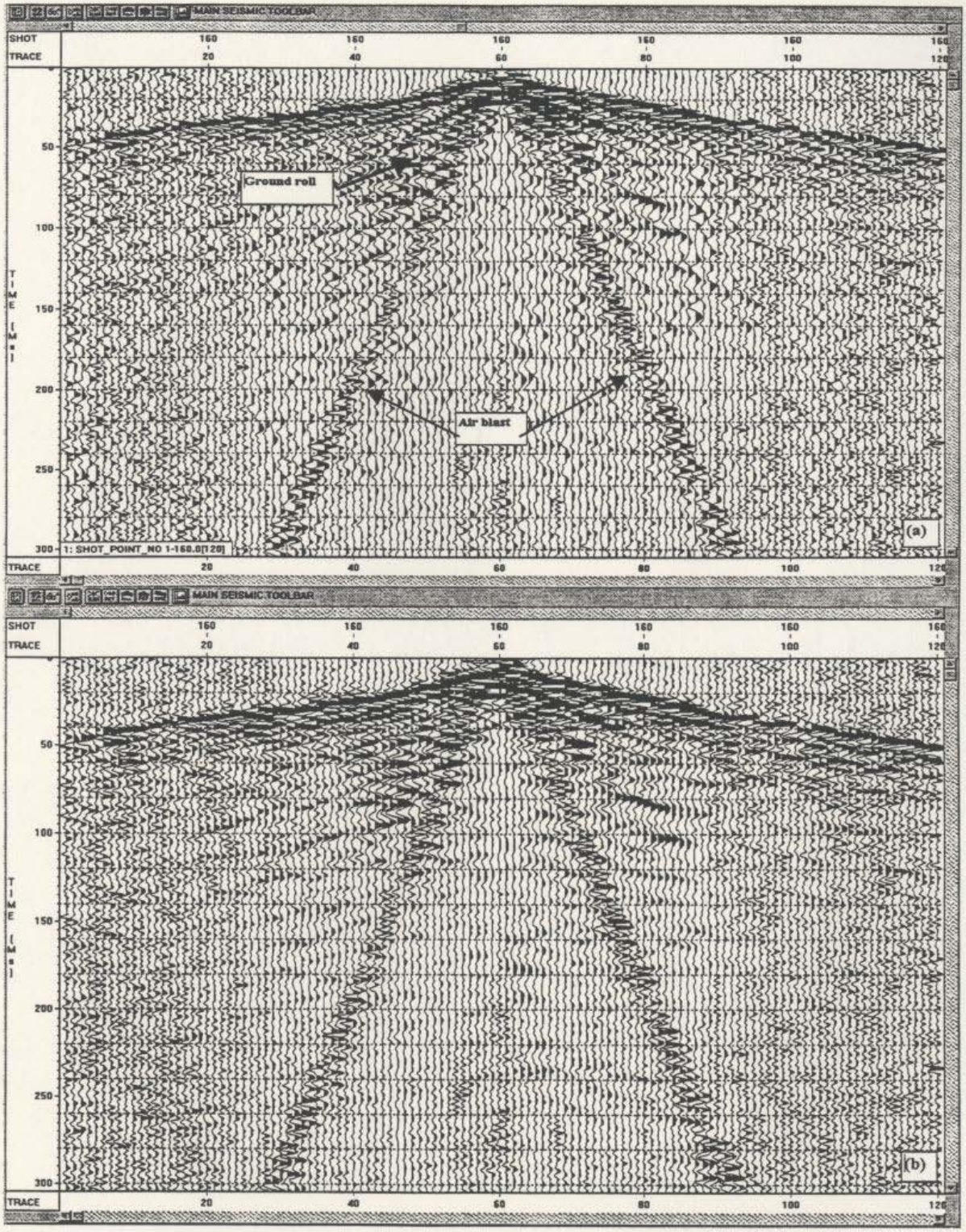

Figure 23 Shot gather before and after f-k filtering

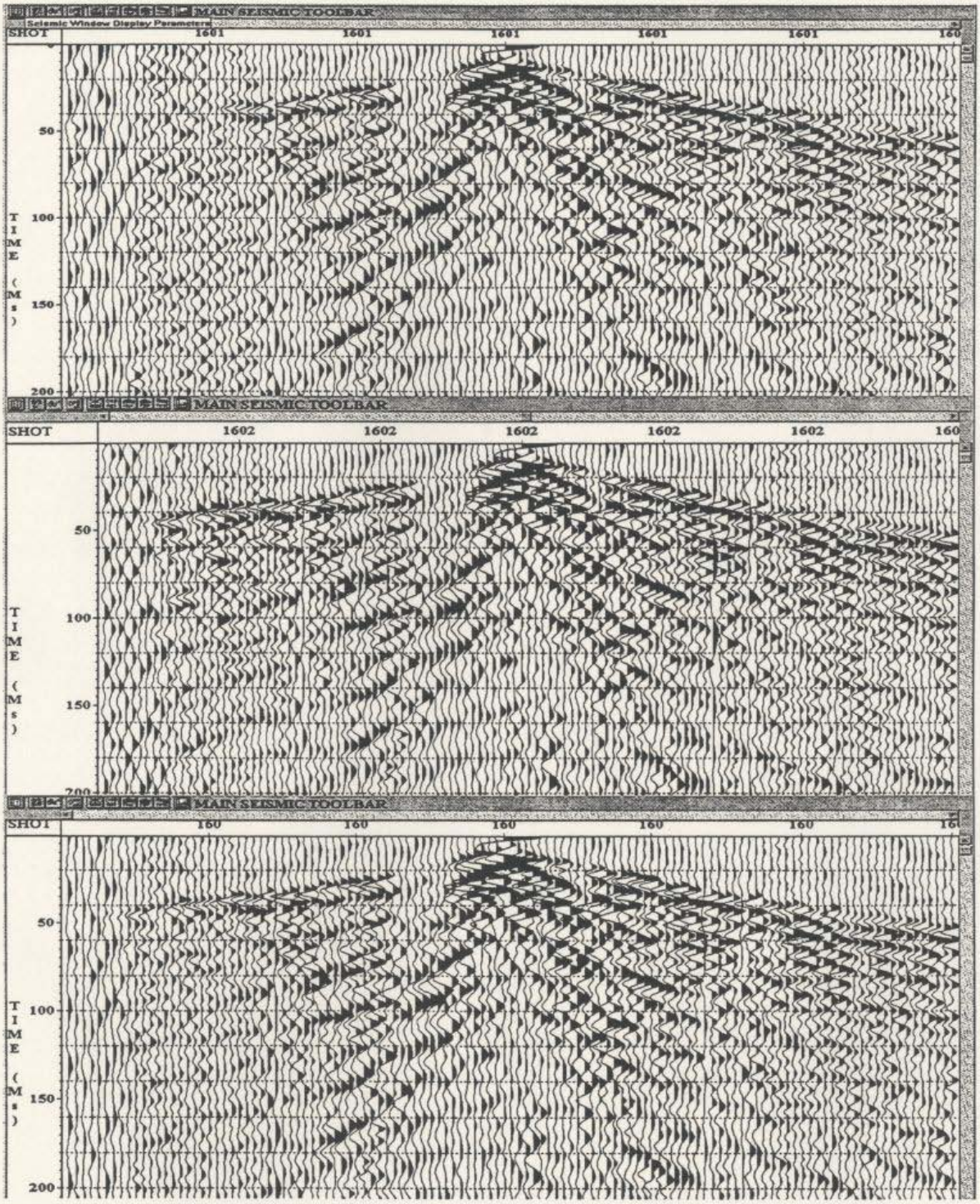

Figure 24 Shot stacking: shot 1601 and shot 1602 stacked as shot 160.

3.3. Summary

For vibratory data, deconvolving the pilot trace before correlation can narrow the wavelet to zero lag to eliminate the ghost noise generated by correlation. Correlating all traces with the deconvolved pilot trace can transform the long records into a preferable normal shot gather. The further deconvolution on correlated data improves the temporal resolution greatly by flattening and broadening wavelet's spectrum. Filtering helps to remove the unwanted noise (i.e. air blast and ground roll) and shot stacking enhances the coherent reflections by reducing the random noise.

As environmental conditions, recording parameters and processing parameters all affect both the amplitude and frequency contents of the seismic signal, a valid source comparison requires that acquisition and processing condition be held as constant as possible.

In this research, three different tests were carried out with five sources. For direct comparison, all of the trace data were processed identically by following the steps below:

- AGC 300ms
- Spiking deconvolution
- F-K filtering to remove air blast and ground roll
- First arrival mute (direct wave and the noise generated by crosscorrelation)
- Band-pass filtering (zero-phase Butterworth 40/60/300/500Hz)

After appling the above specific processing, the SIST records and the hammer source records are transformed to "normal" shot gather seismograms (Figure 26 to Figure 29),

which are now capable of being compared with the data of the shotgun source (Figure 25).

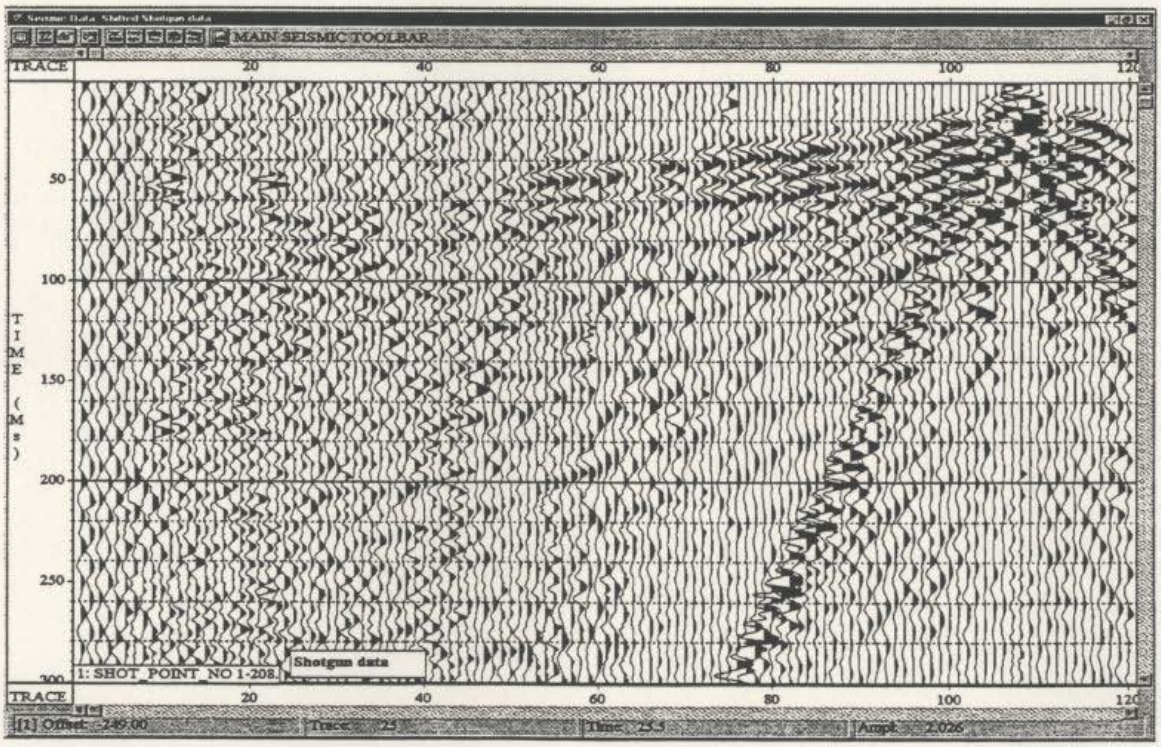

Figure 25 Shot gather of shotgun data after processing

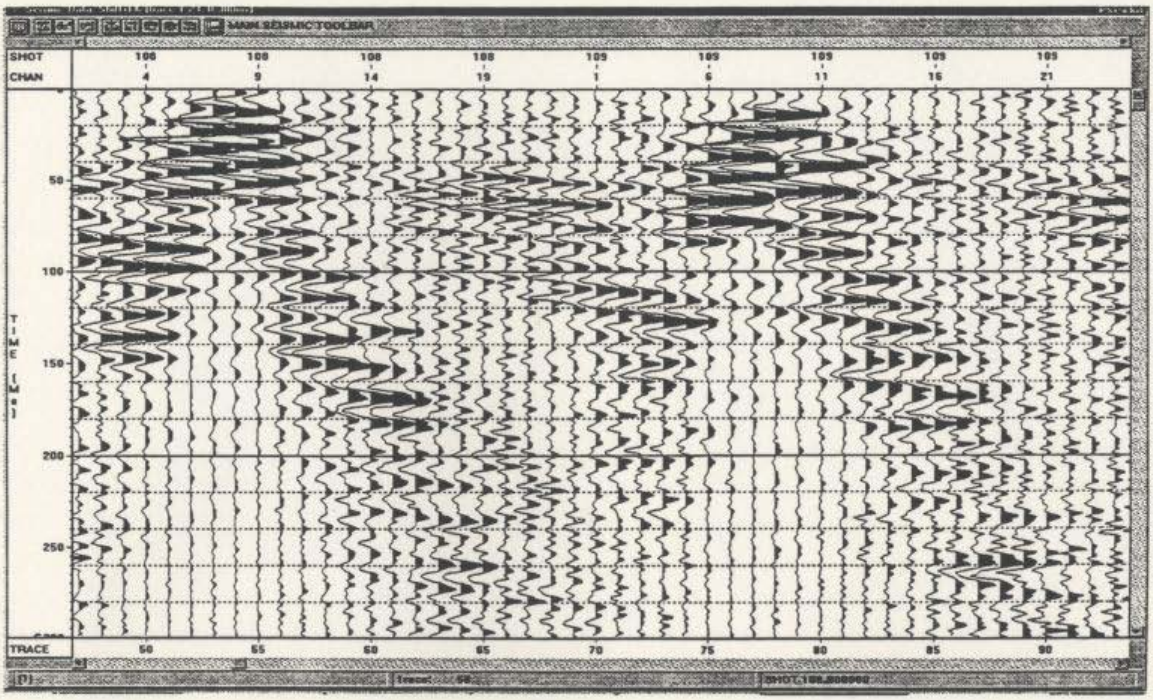

Figure 26 Shot gather of hammer data after processing

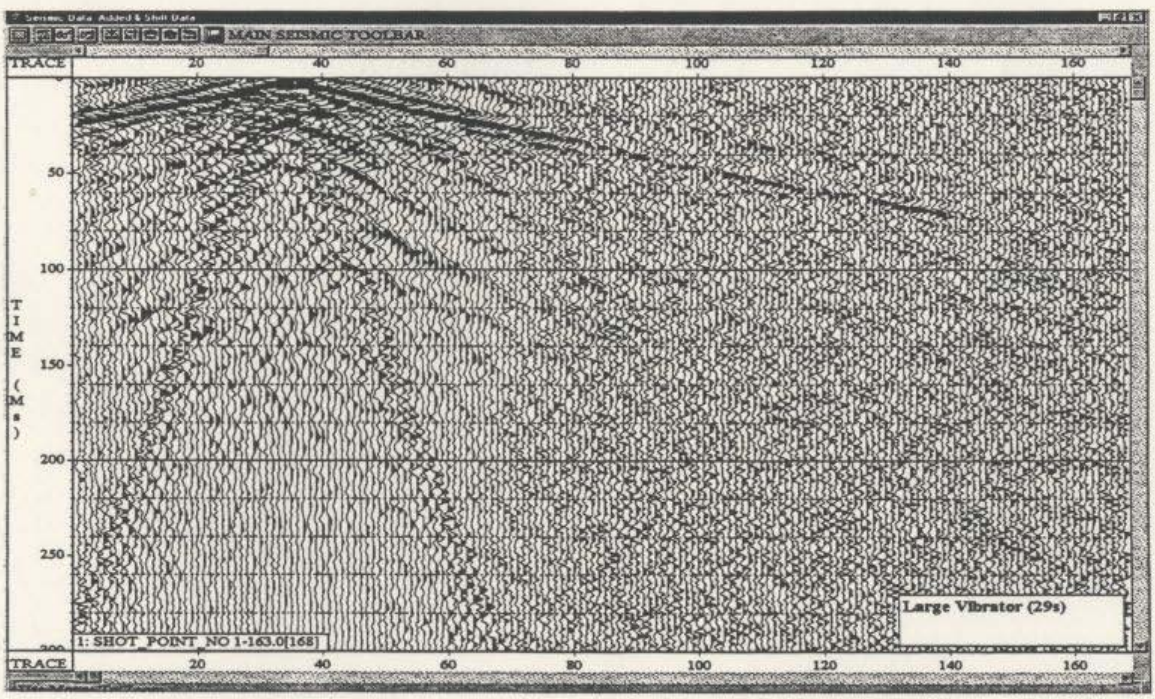

Figure 27 Shot gather of large vibrator source (29s) data after processing

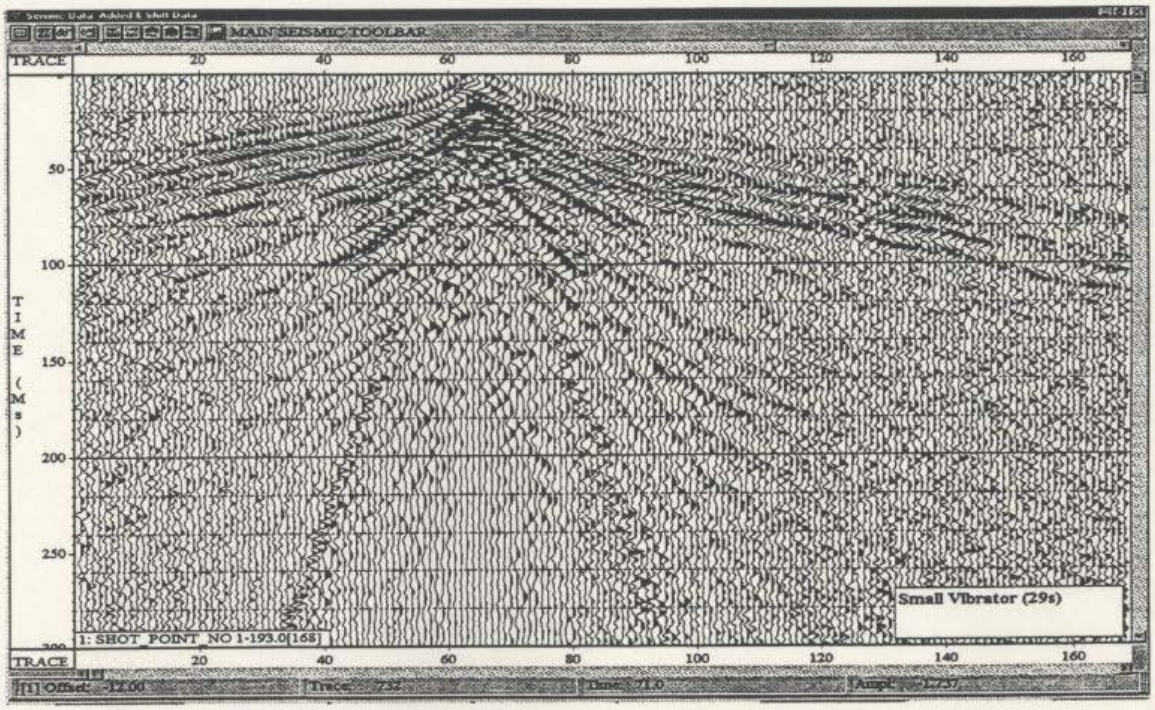

Figure 28 Shot gather of small vibrator source (29s) data after processing

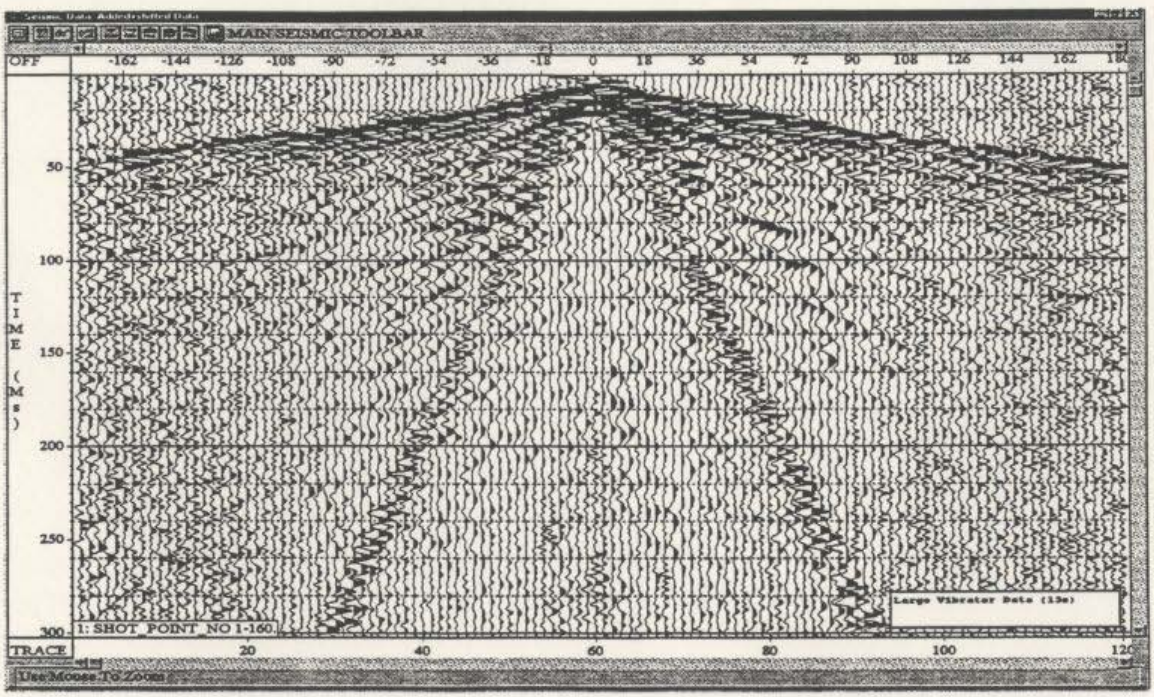

Figure 29 Shot gather of large vibrator source (15s) data after processing

Chapter 4. Data Analysis: Comparison of Sources

This chapter presents the processed data for several high resolution sources.

The pilot trace is an important consideration that affects the resolution. The ideal pilot trace to achieve high resolution is one whose autocorrelation is a minimum phase function, which equals to zero everywhere except at the zero-lag. The compliance with this condition provides an effective means of evaluating the seismic resolution. The nature of the pilot trace in terms of autocorrelation and amplitude spectrum is studied first.

Seismic resolution also depends on the frequency content. High frequency sharpens and narrows the waveshape to increase seismic resolution. This chapter then studies the frequency content by calculating the dominant frequency and bandwidth, from which the maximum resolution limit and diameter of Fresnel zone is derived. As well the energy is calculated relative to both offset and frequency.

Finally, vibratory sources are compared with the shotgun, both quantitatively and graphically. Since the main focus of this research is limited to within several hundred meters of the surface, only the portion of the trace from 0 ms to 250 ms is processed.

4.1. Pilot Signal Specification

The effect of cross-correlating is to replace each replica of the input signal with its autocorrelation that has the same amplitude and polarity as the original spike of the earth response (Geyer, 1970a). Therefore, the sharper the autocorrelation of the pilot trace, the higher the resolution. The characteristics of the autocorrelation signal depend on the amplitude spectrum and duration of the pilot trace. As an essential determiner of seismic resolution, the pilot trace characteristics for four sources will be discussed and compared below.

If f_1 and f_2 represent low and high frequency cutoffs respectively, the frequency range can be quantified as

$\Delta=(f_2-f_1)$ ..... (4.1)

The actual choice of the cutoff amplitude is somewhat subjective. A value of –20dB from the peak is used for this study. Figure 30 is a diagram for picking f_2 and f_1.

The ratio of the cutoff frequencies is defined as $R_f=f_2/f_1$

The bandwidth can be expressed in octaves as

$$R^0{}_f = \frac{\log R_f}{\log 2} \qquad \text{.....(4.2)}$$

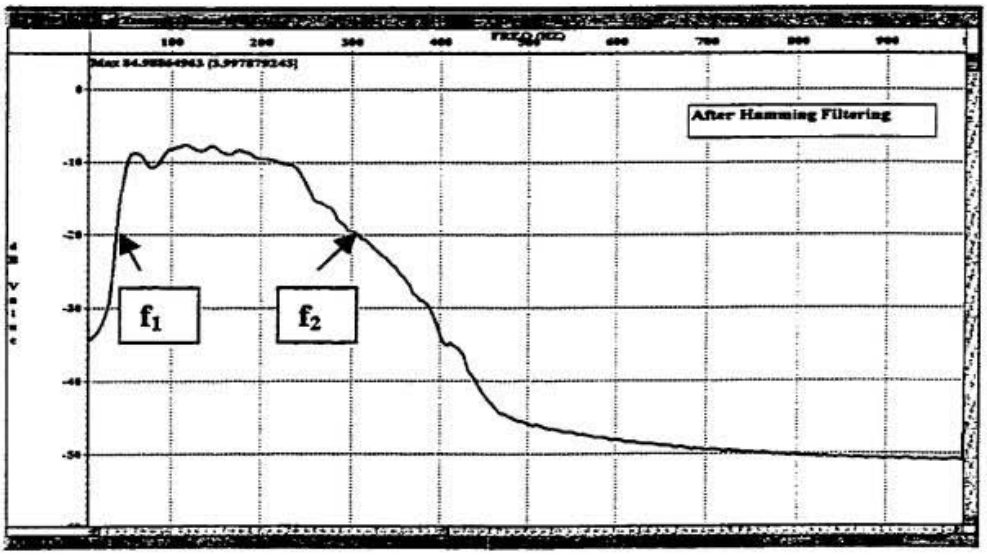

Figure 30 Diagram for picking cutoff frequencies

According to equation (4.1) and (4.2), not only the frequency range but also the bandwidth affects the resolution. The frequency range determines the sharpness of the peak and the bandwidth determines the basic shape of the autocorrelation function (Geyer, 1970b). Because a pilot signal with broad bandwidth yields better resolution than one with narrow bandwidth, the larger $R°_f$ the better the resolution. The average frequency range and bandwidth for each source individually are calculated and listed in Table 1.

As a double check on the pilot trace frequencies, the center peak-to-side lobe amplitude ratio (A_0/A_{SL}) is also computed and compared. The results are listed in Table 1. Since the amplitude of center peak represents the signal on the record while the amplitude of the side lobes represents a signal-generated noise, A_0/A_{SL} represents a theoretical intrinsic

signal-to-noise ratio inherent in the specifications of the pilot trace. In this research, the amplitude of the first side lobes is A_{SL}.

Table 1 Parameter comparison of the pilot signal

Sources	Deconvolution	Frequency range (Hz)	Bandwidth (Octave)	A_0/A_{SL}
Hammer	**NO**	265 (35-300)	3.0	1.6
	YES	475 (25-500)	4.3	7.2
S. Vibrator(29s)	**NO**	100 (55-155)	1.5	1.4
	YES	357 (25-382)	4.0	4.3
L. Vibrator(29s)	**NO**	160 (40-200)	2.3	1.6
	YES	392 (23-415)	4.2	6.1
L. Vibrator(15s)	**NO**	164 (36-200)	2.5	1.6
	YES	575 (25-600)	4.6	10.0

For the pilot signal without deconvolution, the hammer has the largest value for all three parameters in Table 1. For the SIST vibrators, the frequency range is relatively narrow (100, 160, and 164Hz respectively); the largest bandwidth is just 2.5 octaves and the ratios of A_0/A_{SL} are less than two. Obviously, these unsatisfactory pilot specifications will result in poor quality on the correlated data

Deconvolution broadens the frequency range and bandwidth, and increases the signal-noise ratio greatly. The bandwidth for all sources is over 4.0 octaves with the largest at 4.6, and the ratios of A_0/A_{SL} are increased greatly with the largest at 10.

Figure 31 to Figure 38 display the four sources' typical autocorrelation and amplitude spectrum of the pilot trace both with and without deconvolution. They obviously illustrate that the autocorrelation without deconvolution is not a ideal Klauder wavelet. Deconvolution de-scrambles the transients and thereby sharpens the autocorrelation and

broadens the amplitude spectrum. The autocorrelation functions from all four sources are minimum phase because most of their energy concentrates at zero-lag. The hammer source has the least non-causal effect, and the large vibrator (29s) is better than the other two vibrators.

Among the four sources, the large vibrator (15s) has the best frequency range and bandwidth so as to yield the largest A_0/A_{SL} ratio. The hammer is the second best and then the vibrators (29s) are next. The main focus of this research is on the pilot signals with deconvolution processing, which is used as a true correlator in the data processing.

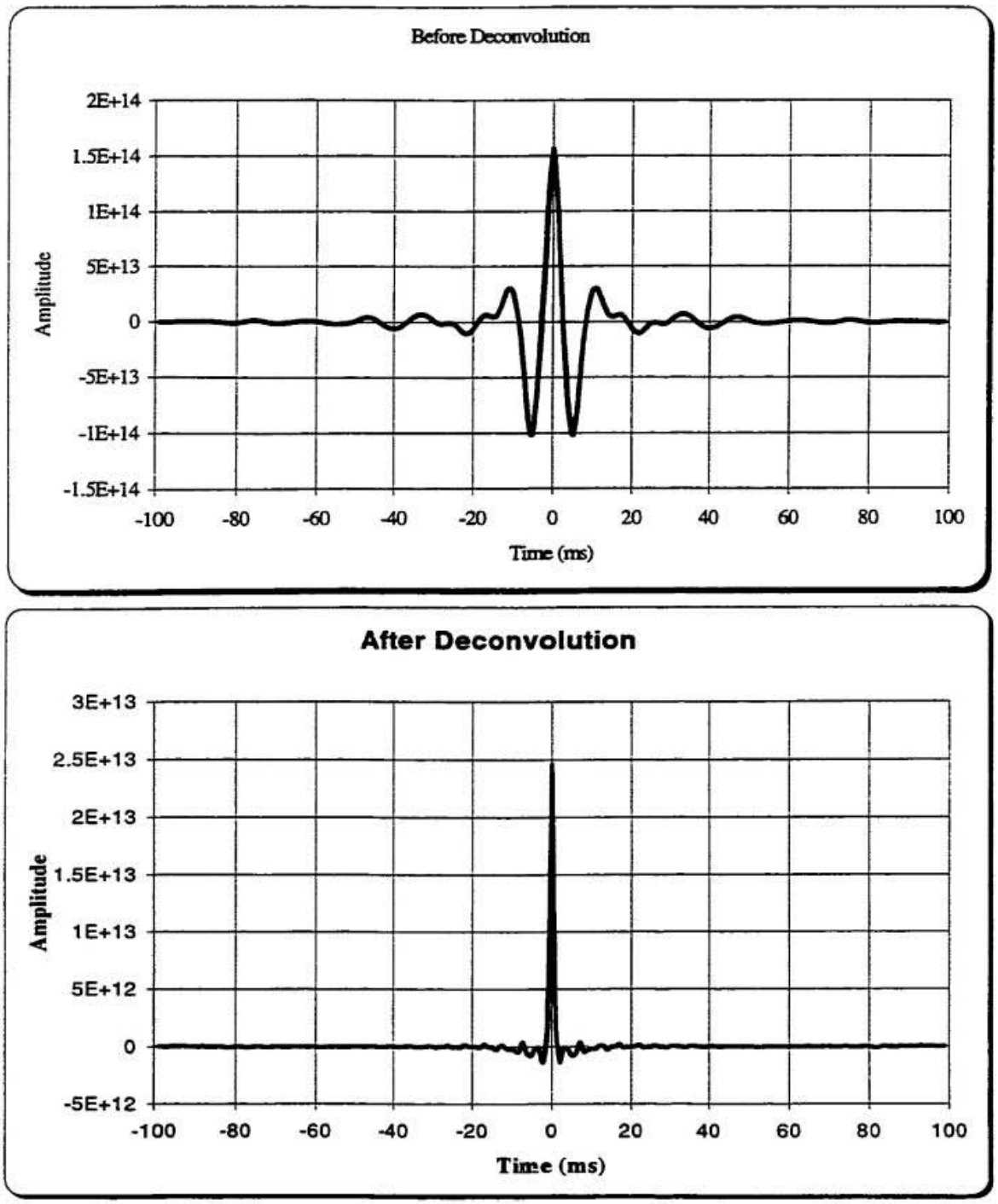

Figure 31 The auto-correlation of the pilot trace (Hammer source)

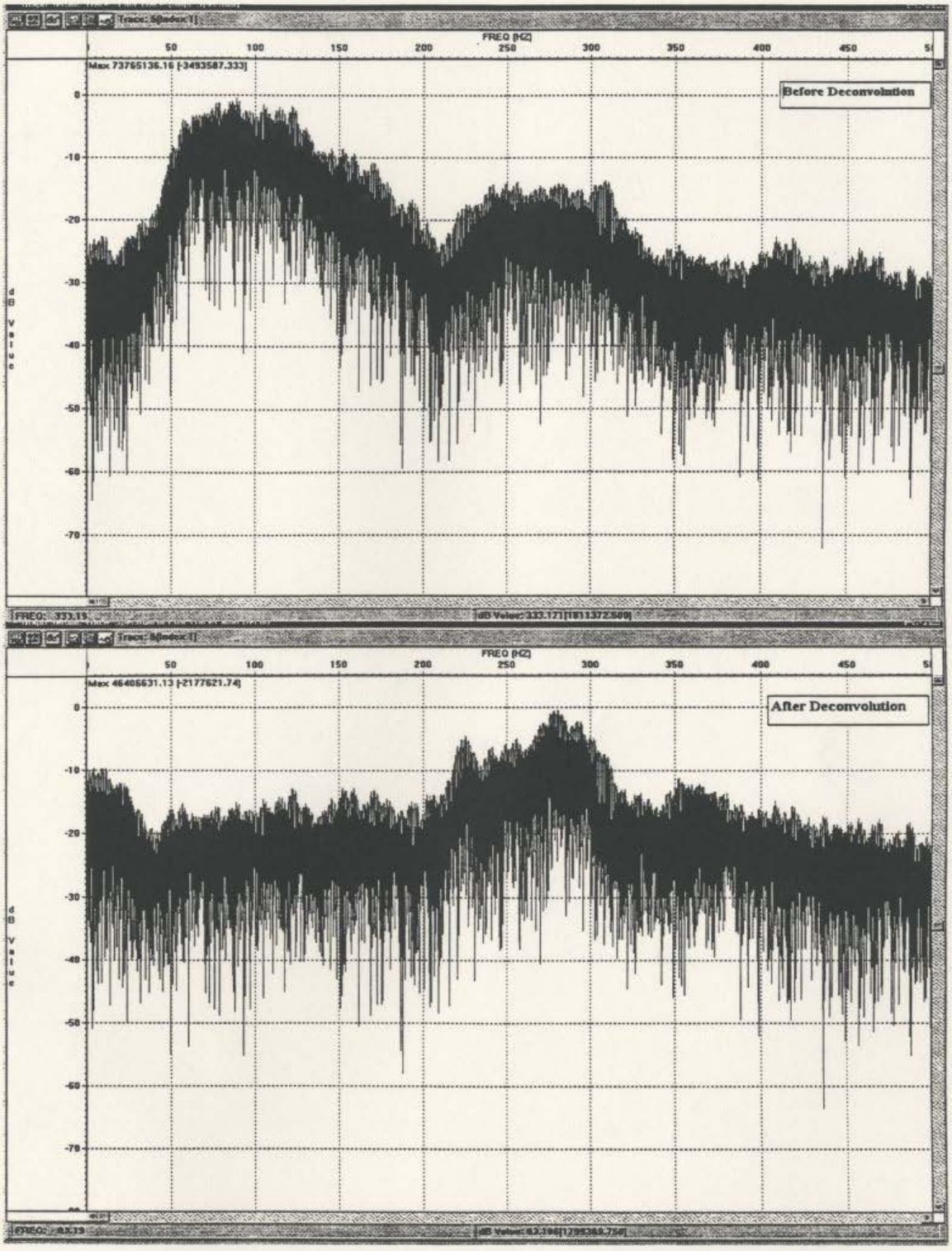

Figure 32 The amplitude spectrum of the pilot trace (Hammer source)

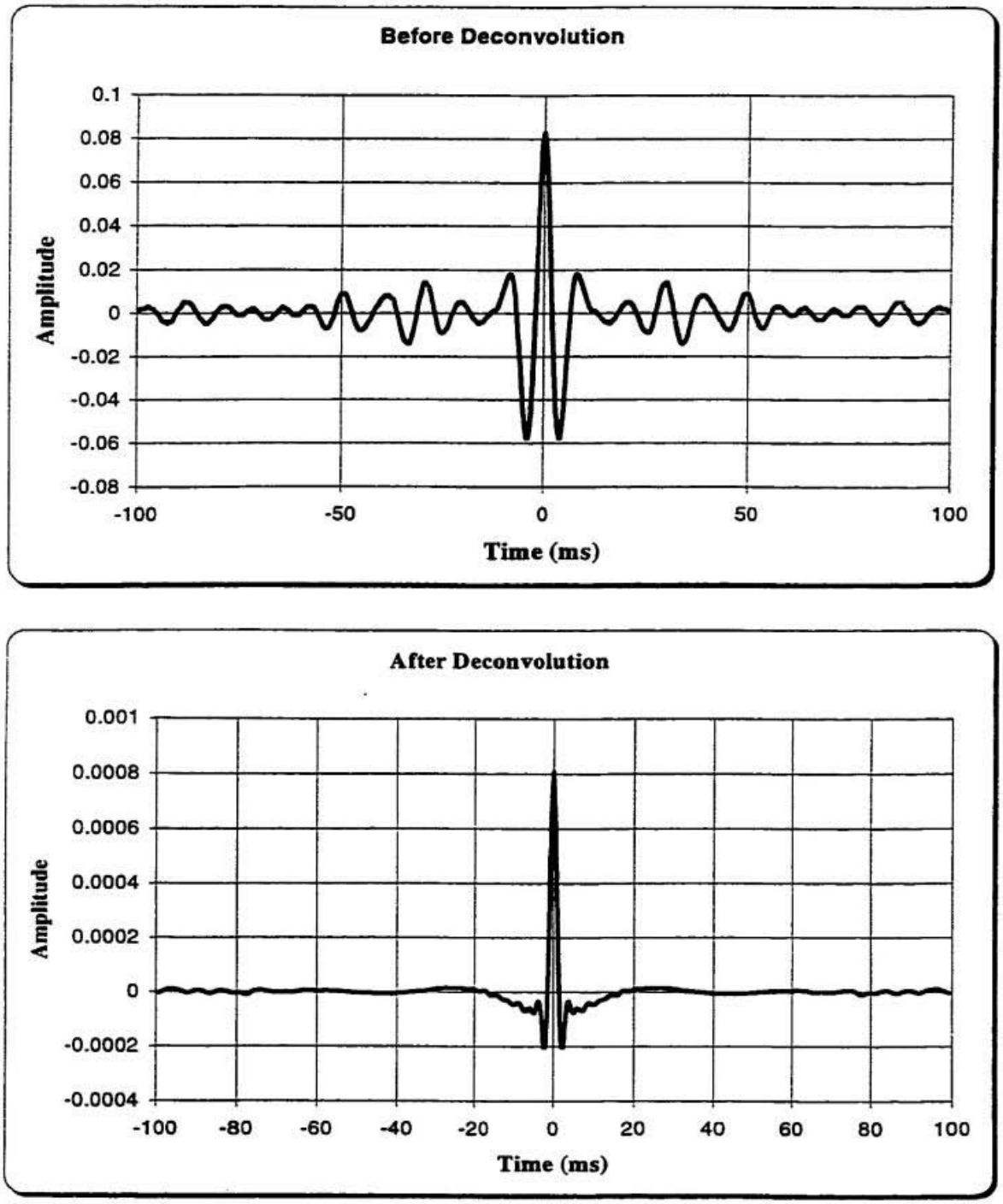

Figure 33 The auot-correlation of the pilot trace (Small vibrator, 29s)

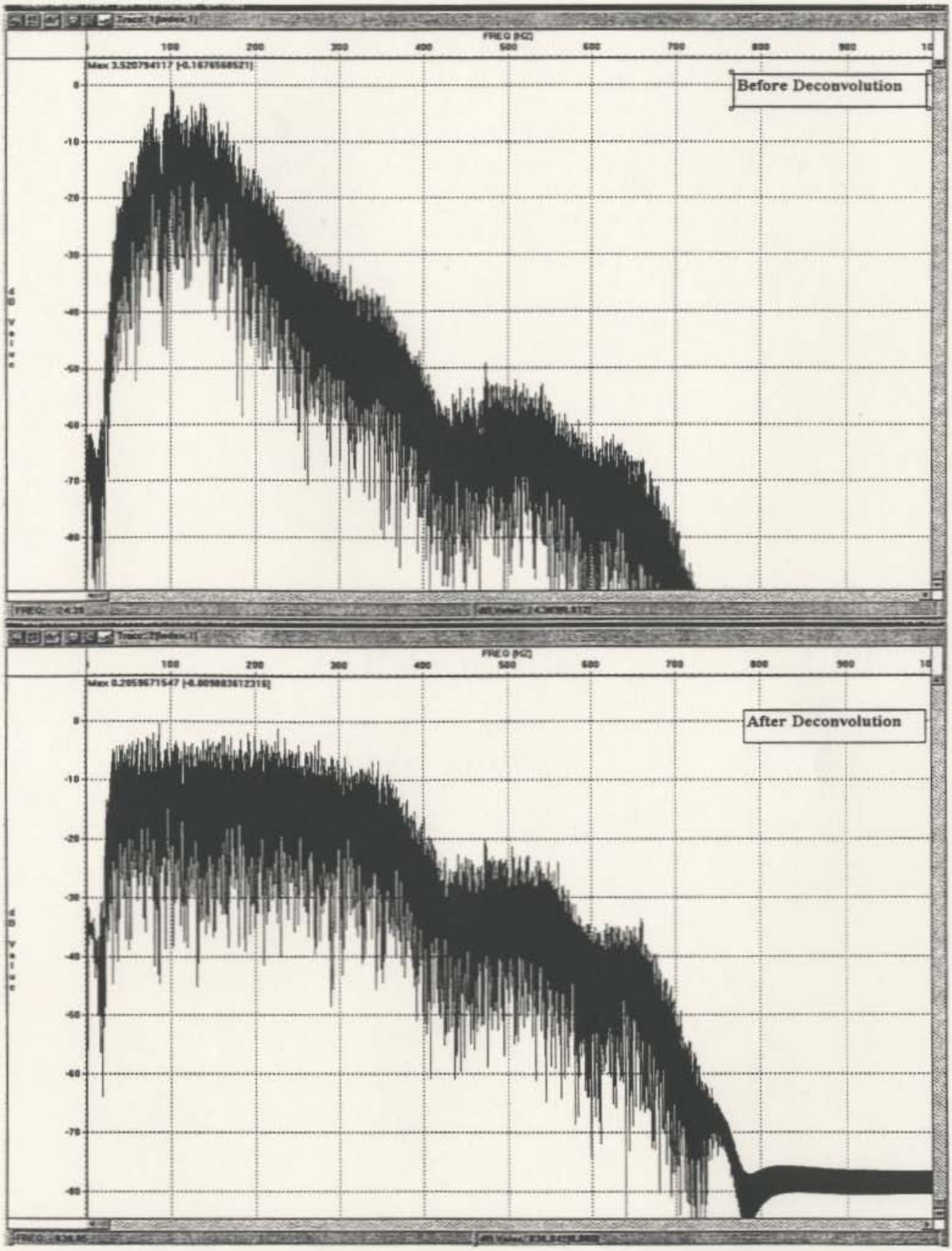

Figure 34 The amplitude spectrum of the pilot trace (Small vibrator, 29s)

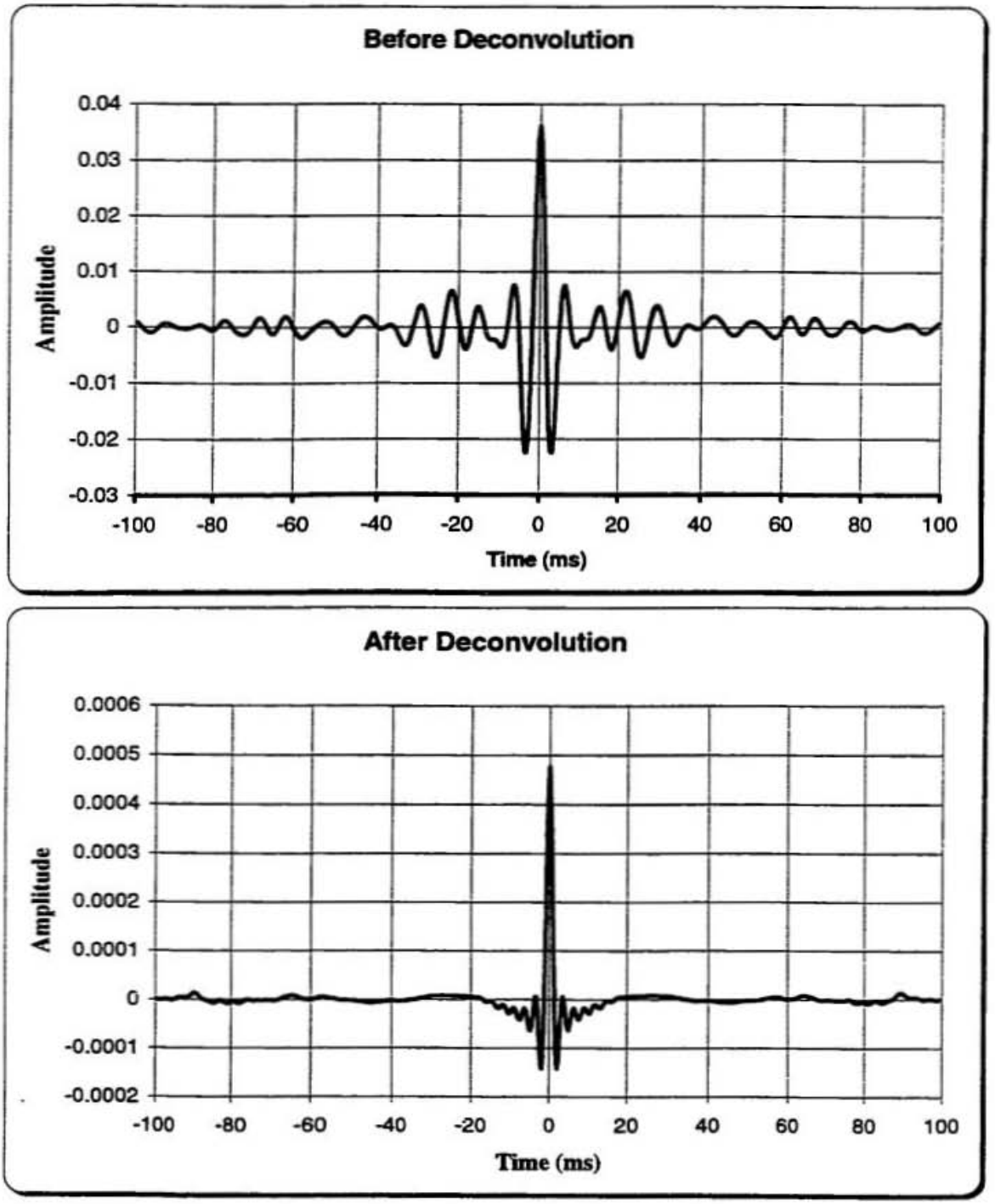

Figure 35 The auto-correlation of the pilot trace (Large vibrator, 29s)

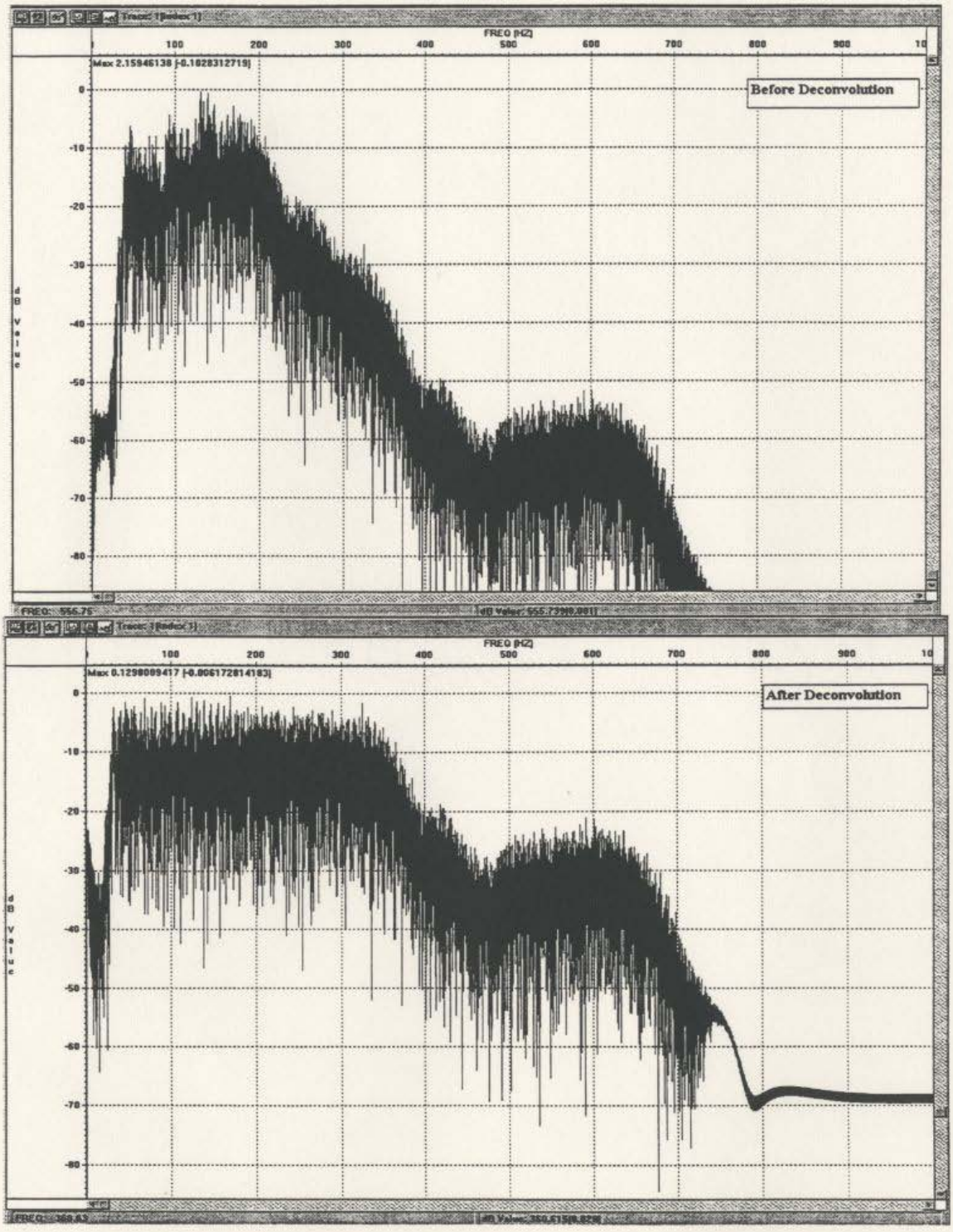

Figure 36 The amplitude spectrum of the pilot trace (Large vibrator, 29s)

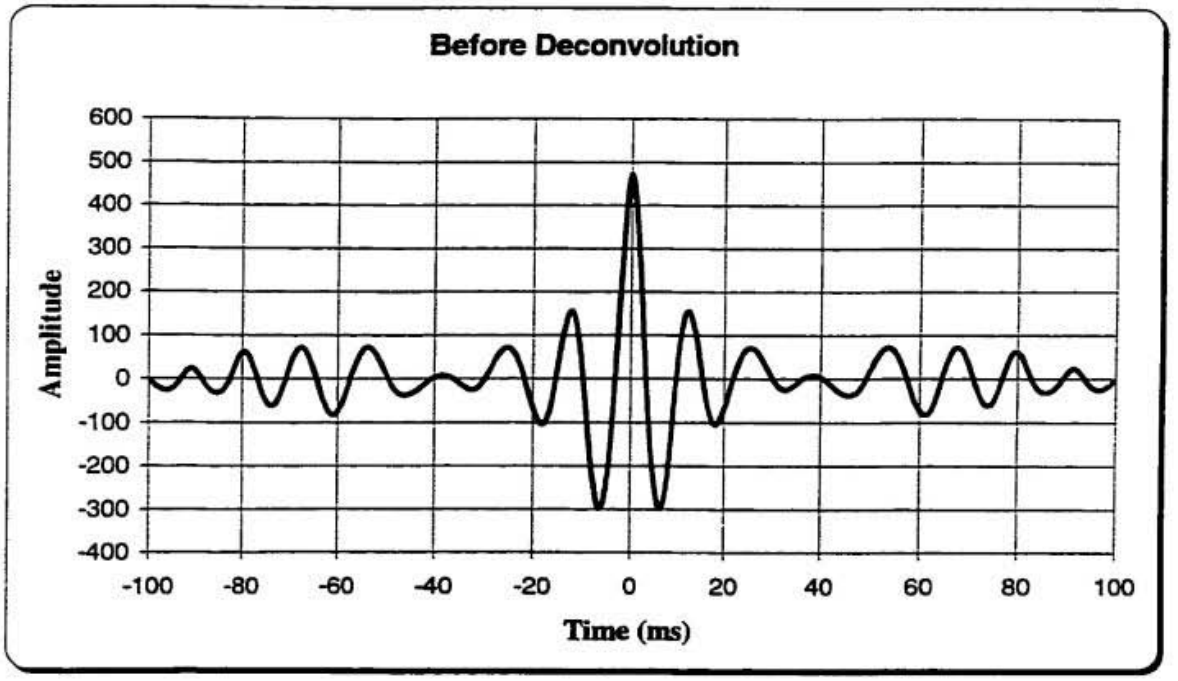

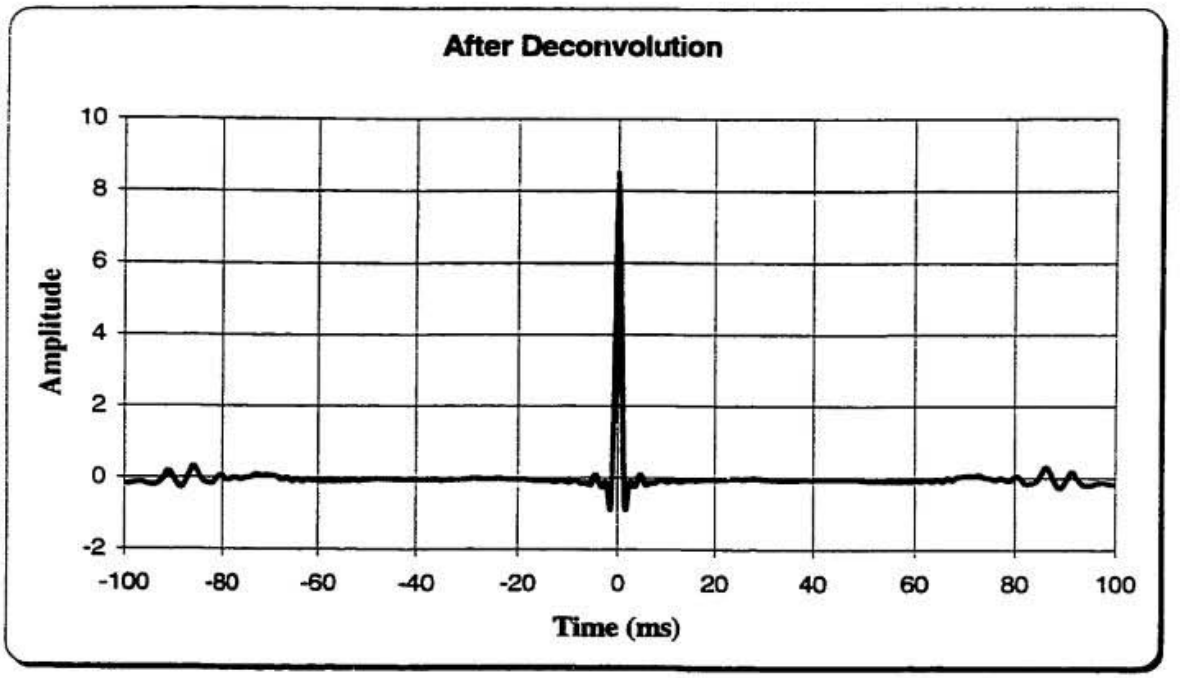

Figure 37 The auto-correlation of the pilot trace (Large vibrator, 15s)

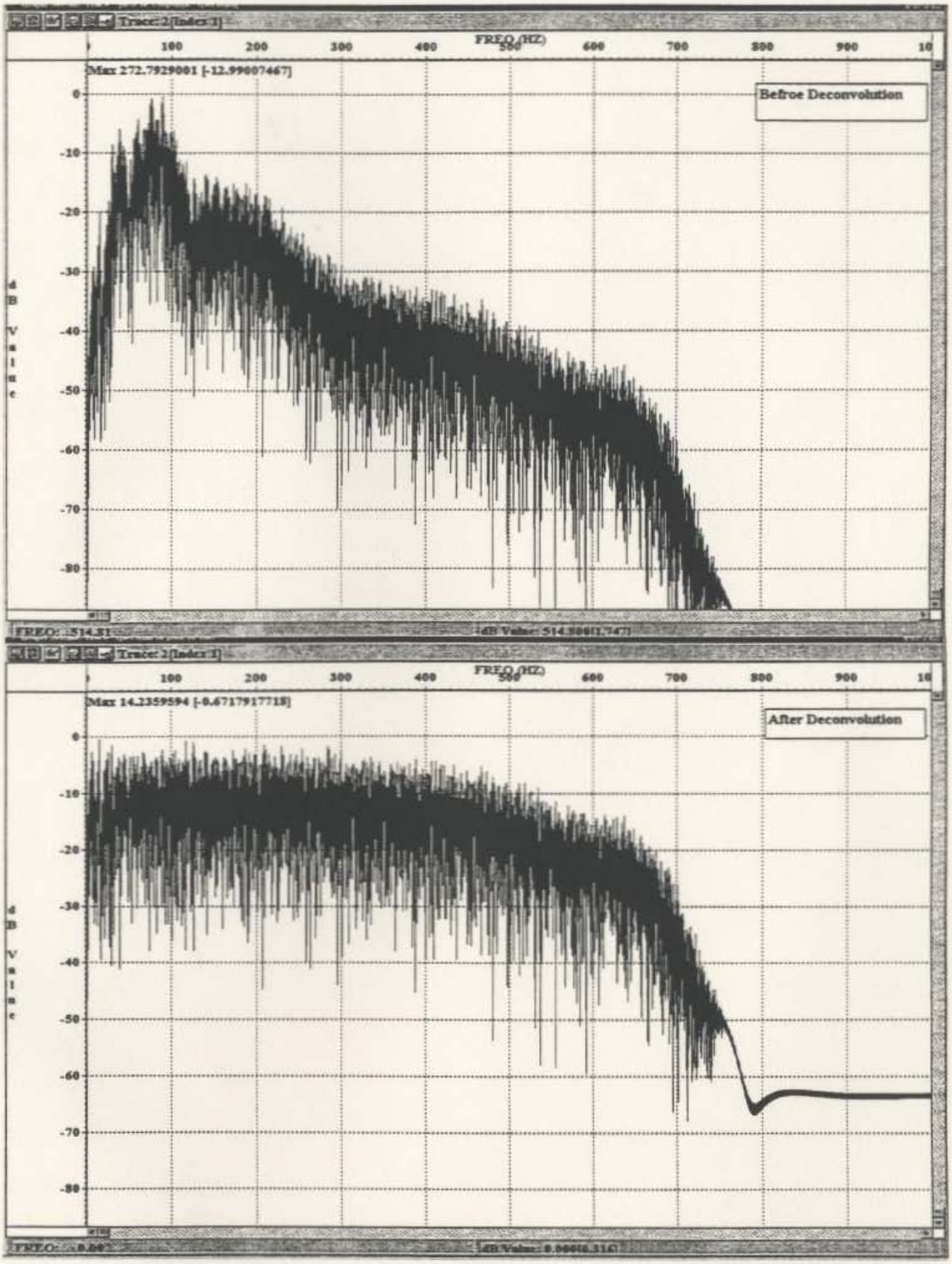

Figure 38 The amplitude spectrum of the pilot trace (Large vibrator, 15s)

4.2. Frequency Content

This section contains the actual calculations. The frequency spectrum of individual traces was calculated to allow comparison of the frequency characteristics. Because the reflections are not clear making it possible to separate them from other seismic energy, all the waves are used to calculate the spectra.

Practically, the raw frequency spectra are too noisy to be compared properly; therefore a five-point Hamming filter is used for smoothing before calculations.

$$\bar{x}_i = \frac{1}{5}(x_{i-2} + x_{i-1} + x_i + x_{i+1} + x_{i+2}) \quad \text{.....(4.3)}$$

Figure 39 shows an example of the spectrum before and after smoothing (from the large vibrator, 15s). The smoothed spectrum clearly indicates the low cutoff frequency f_1 and high cutoff frequency f_2, which yields the dominant frequency by picking the midpoint between f_1 and f_2. f_1 and f_2 are defined in this research to be the beginning and ending frequency of plateau of the amplitude spectrum. Also, the frequency range can be determined easily by subtracting f_1' from f_2' at an appropriate decibel cutoff (-20dB was selected in this research).

To study the frequency characteristics with offset, offset sort processing was applied to calculate average amplitude spectrum statistically at each offset. The dominant frequencies, frequency ranges and bandwidth in octaves for all sources are listed in Appendix A and illustrated in Figure 40, Figure 41 and Figure 42 respectively.

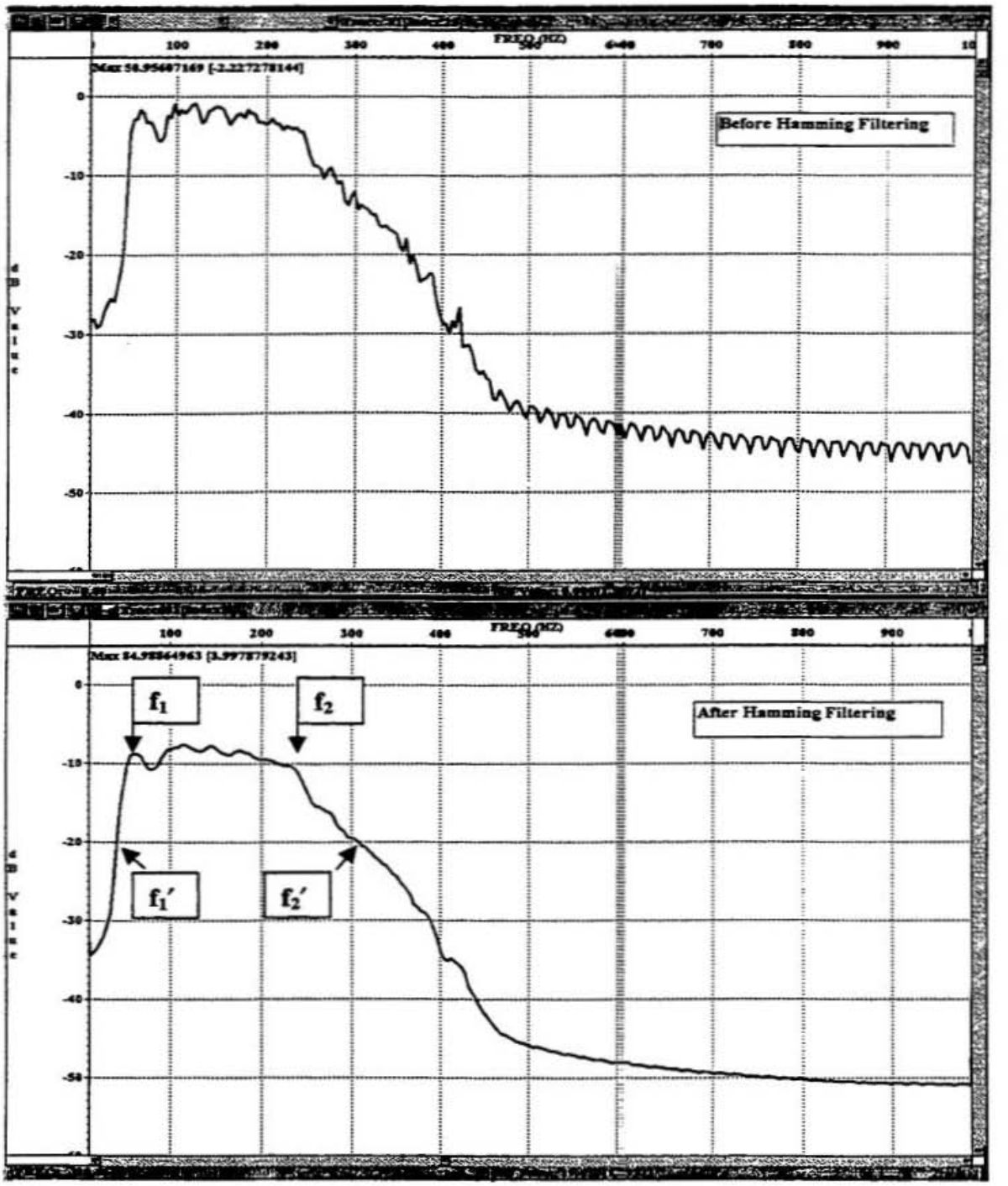

Figure 39 An example of the spectrum before and after Hamming filtering

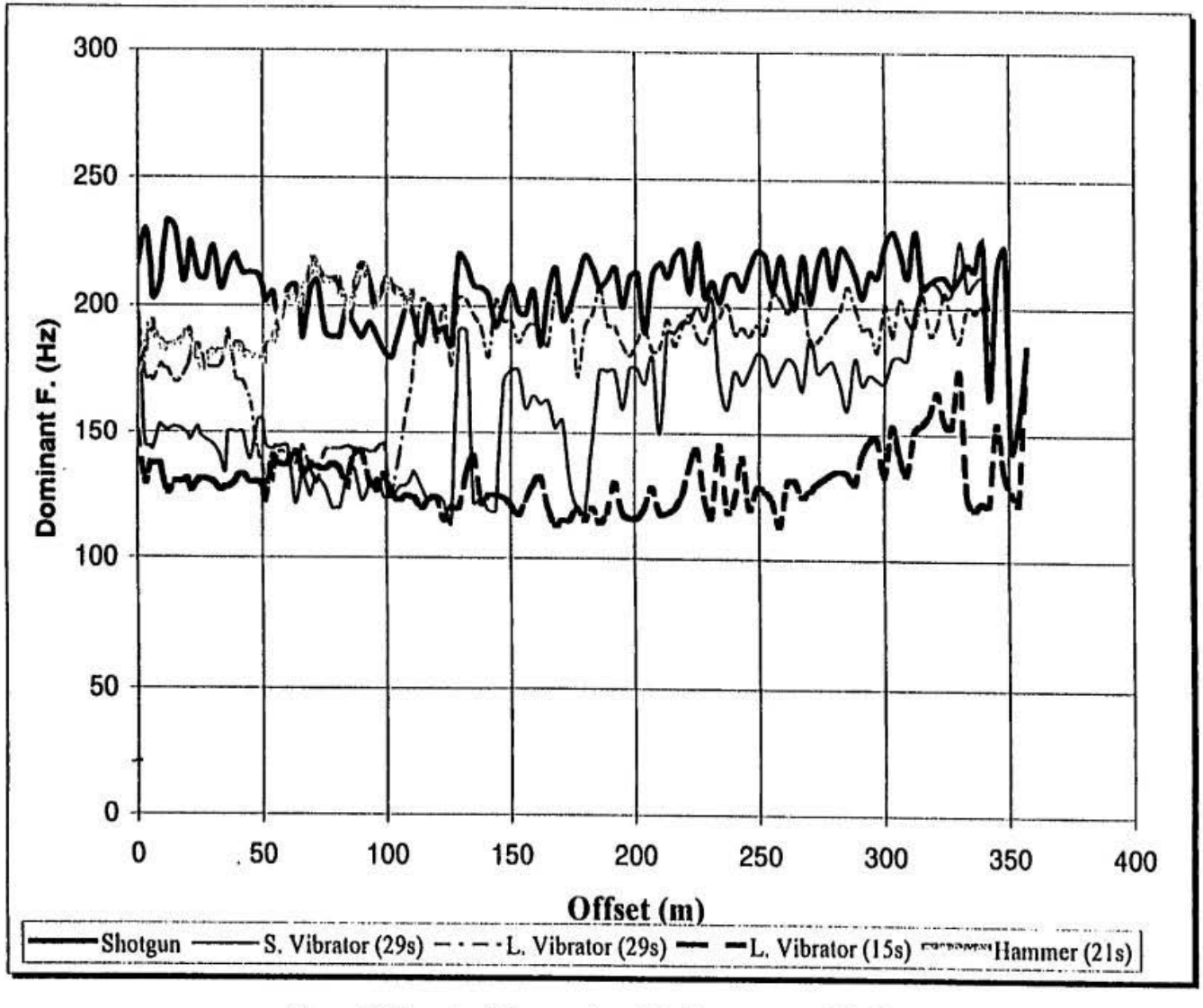

Figure 40 Dominant frequencies of the five sources with offset

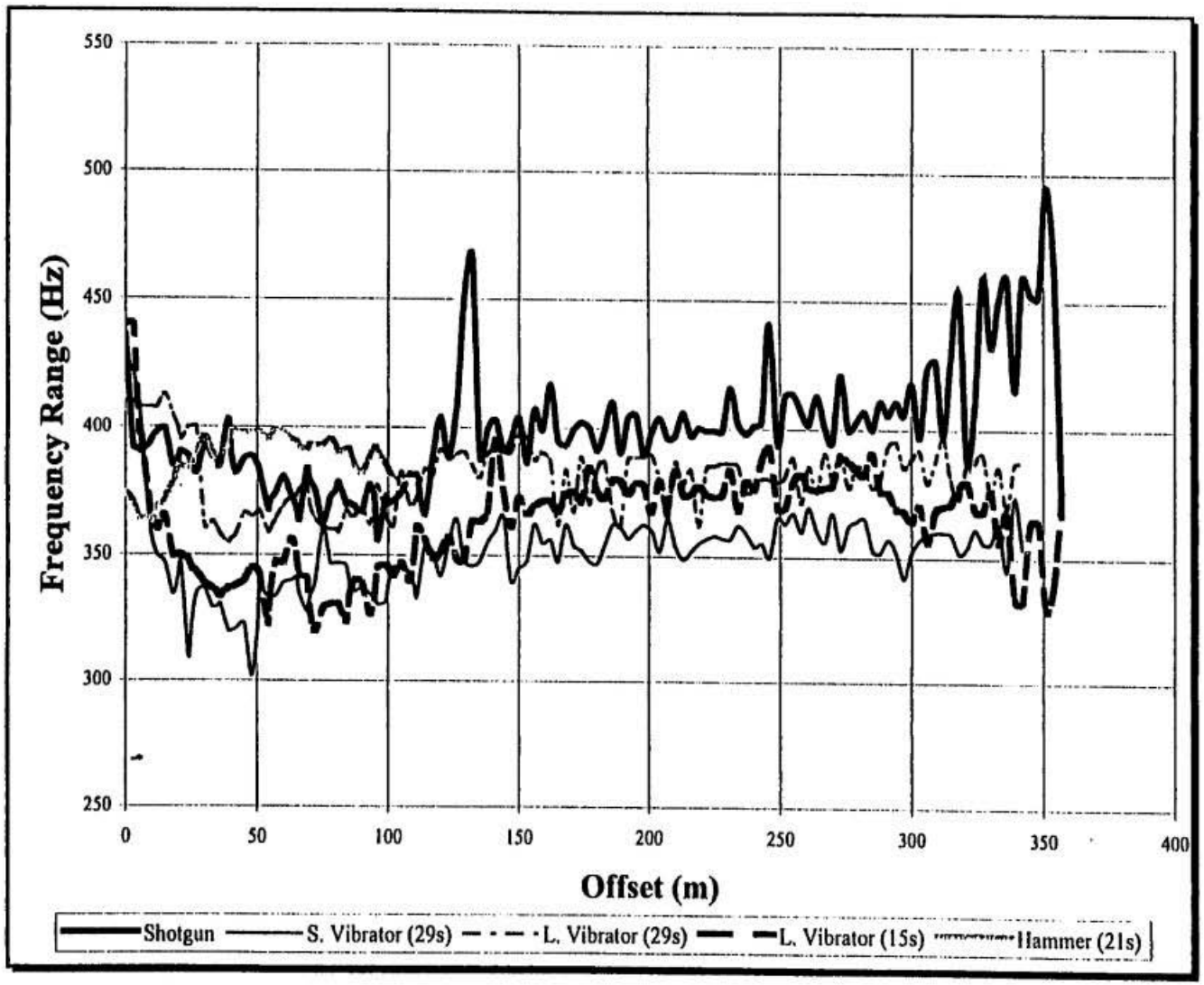

Figure 41 Frequency range (at –20dB) with offset

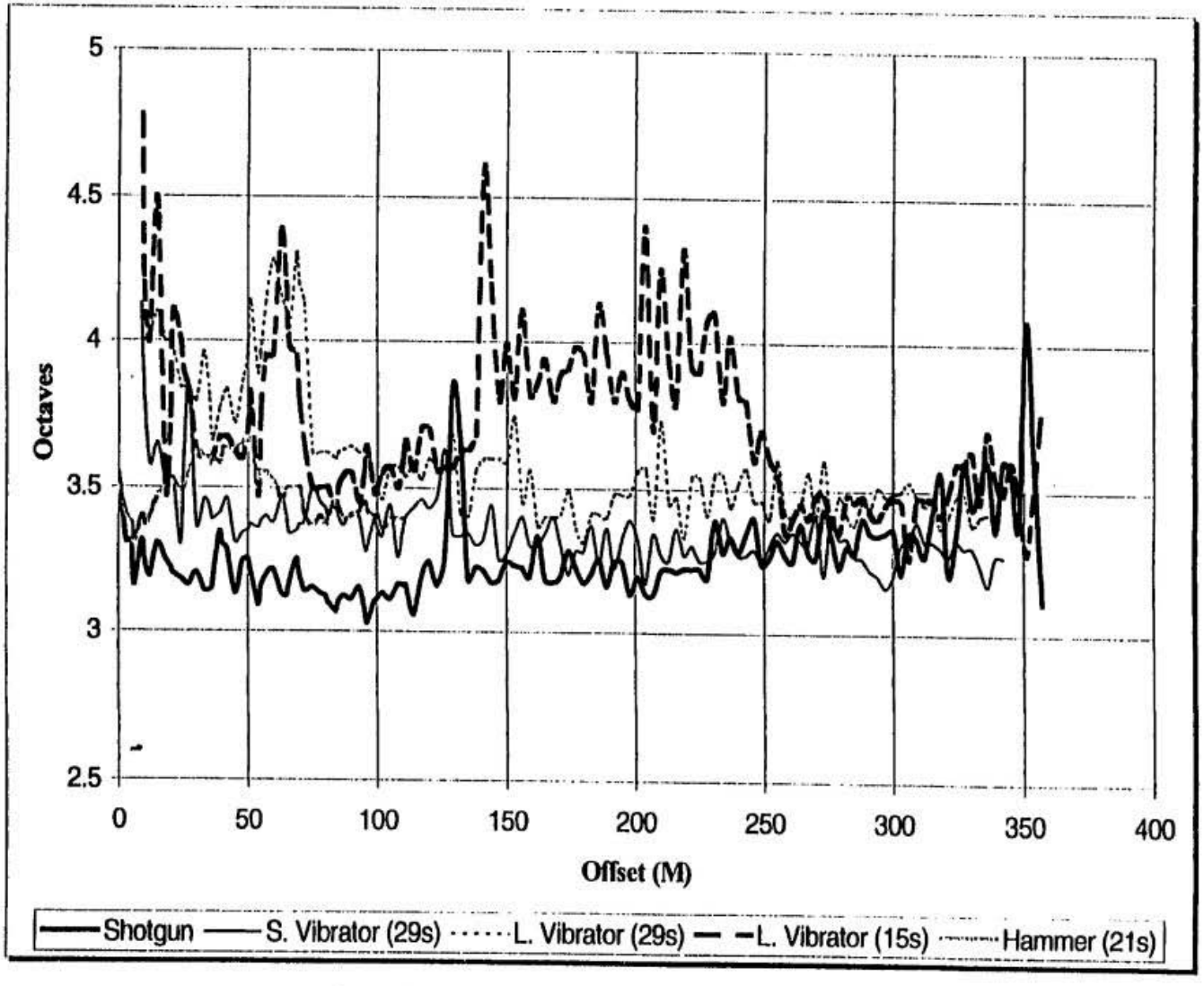

Figure 42 The frequency bandwidth in terms of octave

Figure 40 indicates that the shotgun has the highest dominant frequency. For the SIST vibrator sources, the large vibrator has a higher dominant frequency than the small one. Recording time also affects the frequency content because the frequency of the input wave increases with time. The large vibrator with a 29s recording time has a much higher dominant frequency than the same vibrator with a 15s recording time; furthermore, even the small vibrator with a 29s recording time has a higher dominant frequency than the large one with a 15s recording time.

For near offsets (<100m), the shotgun contains much higher frequencies, but all other sources contain lower frequency content that changes irregularly since the air blast and ground roll contribute unevenly. On far offsets (>100m), the frequencies for all sources increase more or less and keep constant individually except for the small vibrator. Within 110 m, the hammer source's dominant frequency is higher than that of the SIST vibrators and even higher than that of shotgun after 60m. Because its offset is limited to 110 m, the hammer source is impossible to be compared with others for far offsets.

Figure 41 clearly shows that the frequency range has less dependence on offset. After an offset of 150m, they are constant with offset. Among them, the shotgun has the highest bandwidth range at 400 Hz, large vibrators with 29s and 15s recording time have the same value at 380 Hz, and small vibrator offers the lowest one at about 360 Hz. For the same reasons discussed for the dominant frequency, the frequency ranges within near offsets (<100M) fluctuate and they are lower than those for far offsets. The hammer source has the highest value at near offsets.

However, the frequency range alone does not control the frequency affect on resolution properly. Instead, the frequency bandwidth in terms of octaves provides a better explanation. Figure 42 shows the bandwidth with offset, in which the result is something different from that of Figure 41. Large vibrators with both 15s and 29s have higher bandwidth, while the shotgun has the lowest. After offsets of 250m, the bandwidth of all sources tends to be the same at about 3.4 octaves. Table 2 lists the average dominant frequency, frequency range and bandwidth for all sources.

Table 2 Average dominant frequency, frequency range and bandwidth

	Dominant frequency (Hz)	Frequency range (Hz)	Frequency bandwidth (octave)
Shotgun	207	401	3.3
S. Vibrator (29s)	161	352	3.4
L. Vibrator (29s)	181	381	3.5
L. Vibrator (15s)	131	364	3.8
Hammer	194	386	3.5

From a resolution point of view, Widess (1973) defined a layer to be "thin" when its thickness was less than $\lambda/8$, and the maximum resolution achievable may not be better than $\lambda/4$ in practice. Wavelength λ equals to v/f thereby the maximum resolution limit is (v/f)/4. For horizontal resolution, an absolute limit is set by the width of the first Fresnel zone. The diameter of first Fresnel zone, D, is related to the depth of reflector, z, and the dominant wavelength λ (Brouwer and Helbig, 1998).

$$D = \sqrt{\lambda z} \quad \ldots\ldots\ldots\ldots\ldots\ldots\ldots\ldots\ldots\ldots \quad (4.4)$$

Approximately, the velocity v was picked on the data set as 5200 m/s for test 2 and 3, and 4000m/s for test 1. Thus, the maximum resolution limit and diameter of first Fresnel zone can be calculated easily and are listed in Table 3.

Table 3 The maximum resolution limit and the diameter of first Fresnel zone

	Average dominant Frequency (f) (Hz)	Maximum Resolution limit [(v/f)/4] (m)	Diameter of first Fresnel zone $[D=(\lambda z)^{1/2}](m)$
Shotgun	207	6.3	$5.0\ z^{1/2}$
Small Vibrator(29s)	161	8.0	$5.7\ z^{1/2}$
Large Vibrator(29s)	181	7.2	$5.3\ z^{1/2}$
Large Vibrator(15s)	131	9.9	$6.3\ z^{1/2}$
Hammer (21s)	194	5.2	$4.6\ z^{1/2}$

4.3. Energy Versus Offset

Energy level is another important parameter to be compared. Usually, seismic energy attenuates exponentially with distance because of absorption. To obtain an estimate of the relative amounts of seismic energy with offset, relative energy was computed by summing the squares of the amplitude coefficients. The amplitude coefficients are the individual values depicting the amount of signal at particular frequencies.

Ideally, separating different waves and comparing energy from the identical wave is the best way; however, the current data is not good enough to separate different waves properly, thus all waves are included to calculate the energy in this research. Similar to the processing to assess frequency content, an offset sort was completed to get an average energy at different offsets. The result is illustrated in Figure 43.

Energy attenuates exponentially within 100 m. The energy of the shotgun data is the largest and the large vibrators (both 29s and 15s) have more energy than the small vibrator. Obviously, the hammer has lowest energy level, which is about one order lower than that of all the other sources. Beyond 100m, the attenuation rate reduces greatly and the difference in energy from all sources is slight.

The energy was calculated for particular frequencies by the square of the amplitude coefficients at particular frequencies. Since the traces within the offset less than 84m contain air blast and ground roll that failed to be removed by f-k filtering, the energy versus frequency is divided into two parts. One part contains air blast and ground roll

(offset<84M) and the other does not (84M<offset<360M). They are shown in Figure 44 and Figure 45 respectively.

The average relative energy within 84 m (Figure 44) is about three to four times greater than that beyond 84 m (Figure 45). This is due to the geometrical spreading, and the inclusion of the ground roll and the air blast energy. This result agrees with the source test in New Jersey and California (Miller et al, 1986). It is especially noted that the shotgun contributes the largest energy level within 84 m while the large vibrator with 15s recording time becomes the most powerful source beyond 84 m.

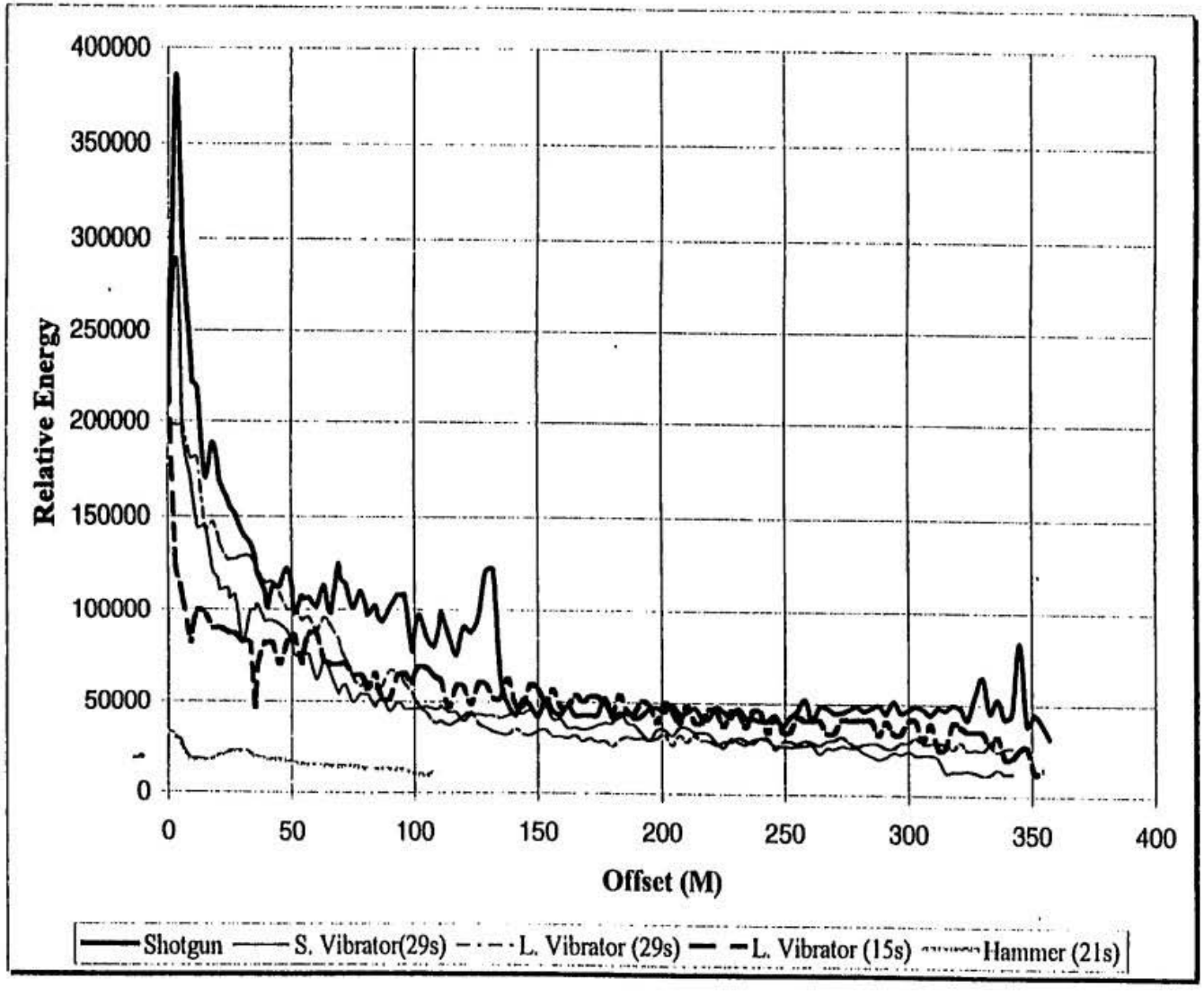

Figure 43 Relative energy with offset for all five sources

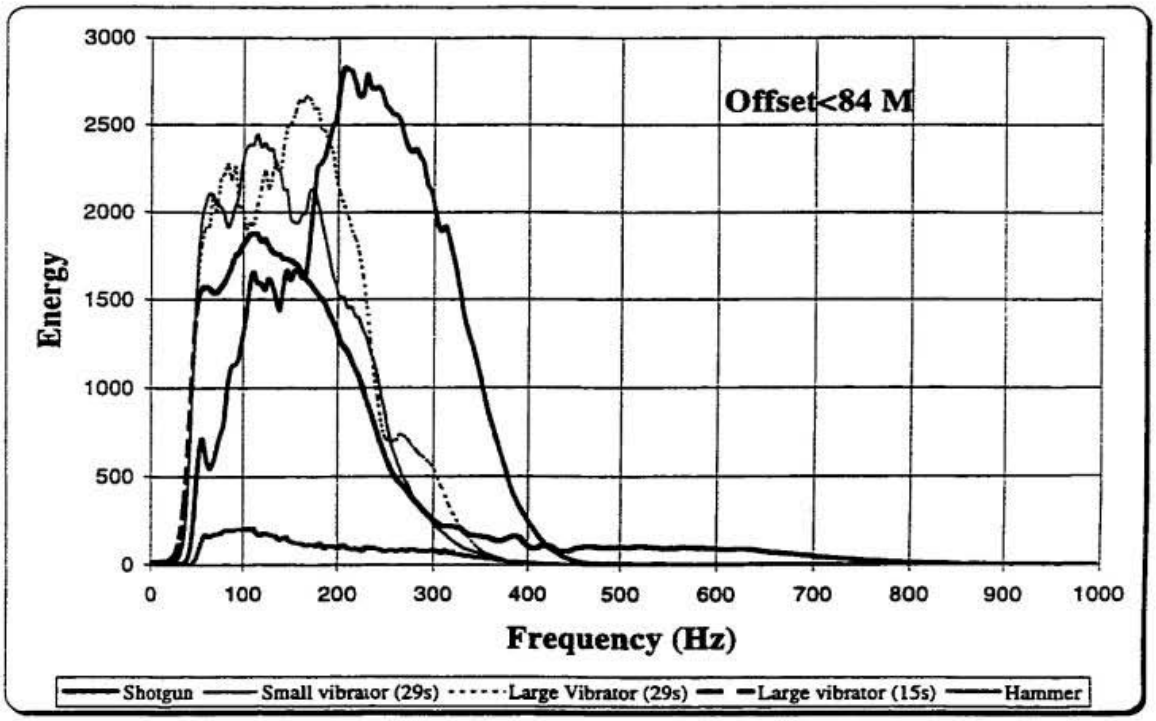

Figure 44 A comparison of relative energy versus frequency (with air blast and ground roll)

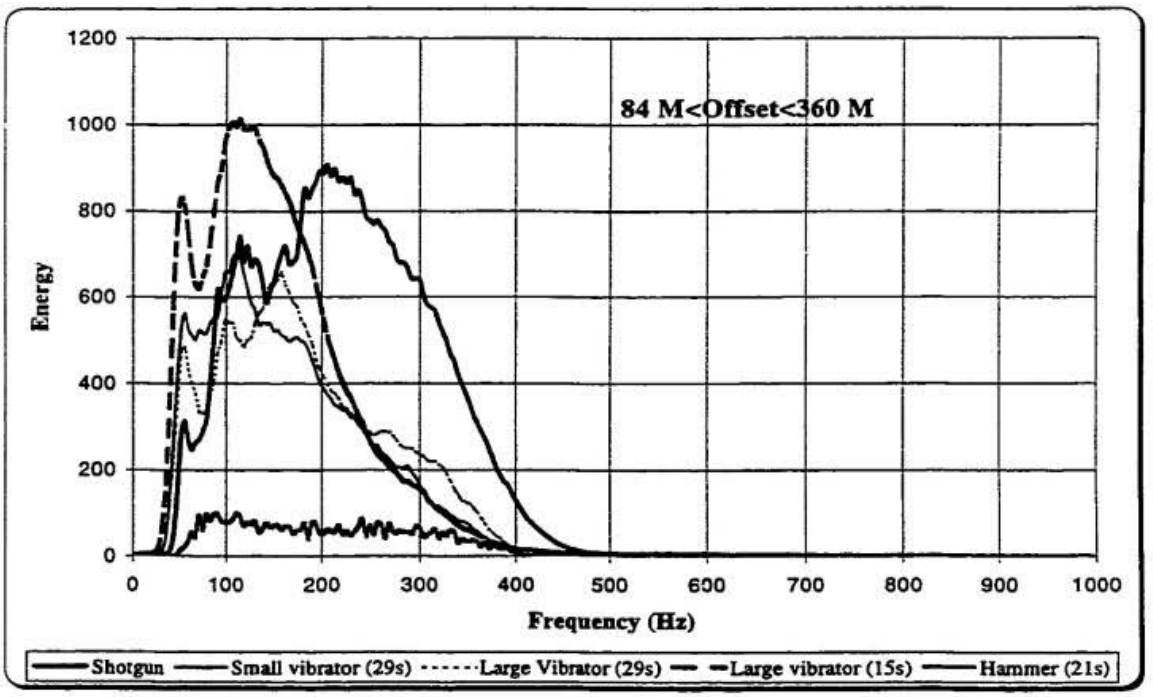

Figure 45 A comparison of relative energy versus frequency (without air blast and ground roll)

Chapter 5. Geological Interpretation

5.1. Geological Setting

The test site for both test 2 and test 3 is located on the Avalon Peninsula, Newfoundland along the Atlantic coast. The seismic array crosses most of the Middle Cove Member (5a) in the Mistaken Point Formation of the Conception group (See Figure 14).

Previous detailed geological mapping at the test site has not been done, but King's (1990) work assesses the regional geological setting. The Conception Group occurs throughout the Avalon Peninsula and is dominated by green to grey siliceous sedimentary rock. The Group outcrops in a 12-km-wide belt between the coastal ranges. The Conception Group is divided into five formations, two of which outcrop in the test site area are the Drook Formation (unit 4) and the Mistaken Point Formation (unit 5).

Green, siliceous volcaniclastic sedimentary rocks of the Drook Formation constitute much of the Conception Group throughout Avalon Peninsula. The average thickness throughout the Formation is 1500 m. The Mannings Hill Member (4d) has characteristic white to yellow and green-weathering thick beds of siliceous sandstone that make the Drook Formation distinctive.

The Mistaken Point Formation corresponds to the upper part of the Torbay Slate. It is composed of relatively less competent rocks than the underlying Drook Formation and forms a structural zone characterized by open to tight folds. The stratigraphic thickness of the formation ranges between 300 to 500 m. The Middle Cove Member (5a) consists of

medium-bedded, graded, fossiliferous sandstone and intercalated variegated tuffs that are present in the lower part of the Mistaken Point Formation. These rocks are well exposed in a 1-km-long coastal belt to the north of Middle Cove. They are a very thick, red tuffaceous mudstone-siltstone unit prominently exposed in steeply dipping beds. Red mudstone and lithic tuff (up to 2 m thick) are interbedded with very fine grained turbidites throughout the unit. Variable amounts of lithic fragments occur in most beds and are mainly rhyolite, rhyolite porphyry, ignimbrite and granophyre.

Figure 46 illustrates the composite stratigraphic section of both the Drook Formation and the Mistaken Point Formation.

King's (1990) regional mapping indicates an open fold (synform) in the Middle Cove Member along the profile of the test 2 and test 3. The Middle Cove Member overlies the Mannings Hill Member and it is this contact that is imaged seismically. The lithologies of the two members are similar and it is likely that it is the change in competency between the Mistaken Point Member and the Mannings Hill Member that gives rise to the reflection.

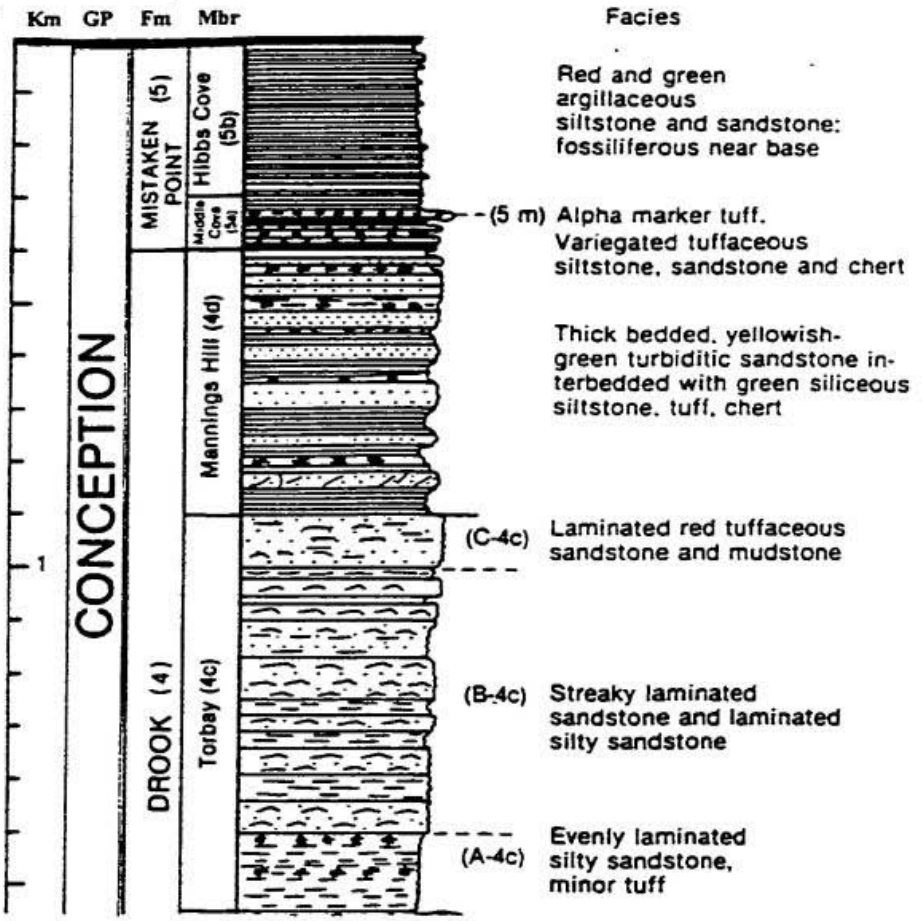

Figure 46 Composite stratigraphic sections of the test 2 - 3 site (after King, 1990)

5.2. Interpretation

Figure 47 to Figure 50 display the four CMP stacked profiles for comparison, in which the vibrator lines are cut short to coincide with the length of the shotgun line.

At the west end (lower CMP number) of the shotgun stacked section (Figure 47), deeper reflectors dominate and the signal is weak. The deepest reflector is located at about 140 ms of two way time. After CMP location 40, four shallower events become prominent with strong signal enhancement and have a similar dip to the east.

In the middle CMP locations of the hammer section (Figure 48), two strong events appear between 40ms and 60 ms. At 20 ms, a reflector crosses the entire profile with weak signal on the middle CMP locations. Because the hammer data were collected at a different site, it is impossible to compare its section with the other sections. It is presented solely to illustrate the quality of the stack to be expected.

Test 2 includes both large and small vibrators with 29s recording time. Because only three shots for each vibrator are available, the fold is not enough to apply CMP stacking well. Thus six shots from two vibrator sources are used together to produce the CMP stack (Figure 49). Lower CMP locations (1 to 60) yield both shallow and relatively deep events while there are only shallow events on the middle CMP locations (60 to 100). These are similar to that of shotgun except the events have higher frequencies and closer events can be separated. After CMP 100, five strong events become clear between 20 ms

and 60 ms. Like the shotgun stacked section, reflectors are not continuous across the entire profile.

The data of the test 3 also yields more events but fails to show the events as clearly as test 2 (Figure 50). A possible reason for this may be the replacement of the pilot trace and the irregular recording time delay on different shots. However, by careful interpretation, the events corresponding to those in test 2 can still be distinguished at almost same locations.

Figure 51 highlights the same event on both the test 2 and the test 3 stacked section. The depth of the event is about 104 m at the center (CMP 70). Compared to the geological structure under the seismic line (Figure 14b), the synform with dip of 20-25° could be about 110 m deep at the center (Figure 51c). The SIST data yield a clear event corresponding to the base of the Middle Cove Member.

Obviously, the SIST vibrator (29s) line (Figure 49) has much better signal-to-noise ratio and is higher resolution than the shotgun data. Although the SIST data (15s) fails to achieve a high quality CMP stack profile, it still provides an improved image compared to the shotgun and shows the potential for shallow high resolution surveying with the SIST technique.

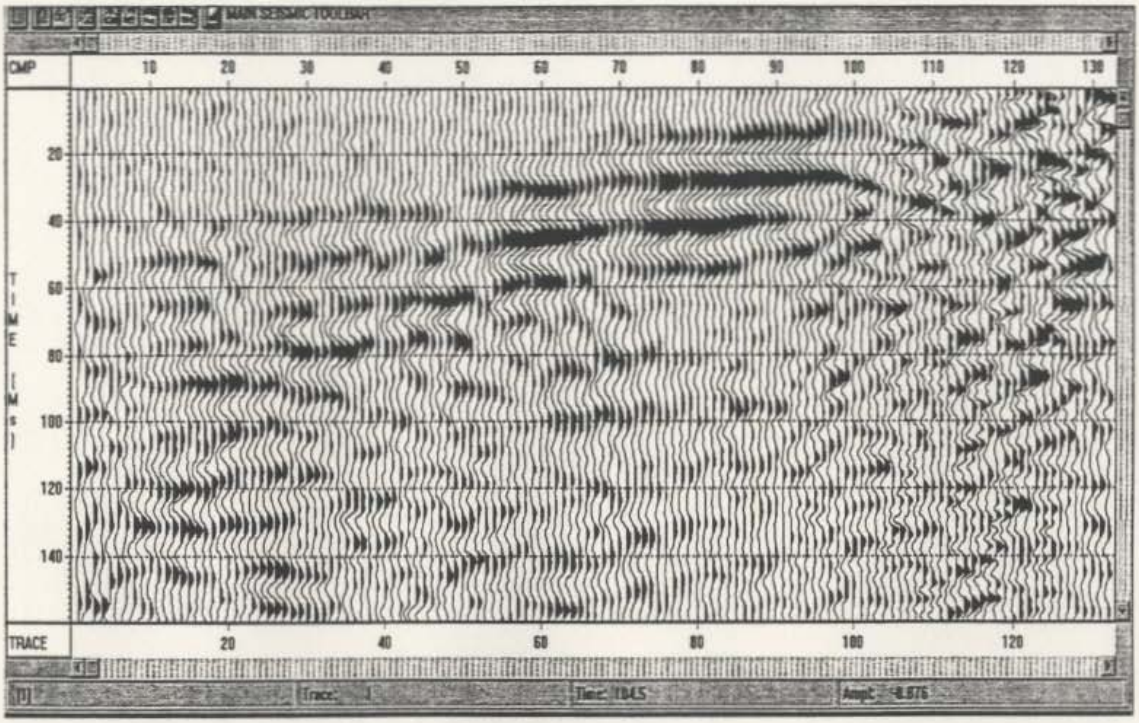

Figure 47 Brute Stack for shotgun data

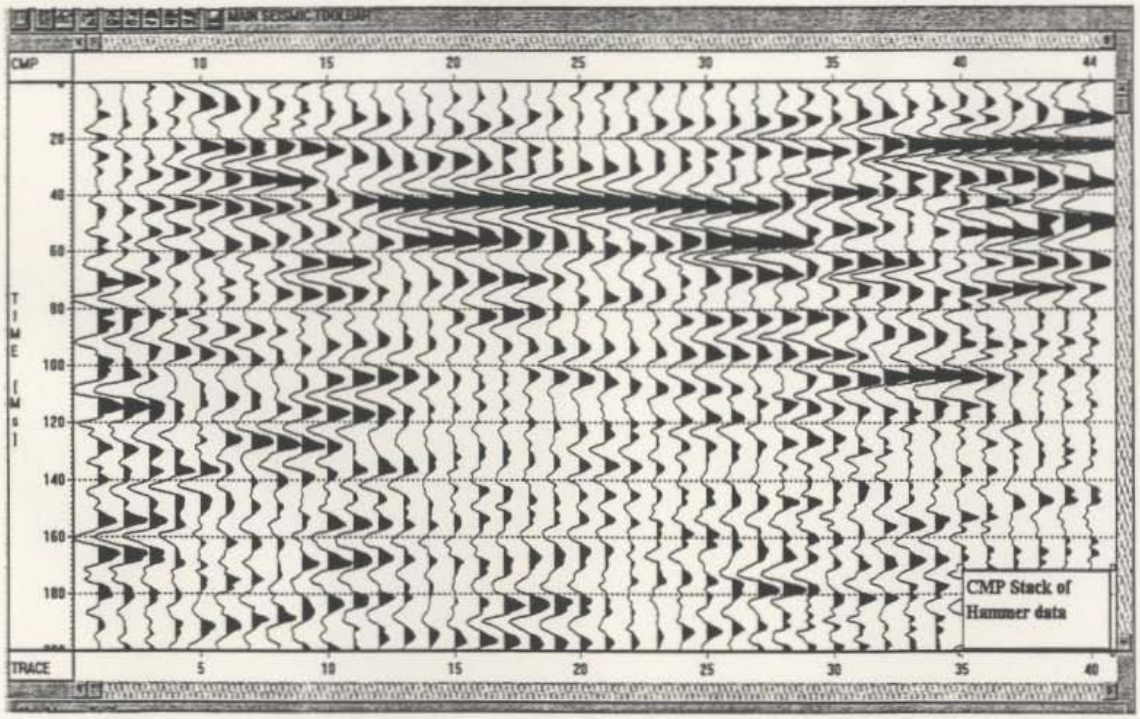

Figure 48 Brute stack for Hammer source data

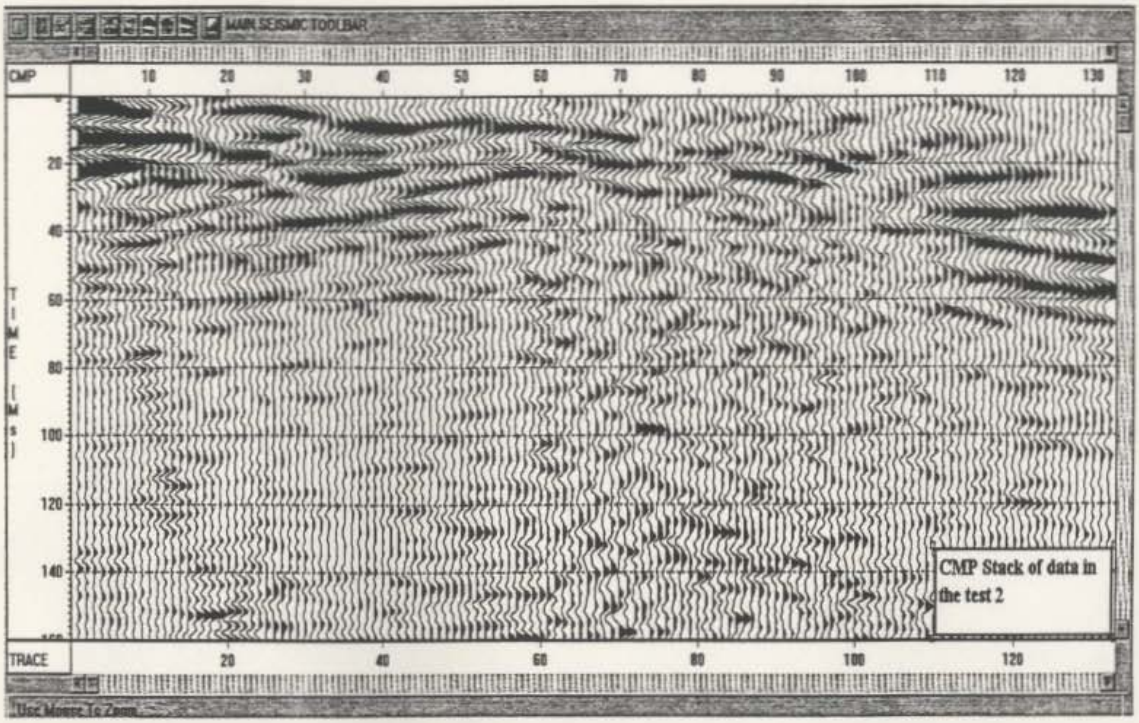

Figure 49 Brute stack for the data of test 2 (both Large and small vibrators, 29s)

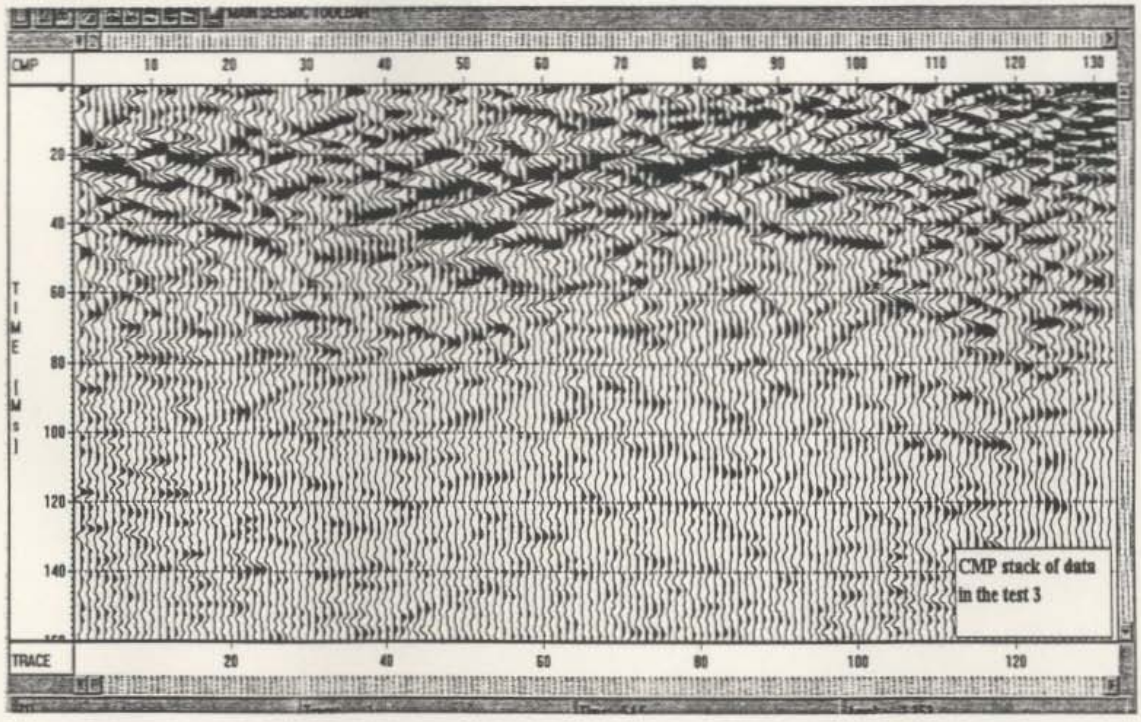

Figure 50 Brute stack for the data of test 3 (Large vibrators, 15s)

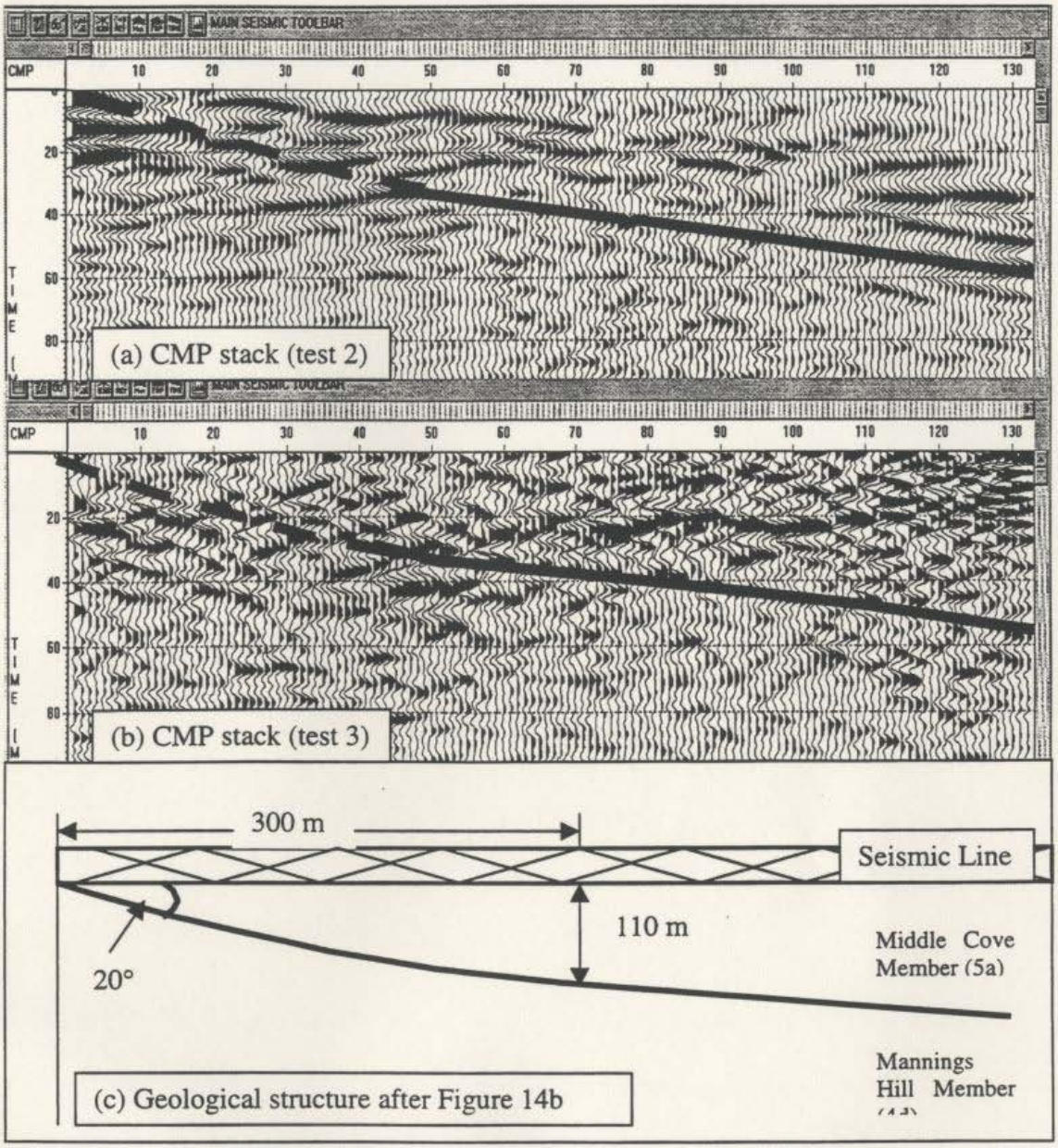

Figure 51 Comparison of SIST stack and geological structure

5.3. Penetration Depths and Limitation

The penetration depth depends on the energy level and frequency content of the source. A larger energy source can achieve deeper penetration while a higher frequency leads to reduced penetration but improved resolution.

The stacked sections indicate that the two-way penetration times are ~100ms, ~60ms and ~60ms for shotgun, the SIST vibrators and the hammer sources respectively. For the velocities 5200m/s for the test 2-3 site and 4000m/s for the test 1 site, the corresponding penetration depths are ~260m, ~150m and ~120m respectively.

The penetration depths in this research are not entirely satisfactory. The 12 gauge shotgun used in this research provides small energy. This weak energy results in the shallow penetration depth. Furthermore, the SIST vibrators generated much weaker energy than shotgun, so as the reflections seldom appear on the data set. The hammer usually offers the weakest energy, which yields the shallowest depth.

Referring to the unstacked data sets is helpful to consider this issue. Figure 25 to Figure 29 display the best shot gathers from each of the different sources. Reflections can be seen at very shallow depths on the shotgun and the large vibrator (29s). The remaining sources fail to provide clear reflections.

The most convincing conclusions arise from the site geological structure. Because the Middle Cove Member (5a) and the Mannings Hill Member (4d) have similar lithologies, their impedance is not markedly different, so the boundary between them could not give

rise to a strong reflection. In the 4d Member, the geological makeup is uniform and seldom provides reflections. In addition, the depth of the base of 4d Member is inferred to be more than 1000 m, which is too deep to be detected by any of these sources.

In addition to the geological structure, data acquisition may be another cause of poor reflections. In this research, the recording system failed to keep the recording delay time identical for each shot due to triggering problems. Before processing, all shot gathers needed to be shifted to a nominal 0 ms manually. Even though this was done meticulously, it is still hard to decide the exact time to be shifted. A difference of even 2-3 ms can destroy the stacking of a reflection.

Chapter 6. Conclusions

In order to study the ability of the vibratory sources to achieve high resolution in near-surface seismic imaging, this research compares three SIST (Swept Impact Seismic Technique) sources and a hammer source with a shotgun source in terms of dominant frequency, frequency bandwidth, energy level, CMP stack and penetration depth. Even though the portable vibratory sources require more effort to achieve superb seismic results, they offer good comparisons for parameter characteristics and interpretation.

Table 2 lists the average dominant frequency and bandwidth of all five sources. The shotgun is the most broadband with a dominant frequency at 207 Hz; the hammer is the second best with 194 Hz. For the three SIST vibrators, the longer recording time generates higher dominant frequencies than the shorter time, and the larger vibrator offers higher dominant frequencies than the smaller one when their recording times are same. Table 3 lists the maximum resolution limit and diameter of first Fresnel zone, which indicates that the best ranking of sources in terms of resolution is a hammer, shotgun, large SIST vibrator (29s), small SIST vibrator (29s) and large SIST vibrator (15s).

However, the SIST vibrators have a higher frequency bandwidth than the shotgun. The large SIST vibrator (15s) has the highest bandwidth of 3.8 octaves. The large SIST vibrator (29s) shares the next best with the hammer at 3.5 octaves, and the shotgun has the smallest bandwidth at 3.3 octaves.

In the near offset (<140m), the energy level of all sources attenuates exponentially with offset. The shotgun generates the strongest energy that is much higher than that of the SIST vibrators. Among the three SIST vibrators, the strongest energy order is large (29s), small (29s) and large (15s). The hammer gives the weakest energy among the five sources and its absolute value is about one order smaller than that of the large vibrator (15s). Beyond offset 140m, the energy attenuation rates become very slight and the shotgun has almost same energy as SIST vibrators. No hammer data is available in this offset range.

Compared with the shotgun, the SIST vibrator CMP stacked sections show higher frequency. Higher frequency bandwidth makes the SIST vibrator capable of better detection of shallow events than the shotgun. On the other hand, the weaker energy limits the SIST vibrator's penetration to about 150 m in depth, while the shotgun attains 260m.

In conclusion, based on their overall performance, especially as evidenced in the stacked section, the SIST vibrator sources used in this research show a great deal of potential to be viable energy sources for high resolution shallow surveys. Their penetration depth, about 150 m, is deep enough for environmental applications, i.e. ground water, but insufficient for mineral exploration, where a target depth of up to 500 m is expected. Imaging to 500 m depth may be attainable by using multiple SIST sources concurrently.

References:

Al-Sadi, H.N., 1980, Seismic exploration: Technique and processing: Birkhauser Verlag Basel, Boston

Baeten, G., and Ziolkowski, A.,1990, The VIBROSEIS Sources, Advances in Exploration Geophysics: Elsevier Science Publishers.

Barbier, M.G., 1982, Pulse coding in Seismology: International Human Resources Development Corporation, Boston.

Berkhout, A.J., 1984, Seismic Resolution: A Quantitative Analysis of Resolving Power of Acoustical Echo Techniques: Geophysical Press, London-Amsterdam.

Black, R.A., 1996, Swept Impact Seismic Technique (SIST): Geophysics, **61**, 1789-1803.

Brouwer, J., and Helbig, K., 1998, Shallow High-Resolution Reflection Seismics: In Handbook Of Geophysical Exploration. Elsevier, Amsterdam.

Burger, H.R., 1992, Exploration Geophysics of the Shallow Subsurface: Prentice Hall, Englewood Cliffs.

Cosma, C., and Enescu, N., 1999, Characterization of Fractured Rock in the Vicinity of tunnels by the Swept Impact Seismic Technique. (Vibrometric technical report)

Cosma, C., Enescu, N., Heikkinen, P., Keskinen, J., and Larion, L., 1998, Seismic investigations at the Grimsel test site and integrated interpretation of results: B-RP VIB 98-001, ANDRA

Geyer, R.L., 1970a, The VIBROSEIS system of seismic mapping: Journal of the Canadian Society of Exploration Geophysicists, **Vol.6 No.1**

Geyer, R.L., 1970b, VIBROSEIS parameter optimization: Oil & Gas Journal, **April 13, April 27**, 114-116.

Greenhalgh, S.A., and Emerson, D.W., 1986, Elastic properties of coal measure rocks from the Sydney Basin, New South Wales: Explor. Geophys., **17,** 157-163.

Helbig, K., Brouwer, J., Dankbssr, J.M., and Jongerius, P., 1985, Shallow high resolution seismics on tidal flats: Acquisition Technology: 55th Ann. Internat. Mtg., Society of Exploration Geophysicists, 165-167.

Hunter, J.A., Pullan, S.E., Burns, R.A., Gagne, R.M., and Good, R.L., 1984, Shallow seismic reflection mapping of the overburden-bedrock interface with the engineering seismograph— Some simple techniques: Geophysics, **49,** 1381-1385

Jenkins, F.A., and White, H.F., 1957, Fundamentals of optic: New York, McGraw-Hill

Jongerius, P., and Helbig, K., 1988, Onshore high resolution seismic profiling applied to sedimentology: Geophysics, **53**, 1276-83

King, A.F., 1990, Geology of the St. John's area, Report 90-2: Geological Survey Branch, Department of Mines and energy, Government of Newfoundland and Labrador.

Li, X.P., Sollner, W., and Hubral, P., 1995, Elimination of harmonic distortion in vibroseis data: Geophysics, **60,** 503-516

Li, X.P., 1997, Elimination of ghost noise in vibroseis data by deconvolution: Geophysical Prospecting, **45**, 909-929

Martin, J.E., and Bacon, W.M., 1993, Simultaneous vibrosis recording: Geophys. Prosp., **41**, 943-967.

Miller, R.D., 1992, Normal moveout stretch mute on shallow-reflection data: Geophysics, **57**, 1502-1507

Miller, R.D., Pullan, S.E., Waldner, J.S., and Haeni, F.P., 1986, Field comparison of shallow seismic sources: Geophysics, **51,** 2067-2092

Miller, R.D., Pullan, S.E., Steeples, D.W., and Hnter, J.A., 1992, Field comparison of shallow seismic sources near Chino, California: Geophysics, **57,** 693-709.

Nickerson, W., 1993, Seismic Data Processing for Engineering and Environmental Application: Course note presented at the Geophysical Section of the Geological Survey of Botswana in Lobatse.

Pullan, S.E., and Hunter, J.A., 1985, Seimic model studies of the overnurden-bedrock reflection: Geophysics, **50**, 1684-1688.

Pullan, S.E., and Hunter, J.A., 1990, Delineation of buried bedrock valleys using the optimum offset shallow seismic reflection technique: Geotechnical and

Environmental Geophysics, **volume 3**: Society of Exploration Geophysicists Investigatios in Geophysics, 75-87.

Pullan, S.E., and MacAulay, H.A., 1987, An in-hole shotgun source for engineering seismic survey: Geophysics, **52**, 985-996

Reynolds, J.M., 1997, An Introduction to Applied and Environmental Geophysics: John Wiley & Son, Chichester.

Sallas, J.J., 1984, Seismic vibrator control and the downgoing P-wave: Geophysics, **49**, 731-740

Schepers, R., 1975, A seismic reflection method for solving engineering problems: J. of Geophysics, **41**, 367-384

Sharma, P. V., 1997, Environmental and Engineering Geophysics: Cambridge University Press, Cambridge.

Sheriff, R.E., 1985, Aspects of seismic resolution: In American Association of Petroleum Geologists Memoir 39, Seismic Stratigraphy II: An Integrated Approach

Sheriff, R.E., and Geldart, L.P., 1995, Exploration Seismology, 2nd edition: Cambridge University Press, Cambridge.

Spencer, C., Thurlow, G., Wright, J.A., White, D., Carrol, P., Milkereit, B., and Reed, L., 1993. A vibroseis reflection seismic survey at the Buchans Mine in central Newfoundland: Geophysics, **58,** 154-166

Steeples, D.W., and Miller, R.D., 1990, Seismic reflection methods applied to engineering. environmental, and groundwater problems: In Geotechnical and Environmental Geophysics. **Vol. 1**. Soc. Explor. Geophys., Tulsa pp1-30.

Steeples, D.W., and Miller, R.D., 1998, Avoiding pitfalls in shallow seismic reflection surveys: Geophysics, **63,** 1213-1224

Steer, D.N., Brown, L.D., Knapp, J.H., and Baird, D.J., 1996, Comparison of explosive and vibroseis source energy penetrating during COCORP deep seismic reflection profiling in the Williston Basin: Geophysics, **61,** 211-221

Widess, M.B., 1973, How thin is a thin bed?: Geophysics, **38,** 1176-1180.

Yilmaz, O., 1987, Seismic Data Processing: Society of Exploration Geophysicists, Tulsa.

Bibliography:

Anstey, N.A., 1963, VIBROSEIS gentle message obtains structural data safely, economically: Oil & Gas Journal, March 18, 110-118.

Bachrach, R., and Nur A., 1998a, High-resolution shallow-seismic experiments in sand, Part I: Water table, fluid flow, and saturation: Geophysics, **63**, 1225-1233

Bachrach, R., and Nur A., 1998b, High-resolution shallow-seismic experiments in sand, Part II: Water table, fluid flow, and saturation: Geophysics, **63**, 1234-1240

Black, R.A., Steeples, D.W., and Miller, R.D., 1994, Migration on shallow seismic reflection data: Geophysics, **59,** 402-410

Chapman, W.L., Brown, G.L., and Fair, D.W., 1988, The VIBROSEIS system: a high-frequency tool: Geophysics, **46:**

Cordier, Jean-Pierre, 1985, Velocities in Reflection Seismology: D. Reidel Publishing Company, Dordrecht, Holland.

Dieter V., 1995, Environmental Geophysics — A Practical Guide: Springer—Verlag, Berlin.

Dobrin, M.B., and Savit, C.H., 1988, Introduction to Geophysical Prospecting, 4th Edition: McGraw-Hill Book Company, New York.

Dohr, G., 1981, Applied Geophysics— Introduction to Geophysical Prospecting: Halsted Press, New York.

Evans, A.M., 1995, Introduction to Mineral Exploration: Blackwell Sciences Ltd., Oxford.

Foufoula-Georgiou, E., and Kumar, P., 1994, Wavelets in Geophysics: Academic Press, San Diego.

Geissler, P.E., 1989, Seismic reflection profiling for groundwater studies in Victoria, Australia: Geophysics, **54,** 31-37.

Gendzwill, D.J., and Brehm, R., 1993, High resolution seismic reflections in a potash mine: Geophysics, **58,** 741-748.

Ghose, R., 1998, Shallow to very shallow, high-resolution reflection seismic using a portable vibrator system: Geophysics, **63,** 1295-1309

Gibowicz, S.J., and Kijko, A., 1993, An Introduction to Mining Seismology: Academic Press, San Diego.

Goupillaud, P.L., 1976, Signal design in the "VIBROSEIS" technique: Geophysics, **41,**

Hatton, L., Worthington, M.H., and Makin, J., 1986, Seismic Data Processing: Theory and Practice: Blackwell Scientific Publication, Oxford.

Jeng, Y., 1995, Shallow seismic investigation of a site with poor reflection quality: Geophysics, **60,** 1715-1726

Kanasewich, E.R., 1990, Seismic Noise Attenuation: Geophysical Press, London-Amsterdam.

Keys, W.S., 1997, A Practical Guide to Borehole Geophysics in Environmental Investigations: Lewis Publishers, Boca Raton.

Knapp, R.W., 1993, Energy distribution in wavelets and implications on resolving power: Geophysics, **58,** 39-46

Knapp, R.W., and Steeples, D.W., 1986a, High resolution common depth point seismic reflection profiling instrumentation: Geophysics, **51,** 276-282.

Knapp, R.W., and Steeples, D.W., 1986b, High resolution common depth point seismic reflection profiling instrumentation: Geophysics, **51,** 283-294.

Landrum, Ralph, A., Jr., 1967, Extraction of signals from random noise by crosscorrelarion: paper at 37th Annual International Meeting of Society of Exploration Geophysicists in Oklahoma.

Lankston, R.W., 1990, High-resolution seismic data acquisition and interpretation: In Geotechnical and Environmental Geophysics, **Vol. 1**. Soc. Explor. Geophys., Tulsa, PP 45-74.

Marschall, R., 1990, Aspects of Seismic Reflection Data Processing: Kluwer Academic Publishers, Dordrecht.

Mendecki, A.J., 1997, Seismic Monitoring in Mines: Chapman & Hall, London.

Miller, R:D., Anderson, N.L., Feldman, H.R., and Franseen, E.K., 1995, Vertical resolution of seismic survey in stratigraphic sequences less than 100 m deep in southeastern Kansas: Geophysics, **60,** 423-430

Miller, R.D., and Steeples, D.W., 1994, Application of shallow high-resolution seismic reflection to various environmental problems: J. Appl. Geophys. **31,** 65-72.

Milsom, J., 1996, Field Geophysics: John Wiley & Sons, Chichester.

Nelson, H.R., 1983, New Technologies in Exploration Geophysics: Trends and New Developments in Exploration Methods Using Reflection Methods: Gulf Publishing Company.

Okaya, D.A., Karageorg, E., McEvilly, T.V., and Malin, P., 1992, Removing vibrator-induces correlation artifacts by filtering frequency-uncorrelated space: Geophysics, **57,** 916-926

Parker, J.C., Pelton, J.R., and Dougherty, M.E., 1993, A versatile shotgun source for engineering and groundwater seismic surveys: Geophysics, **58,** 1511-1516

Polom, U., 1997, Elimination of source-generated noise from correlated vibroseis data (the 'ghost-sweep' problem): Geophysical Prospecting, **45,** 571-591

Pritchett, W.C., 1990, Acquiring Better Seismic Data: Chapman and Hall, New York.

Scales, J.A., 1995, Theory of Seismic Imaging: Springer-Verlag, Berlin.

Scherbaum, F., 1994, Basic Concepts in Digital Signal Processing for Seismologists: Springer-Verlag, Berlin.

Schrodt, J.K., 1987, Techniques for improving VIBROSEIS Data: Geophysics, **52,** No.4

Steeples, D.W., 1984, High-resolution seismic reflections at 200 Hz: Oil & Gas Journal, **Dec. 3**

Tantham, R.H., and McCormack, M.D., 1991, Multicomponent Seismology in Petroleum Exploration: Society of Exploration Geophysicists, Tulsa.

Waters, K.H., 1981, Reflection Seismology: A Tool For Energy Resource Exploration, 2nd edition: John Wiley & Son.

Ziolkowski, A.M., and Lerwill, W.E., 1979, A simple approach to high resolution seismic profiling for coal: Geophysical Prospecting, **27,** 360-393.

Appendix A: Table of f_{max}, Δ and R_f

Table of dominant frequency, frequency range and bandwidth (octave) with offset

Offset	Shotgun				S. Vibrator (29s)				L. Vibrator (29s)				L. Vibrator (15s)				Hammer (21s)			
	No.	Fmax	f2-f1	Rf	No.	Fmax	f2-f1	Rf	No.	Fmax	f2-f1	Rf	No.	Fmax	f2-f1	Rf	No.	Fmax	f2-f1	Rf
0	5	217	436	3.54	3	196	429		3	197	410		38	150	440		16	175	374	3.5
3	9	230	392	3.31	6	145	421		6	172	410		75	130	440					
5																	18	193	364	3.37
6	9	203	390	3.16	6	143	400		6	171	408		73	137	397					
9	5	209	393	3.31	6	153	364	4.13	6	177	408	4	42	137	371	4.78				
10																	17	183	363	3.37
12	8	233	398	3.19	6	151	350	3.58	6	175	408	4	71	126	360	4				
15	8	230	399	3.3	6	152	347	3.65	6	170	413	4.1	72	130	365	4.49	18	185	372	3.47
18	5	210	385	3.25	6	151	335	3.52	6	173	405	4	40	130	350	3.5				
20																	18	190	384	3.5
21	7	225	390	3.2	6	147	347	3.53	6	181	395	3.98	70	127	350	4.1				
24	7	212	388	3.18	6	152	310	3.3	6	185	400	3.84	69	130	348	4				
25																	18	175	384	3.5
27	5	211	382	3.16	6	147	335	3.85	6	177	400	3.84	41	131	343	3.83				
30	6	223	392	3.2	4	145	337	3.37	4	176	361	3.8	67	130	339	3.62	17	182	396	3.62
33	6	207	388	3.14	4	140	330	3.46	6	177	363	3.96	67	127	337	3.6				
35																	16	182	384	3.58
36	5	215	385	3.15	4	150	331	3.39	6	190	358	3.66	40	128	334	3.6				
39	5	220	403	3.34	4	150	320	3.41	6	172	355	3.77	66	130	337	3.67				
40																	14	185	398	3.63
42	5	213	382	3.28	4	150	321	3.46	6	170	358	3.83	66	133	338	3.67				
45	5	213	387	3.13	4	139	323	3.31	6	162	366	3.72	39	130	340	3.62	13	180	398	3.63
48	5	212	388	3.24	4	155	302	3.34	6	142	365	3.86	65	130	345	3.6				

Offset	Shotgun				S. Vibrator (29s)				L. Vibrator (29s)				L. Vibrator (15s)				Hammer (21s)			
	No.	Fmax	f2-f1	Rf	No.	Fmax	f2-f1	Rf	No.	Fmax	f2-f1	Rf	No.	Fmax	f2-f1	Rf	No.	Fmax	f2-f1	Rf
50																	11	178	398	3.67
51	5	202	382	3.21	4	145	336	3.37	6	130	367	4.14	65	123	342	3.82				
54	5	205	368	3.09	4	143	334	3.36	6	130	359	3.89	38	140	323	3.47				
55																	10	190	396	3.55
57	5	195	374	3.19	6	144	334	3.4	6	142	364	4.13	63	137	347	3.95				
60	5	206	380	3.21	5	144	339	3.38	5	140	369	4.28	63	137	347	3.95	9	203	398	3.52
63	5	208	373	3.13	6	122	340	3.46	6	137	372	4.16	37	142	356	4.38				
65																	9	200	394	3.5
66	5	188	364	3.16	6	133	335	3.34	6	144	375	4	61	133	342	3.99				
69	5	205	383	3.25	6	125	328	3.35	6	135	377	4.13	61	137	341	3.95				
70																	8	218	393	3.5
72	5	210	375	3.14	6	131	339	3.38	5	130	364	4.13	36	136	320	3.64				
75	5	190	363	3.15	6	128	360	3.5	5	142	361	3.62	59	135	329	3.5	8	210	393	3.37
78	5	188	372	3.13	6	120	347	3.45	5	143	360	3.62	59	137	331	3.5				
80																	7	210	392	3.37
81	5	188	378	3.1	6	120	347	3.41	5	143	359	3.62	35	135	331	3.5				
84	5	200	370	3.07	6	132	346	3.44	5	144	367	3.6	57	128	324	3.43				
85																	6	196	391	3.43
87	5	192	369	3.12	6	135	336	3.37	5	143	365	3.63	57	141	340	3.54				
90	5	188	367	3.11	6	123	337	3.41	5	143	368	3.64	34	141	339	3.55	5	216	382	3.4
93	5	193	377	3.15	6	129	335	3.4	5	142	362	3.62	55	130	327	3.45				
95																	4	200	392	3.45
96	5	188	356	3.03	6	131	331	3.28	5	143	377	3.64	55	127	345	3.64				
99	5	182	372	3.1	6	124	332	3.39	5	145	365	3.5	33	133	346	3.48				
100																	3	210	383	3.4
102	5	180	371	3.13	6	124	345	3.33	4	127	361	3.46	33	125	342	3.55				
105	5	190	374	3.11	6	128	345	3.44	4	140	382	3.57	53	123	347	3.57	2	205	379	3.39
108	5	200	381	3.16	6	129	343	3.26	4	160	370	3.57	32	125	340	3.5				
110																	1	205	379	3.39
111	5	195	381	3.16	6	134	334	3.4	4	182	372	3.54	51	124	361	3.66				

Offset	Shotgun				S. Vibrator (29s)				L. Vibrator (29s)				L. Vibrator (15s)				Hammer (21s)			
	No.	Fmax	f2-f1	Rf	No.	Fmax	f2-f1	Rf	No.	Fmax	f2-f1	Rf	No.	Fmax	f2-f1	Rf	No.	Fmax	f2-f1	Rf
114	5	185	366	3.06	6	128	353	3.43	4	202	383	3.57	51	120	356	3.56				
117	5	200	388	3.18	6	123	351	3.46	4	200	381	3.53	31	123	349	3.7				
120	5	190	404	3.24	6	125	342	3.43	4	186	391	3.6	49	124	351	3.7				
123	5	191	388	3.16	6	122	354	3.47	4	200	387	3.56	49	115	357	3.56				
126	5	185	407	3.24	6	114	364	3.63	4	177	389	3.56	29	120	349	3.57				
129	5	220	450	3.85	6	190	348	3.34	4	203	390	3.68	48	120	348	3.57				
132	5	216	466	3.65	6	190	346	3.33	3	202	385	3.41	47	133	363	3.63				
135	5	208	388	3.18	6	122	348	3.34	3	196	380	3.4	28	140	363	3.63				
138	5	207	399	3.22	6	124	355	3.3	3	191	389	3.56	46	122	367	3.68				
141	5	204	403	3.21	6	119	360	3.32	3	180	391	3.9	45	125	395	4.6				
144	5	192	391	3.17	6	119	365	3.44	3	202	390	3.6	27	125	375	4.2				
147	5	200	395	3.18	6	170	340	3.25	3	194	390	3.6	44	124	361	3.8				
150	5	208	404	3.24	6	175	345	3.27	3	194	398	3.59	43	121	372	3.99				
153	5	198	386	3.23	6	175	348	3.34	3	186	396	3.34	26	117	366	3.81				
156	5	197	407	3.22	6	160	362	3.4	3	191	387	3.6	42	123	369	4.11				
159	5	206	399	3.19	6	165	355	3.3	3	183	390	3.3	41	129	371	3.82				
162	5	185	417	3.33	5	162	356	3.3	3	190	386	3.3	26	132	371	3.86				
165	5	205	395	3.18	5	163	348	3.34	3	185	362	3.34	39	120	367	3.94				
168	5	215	393	3.17	5	152	362	3.4	3	205	383	3.6	39	113	373	3.8				
171	5	195	399	3.19	5	155	354	3.3	3	195	367	3.3	24	115	375	3.89				
174	5	200	402	3.28	5	130	352	3.2	3	200	388	3.2	38	115	371	3.91				
177	5	210	400	3.22	5	120	348	3.28	3	173	370	3.28	38	120	384	3.98				
180	5	220	391	3.17	5	118	347	3.28	3	192	383	3.28	22	115	375	3.96				
183	5	215	399	3.2	5	147	354	3.37	3	197	386	3.37	36	120	372	3.8				
186	5	208	410	3.25	5	175	362	3.24	3	207	367	3.24	36	114	379	4.13				
189	5	211	390	3.16	5	175	361	3.36	3	193	362	3.36	20	118	379	3.97				
192	5	215	404	3.24	4	175	357	3.22	3	192	387	3.22	35	130	374	3.8				
195	5	200	405	3.24	4	160	360	3.32	3	185	388	3.32	35	118	378	3.9				
198	5	212	389	3.13	4	176	362	3.39	3	181	388	3.39	18	116	377	3.8				
201	5	213	398	3.19	4	176	360	3.32	3	186	389	3.32	33	116	367	3.78				

Offset	Shotgun				S. Vibrator (29s)				L. Vibrator (29s)				L. Vibrator (15s)				Hammer (21s)			
	No.	Fmax	f2-f1	Rf	No.	Fmax	f2-f1	Rf	No.	Fmax	f2-f1	Rf	No.	Fmax	f2-f1	Rf	No.	Fmax	f2-f1	Rf
204	5	190	404	3.13	4	170	352	3.17	3	193	380	3.17	33	120	379	4.4				
207	5	213	396	3.13	4	180	364	3.34	3	183	365	3.34	17	128	369	3.7				
210	5	217	397	3.21	4	150	354	3.27	3	184	386	3.27	31	118	383	4.25				
213	5	212	406	3.22	4	190	349	3.25	3	195	378	3.25	31	118	374	3.95				
216	5	220	397	3.21	4	190	352	3.36	3	185	383	3.36	16	120	374	3.8				
219	5	222	400	3.22	4	194	355	3.27	3	192	362	3.27	29	125	377	4.32				
222	5	206	399	3.22	3	194	357	3.3	3	197	384	3.3	29	136	374	3.92				
225	5	225	399	3.22	3	200	358	3.25	3	189	385	3.25	15	143	373	3.9				
228	5	204	399	3.19	3	195	357	3.25	3	186	386	3.25	27	124	374	4.07				
231	5	210	416	3.39	3	203	357	3.28	3	193	386	3.28	27	117	383	4.1				
234	5	202	402	3.28	3	171	362	3.4	3	196	385	3.4	14	145	368	3.8				
237	5	212	398	3.33	3	160	359	3.32	3	201	375	3.32	25	119	379	4.02				
240	5	213	401	3.28	3	175	354	3.27	3	190	376	3.27	25	123	376	3.82				
243	5	207	403	3.34	3	170	355	3.27	3	192	380	3.27	13	140	387	3.8				
246	5	216	441	3.4	3	175	350	3.29	3	189	380	3.29	23	120	392	3.6				
249	5	222	394	3.24	3	182	365	3.25	3	193	379	3.25	23	128	369	3.7				
252	5	220	413	3.26	3	180	363	3.3	3	190	381	3.3	12	127	369	3.6				
255	5	207	414	3.32	3	170	367	3.35	3	205	388	3.35	21	123	379	3.55				
258	5	220	407	3.27	3	175	360	3.32	3	203	371	3.32	21	113	382	3.35				
261	5	208	402	3.25	3	180	369	3.35	3	198	385	3.38	11	130	377	3.4				
264	5	200	413	3.38	3	178	360	3.32	3	203	375	3.32	19	131	376	3.45				
267	5	220	401	3.28	3	168	356	3.31	3	205	390	3.34	19	125	377	3.4				
270	5	202	395	3.26	3	188	367	3.41	3	186	381	3.74	10	127	378	3.48				
273	5	217	421	3.43	3	175	353	3.2	3	187	390	3.5	17	130	388	3.48				
276	5	223	400	3.34	3	177	362	3.4	3	191	377	3.7	17	132	387	3.41				
279	5	208	403	3.23	3	179	364	3.33	3	195	385	3.36	9	134	384	3.35				
282	5	223	407	3.3	3	170	365	3.33	3	199	384	3.33	15	135	382	3.48				
285	5	220	400	3.28	2	160	353	3.27	3	208	377	3.27	15	134	390	3.46				
288	5	213	411	3.4	2	180	352	3.26	3	200	380	3.26	8	130	376	3.48				
291	5	204	406	3.35	2	170	357	3.22	3	192	393	3.22	13	141	375	3.42				

Offset	Shotgun				S. Vibrator (29s)				L. Vibrator (29s)				L. Vibrator (15s)				Hammer (21s)			
	No.	Fmax	f2-f1	Rf	No.	Fmax	f2-f1	Rf	No.	Fmax	f2-f1	Rf	No.	Fmax	f2-f1	Rf	No.	Fmax	f2-f1	Rf
294	5	214	411	3.34	2	174	352	3.2	3	192	395	3.2	13	147	369	3.4				
297	5	212	406	3.35	2	172	342	3.16	3	183	385	3.16	7	148	368	3.45				
300	5	225	418	3.36	2	171	352	3.2	3	201	388	3.2	11	133	364	3.47				
303	5	230	397	3.21	2	180	357	3.31	3	189	391	3.31	11	153	370	3.46				
306	5	222	424	3.35	2	181	359	3.32	3	203	379	3.32	6	141	356	3.26				
309	5	212	427	3.33	2	180	360	3.39	3	195	387	3.39	9	134	368	3.47				
312	5	230	398	3.27	2	198	360	3.32	3	193	396	3.32	9	151	370	3.47				
315	5	208	429	3.42	1	208	359	3.32	3	205	380	3.32	5	154	371	3.47				
318	5	210	453	3.56	1	210	352	3.3	3	190	373	3.3	8	158	377	3.41				
321	5	212	388	3.21	1	209	354	3.27	3	193	386	3.27	8	167	379	3.49				
324	4	212	409	3.34	1	204	361	3.32	3	206	387	3.32	4	155	369	3.59				
327	4	208	459	3.6	1	206	356	3.3	3	193	390	3.3	7	153	368	3.59				
330	4	212	433	3.44	1	226	356	3.3	3	187	375	3.3	7	175	375	3.63				
333	3	217	450	3.52	1	207	363	3.24	3	200	385	3.24	3	125	356	3.46				
336	3	215	459	3.6	1	210	345	3.17	3	198	369	3.17	5	120	367	3.7				
339	3	225	416	3.36	1	212	373	3.27	3	200	386	3.27	5	123	334	3.54				
342	2	165	459	3.6		200	354	3.27	3	186	387	3.27	2	122	333	3.49				
345	2	216	453	3.56									3	154	363	3.6				
348	2	223	452	3.38									3	134	364	3.48				
351	1	144	495	4.08									1	127	330	3.28				
354	1	155	462	3.58									1	123	340	3.53				
357	1	185	367	3.11									1	190	375	3.79				
Ave.		207	401	3.27		161	352	3.42		181	381	3.51		131	364	3.83		194	386	3.48

Note: "No." presents the number of the traces with same offset.
"Fmax" presents the dominant frequency.